INFORMATION TO USERS

This manuscript has been reproduced from the microfilm master. UMI films the text directly from the original or copy submitted. Thus, some thesis and dissertation copies are in typewriter face, while others may be from any type of computer printer.

The quality of this reproduction is dependent upon the quality of the copy submitted. Broken or indistinct print, colored or poor quality illustrations and photographs, print bleedthrough, substandard margins, and improper alignment can adversely affect reproduction.

In the unlikely event that the author did not send UMI a complete manuscript and there are missing pages, these will be noted. Also, if unauthorized copyright material had to be removed, a note will indicate the deletion.

Oversize materials (e.g., maps, drawings, charts) are reproduced by sectioning the original, beginning at the upper left-hand corner and continuing from left to right in equal sections with small overlaps.

Photographs included in the original manuscript have been reproduced xerographically in this copy. Higher quality 6" x 9" black and white photographic prints are available for any photographs or illustrations appearing in this copy for an additional charge. Contact UMI directly to order.

ProQuest Information and Learning
300 North Zeeb Road, Ann Arbor, MI 48106-1346 USA
800-521-0600

EFFECT OF VEGETATION CHARACTERISTICS ON NEAR SOIL MOISTURE RETRIEVAL USING MICROWAVE REMOTE SENSING TECHNIQUE

By

Khil-Ha Lee

A Dissertation Submitted to the Faculty of the

DEPAERMENT OF HYDROLOGY AND WATER RESOURCES

In Partial Fulfillment of the Requirements

For the Degree of

DOCTOR OF PHILOSOPHY

WITH A MAJOR IN HYDROLOGY

In the Graduate College

THE UNIVERSITY OF ARIZONA

2002

THE UNIVERSITY OF ARIZONA ®
GRADUATE COLLEGE

As members of the Final Examination Committee, we certify that we have read the dissertation prepared by KHIL-HA LEE

entitled EFFECT OF VEGETATION CHARACTERISTICS ON NEAR SOIL MOISTURE RETRIEVAL USING PASSIVE MICROWAVE REMOTE SENSING TECHNIQUE

and recommend that it be accepted as fulfilling the dissertation requirement for the Degree of Doctor of Philosophy

Dr. W. James Shuttleworth	Date 4/1/02
Dr. Soroosh Sorooshian	Date 4/1/02
Dr. Eleanor J. Burke	Date 4/1/02
Dr. Juan B. Valdes	Date 4/1/02
Dr. Kevin E. Lansey	Date 4/1/02

Final approval and acceptance of this dissertation is contingent upon the candidate's submission of the final copy of the dissertation to the Graduate College.

I hereby certify that I have read this dissertation prepared under my direction and recommend that it be accepted as fulfilling the dissertation requirement.

Dissertation Director Dr. W. James Shuttleworth	Date 4/4/02

STATEMENT BY AUTHOR

This dissertation has been submitted in partial fulfillment of requirements for an advanced degree at The University of Arizona and is deposited in the University Library to be made available to borrowers under rules of the Library.

Brief quotations from this dissertation are allowable without special permission, provided that accurate acknowledgment of source is made. Requests for permission for extended quotation from or reproduction of this manuscript in whole or in part may be granted by the head of the major department or the Dean of the Graduate College when in his or her judgment the proposed use of the material is in the interests of scholarship. In all other instances, however, permission must be obtained from the author.

SIGNED: 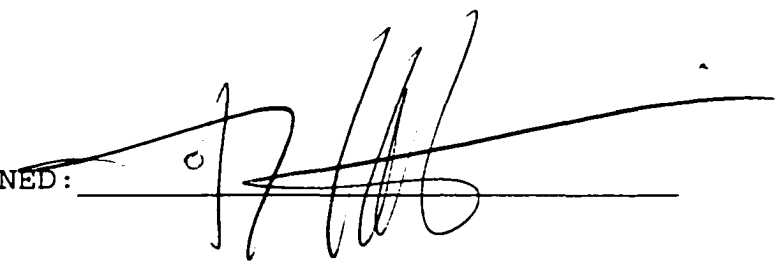

TABLE OF CONTENTS

TABLE OF CONTENTS (continued)

TABLE OF CONTENTS (continued)

LIST OF ILLUSTRATIONS

APPENDIX A

LIST OF ILLUSTRATIONS (continued)

APPENDIX B

LIST OF ILLUSTRATIONS (continued)

APPENDIX C

APPENDIX D

LIST OF ILLUSTRATIONS (continued)

LIST OF TABLES

MAIN TEXT

APPENDIX A

APPENDIX B

APPENDIX C

LIST OF TABLES (continued)

APPENDIX D

ABSTRACT

Passive microwave remote sensing has shown potential for monitoring near surface soil moisture. However, both near-surface soil moisture and the vegetation overlying the soil contribute to microwave emission and an effective way to specify the effect of vegetation is crucial for the retrieval of soil moisture from microwave observations. This dissertation presents a new approach to representing the effect of vegetation on microwave emission by extending an existing model (Wilheit, 1978) of the coherent propagation of electromagnetic radiation through a stratified medium. The resulting multi-layer microwave emission model is plausibly realistic in that it captures the behavior of the vegetation canopy by considering the dielectric permittivity of the mixture of air and vegetation matter in the canopy and recognizing the vertical distribution of dielectric permittivity through the canopy. The model parameters required to specify the dielectric profile within the canopy are not usually available from data taken in typical field experiments, particularly the parameters that quantify the way the dielectric permittivity of the vegetation and air mix together to give the dielectric permittivity of the canopy. Thus, the feasibility of specifying these parameters using an advanced single-criterion, multiple-parameter optimization technique was investigated. The resulting model was also applied to investigate the sensitivity of microwave emission to specific vegetation parameters.

The study continued with an investigation of how the presence and nature of vegetation cover influences the values of geophysical variables retrieved from multi-angle microwave radiometer spectrometer observations, using the upcoming Soil Moisture Ocean Salinity (SMOS) mission as a case study. The extended version of the Wilheit (1978) model was used to calculate synthetic observations of microwave brightness temperature at the look-angles proposed for the SMOS mission for three different soil moisture states (wet, medium, and dry) and four different vegetation covers (grass, crop, shrub, and forest). A retrieval approach that simulates that proposed for SMOS, which assumed the simple Fresnel model of microwave emission and used advance optimization techniques, was used to determine the preferred set of soil moisture, vegetation water content, and surface temperature for each set of synthetic observations. It was shown that retrieved values are only accurate when the effective values of the opacity coefficient used in the Fresnel model are made to vary in a prescribed way with look-angle, soil moisture status, and vegetation. The errors in retrieved values that may be induced by poor specification of vegetation cover were investigated by imposing random errors in the values of vegetation-related parameters in the forward calculations of synthetic observations made with the extended Wilheit model. The results show that poorly specified vegetation can result in both random and systematic errors in the retrieved values of the geophysical variables.

This dissertation is supplemented by description of additional related research to which the candidate made a contribution. Specifically, an investigation of alternative procedures for assimilating area-average estimates of surface soil moisture into Land Data Assimilation Systems, and an investigation of a novel field instrument to measure area-average sensible heat flux.

1. INTRODUCTION

Evaporation from bare soil or from soil beneath vegetation, infiltration into the soil, and, thus, surface runoff, are important aspects of the land-surface water and energy balance that are controlled by near surface soil moisture (often defined to be that present in the uppermost 5 cm). Moreover, the uptake of soil water by vegetation for transpiration is, in part, controlled by soil moisture in the plants' rooting zone. Consequently, water and energy fluxes at the land surface/atmosphere interface depend strongly on soil-moisture status (Kerr et al., 2001). Weather and climate are, in turn, significantly influenced by the local and regional availability of the soil moisture via the evaporation and transpiration processes.

Ground-based measurements of soil moisture are usually point measurements and it is difficult and time consuming to measure the temporal and spatial variability in this way. Moreover it is hard to conceive how the large- (meso-, continental- or global-) scale estimates of soil moisture needed to initiate atmospheric models, or for assimilation into them, could feasibly or economically be made using single-point ground based soil moisture sampling.

Although soil moisture is well known to be important to atmospheric and hydrologic models, to date, there is no direct global measurement of it (Kerr et

al., 2001). However, many observational and modeling studies have shown the potential of passive microwave remote sensing, particularly L-band (1.4 GHz frequency), for estimating near-surface soil moisture (Calvet et al., 1995; Chanzy et al., 1997; Jackson et al., 1999; Teng et al., 1993; Wang et al., 1990; Wigneron et al., 2000). Passive microwave radiometry at low frequencies (L- band: 1.4 GHz, 21cm) has been selected by the European Space Agency (ESA) for use in the Soil Moisture Ocean Salinity (SMOS), which has a proposed launch date in the 2003-2005 time frame (http://www.cesbio.upstlse.fr/indexsmos.html). The SMOS mission will be based on a dual polarization, L-band radiometer with an innovative aperture synthesis concept (a two-dimensional interferometer) that can achieve an on-the-ground resolution of ~50 km near the edge of the swath, coupled with multi-angular acquisition designed to deliver several key land-surface variables, namely, near-surface soil moisture, vegetation water content, and effective temperature (Kerr et al., 2001; Wigneron et al., 2000).

Although L-band microwave remote sensing techniques have potential capability for estimating surface soil moisture, the ability to retrieval using multi-angular viewing configurations with large footprints that sample heterogeneous surface variables has not yet been proven. Moreover, L-band remote sensing can measure soil moisture only within top 5cm of the soil, and merely modifying surface soil moisture during assimilation does not by itself provide a sufficiently strong updating of the deeper soil moisture profile (Houser et al. 1998). Further

study is needed to develop understanding of how to apply the information in remotely sensed surface soil moisture estimates to the deeper soil layers. Some studies of how to integrate remotely sensed soil moisture into a hydrological model have been attempted (Houser et al. 1998; Reichle et al., 2001), but so far the results are less than satisfactory.

Modeling studies have shown that integrating the description of the land surface water and energy exchange with the description of the microwave emission from the soil-vegetation-atmosphere interface can give good prediction of the time courses of the microwave brightness temperature (Liou et al., 1998; Galantowicz et al., 1999; Burke et al., 1997; 1998; 2001). However, it is well recognized in such models that the relationship between microwave brightness temperature and surface soil moisture can be influenced by several auxiliary factors, including soil properties and the nature and form of the overlying vegetation (Schmugge, 1998; Wigneron et al., 1998, Lee et al., 2002). Hence accurate description of the vegetation is necessary when estimating surface soil moisture. The importance of vegetation on surface soil moisture retrieval is especially significant for the SMOS mission, because the radiometer will monitor land surface areas typically at 50 km resolution and vegetation is not expected to be homogeneous over such an area. It is also significant that vegetation biomass is itself a surface variable that is to be monitored during the SMOS mission.

Even though the simple vegetation model suggested by Jackson and Schmugge (1991) is much used in many surface soil moisture retrievals, the opacity coefficient, *b*, used in their model is not a simple parameter. Recent work has shown that the opacity coefficient depends on both the gravimetric water content of vegetation (Wigneron et al., 1996; W; 2000; Le Vine and Karam, 1996) and the temperature (Wigneron et al., 2000). In addition, the canopy type and structure (Jackson and Schmugge, 1991), the polarization (van de Griend and Owe, 1996) and wavelength of the radiation (Jackson and Schmugge, 1991), and the look-angle of the sensor (van de Griend and Owe, 1996) may also influence the opacity coefficient.

The model describing the vegetation suggested by Wigneron et al. (1993) is complete and descriptive but arguably too complicated to be routinely applied in the field. Since the model requires the sophisticated knowledge of the vegetation canopy, inversion may be very complex. Hence, a realistic model of intermediate complexity is required, that adequately captures most of important features of vegetation (such as the canopy type/structure, polarization, wavelength, look angle, temperature, and vegetation water content). In this study a new approach to modelling the effect of the vegetation on passive microwave emission is developed and explored which is based on an existing radiative transfer model (Wilheit, 1978). This new modeling approach is used to test

retrieval capability for the multi-angle, L-band, passive microwave observations such as will be provided during the SMOS mission.

This dissertation includes four papers. The first paper, given in Appendix A, addresses modeling the effect of vegetation on the microwave emission and introduces and applies the new approach mentioned above. This paper also investigate how to specify parameters in the new model from typical field measurements, especially those that cannot be measured directly, such as the effect of non-linear mixing of the dielectric permittivities in the canopy. It also describes how the model was applied to investigate the sensitivity of the microwave emission to specific vegetation parameters. The new model is then applied in the second paper, given in Appendix B, to calculated microwave brightness temperatures that simulate those to be measured during the SMOS mission. In this way, the retrieval capability of the algorithm proposed for SMOS is evaluated for different types of vegetation cover and in different soil moisture conditions.

The above two papers are the main products of this doctoral research program, but two additional papers are included in this thesis. The third paper, given in Appendix C, introduces and investigates a new method for propagating remotely sensed surface soil moisture information more effectively into the deeper soil layers in a hydrological model. This paper also investigates alternative methods for distributing large area average, remotely sensed surface

soil moisture between separate patches in a hydrological model that uses the "mosaic" approach. Finally, the fourth paper, given in Appendix D, describes a field study in which the candidate participated that investigated a novel field instrument, the scintillometer, capable of measuring area-average sensible heat flux.

2. PRESENT STUDY

2.1 BACKGROUND OF THE RESEARCH

2.1.1 Remote Sensing of Soil Moisture

In principle, radiation from across the whole electromagnetic spectrum can be used to provide remotely sensed estimates of soil moisture. However, in practice some wavelengths are more suitable than others. The surface albedo for solar radiation in the visible portion of the spectrum (0.4 - 0.7 μm) depends strongly on the surface wetness of the soil, and this is the basis for attempts to remote sensing soil moisture in the visible waveband. It is, however, very difficult to relate surface albedo and surface soil moisture in a unique way, not least because this relationship is so strongly influenced by soil surface roughness and land cover characteristics. Thermal infrared can also be used to measure the surface soil moisture content because the diurnal cycle of thermal infrared emission is influenced by the thermal conductivity and heat conductivity of soil that is in turn affected by soil wetness. However, remote sensing of soil moisture at this wavelength is restricted to bare soil. Both thermal and visible wavelengths do not penetrate clouds.

One major advantage of microwave remote sensing (typically in the frequency range 0.3 - 300 GHz) is that the radiation passes through the air and clouds with much less attenuation, so it is potentially applicable in all weather conditions. Both active and passive microwave remote sensing can be used to measure the surface soil moisture content. In active microwave remote sensing, the radar emits radiation and detects its return. Satellite based radar that monitor soil moisture can operate at very high spatial resolutions (~ m's). Passive microwave sensors only receive microwave signals emitted by the Earth, so the signal is relatively weak compared to a radar signal and it is harder to achieve high spatial resolutions. Even with limitations on the resolution, passive microwave remote sensing is currently the preferred approach to indirect sensing of soil moisture. This is mainly because the effects of vegetation and soil surface roughness are easily quantifiable.

2.1.2 Passive Microwave Remote Sensing

Passive microwave remote sensing systems operating at L-band (21cm, 1.4 GHz) and/or C-band (6cm, 5.6GHz) frequencies are recognized as being a promising tool to measure soil moisture in the (~5cm) surface layer of soil (Schmugge, 1998; Jackson et al, 1999; Njoku and Li, 1999). Studies have shown that accurate values of the near-surface soil moisture can be retrieved even

when there is a significant vegetation canopy covering the ground (Jackson and Schmugge, 1991). For example, Jackson et al. (1999) present validated soil moistures derived from the Electronically Scanned Thinned Array Radiometer (ESTAR), which was flow during the Southern Great Plains hydrology experiment (SGP97). The prospects for a passive microwave mission that will provide global estimates of soil moisture are good. The AMSR mission, due for launch in spring 2002, contains a C-band passive microwave radiometer, which will provide large-scale estimates of soil moisture under sparse to moderate vegetation. This is not the ideal configuration for soil moisture remote sensing. However the SMOS mission, which has been selected for launch by the European Space Agency (ESA), detects at L-band, and can detect soil moisture under denser vegetation. SMOS uses two-dimensional aperture synthesis to provide brightness temperatures at a range of look angles over the same area (Kerr et al., 2001; Wigneron et al., 2000).

The effectiveness of microwave remote sensing of soil moisture relies on the fact that there is a large difference between the dielectric of the soil particles (~ 4) and air (~ 1) and the dielectric of water (~ 80). The dielectric constant is inversely proportional to the emissivity of a substance. For example, a dry soil will have a low dielectric constant and high emissivity whereas a wet soil will have a high dielectric constant and low emissivity. The effect of vegetation on the

microwave emission from the soil surface is strongly influenced by the imaginary part of the dielectric constant (Schmugge and Jackson, 1992).

Thus, knowledge of the dielectric constant for vegetation and soil medium (see section 2.4 and 2.5) is crucial, and the passive microwave remote sensing of soil moisture greatly benefits from relevant ancillary information on soil texture, soil surface roughness, vegetation geometry and composition, and vegetation cover type (etc.). In addition, horizontal inhomogeneities in vegetation geometry, cover type, and composition impact the dielectric properties and surface roughness of the vegetation cover, although further studies are needed to quantify the importance of these. Large-scale topography affects the microwave signal by introducing variations in the effective look-angle and it has been suggested that this can be considered to be macro-scale surface roughness (Kerr et al., 2001, Matzler and Standley, 2000).

2.1.3 Microwave emission models for bare soils

The radiation received by a microwave sensor is quantified in terms of the brightness temperature, T_B, which, for a soil medium, can be expressed as follows:

$$T_B(\theta, p) = e_s(\theta, p) T_s \qquad (2.1)$$

in which $T_B(\theta, p)$ in $^{\circ}K$ is the microwave brightness temperature, $e_{\nu}(\theta, p)(0 \le e_{\nu} \le 1)$ is the polarized specular emissivity of the soil medium, and T_S is the physical temperature of the soil medium. In all of the models discussed in this section scattering effects are assumed to be negligible.

For homogeneous media, i.e., media with constant moisture and temperature profiles, the emissivity for a smooth surface can be calculated from the dielectric properties of the soil using the Fresnel equations for surface reflectivity, where the emissivity is one minus the reflectivity:

$$r_h = \frac{\varepsilon \cos\theta - \sqrt{\varepsilon - \sin^2\theta}}{\varepsilon \cos\theta + \sqrt{\varepsilon - \sin^2\theta}} \qquad r_v = \frac{\cos\theta - \sqrt{\varepsilon - \sin^2\theta}}{\cos\theta + \sqrt{\varepsilon - \sin^2\theta}} \tag{2.2}$$

where r_h and r_v are the horizontal and vertical reflectivity, respectively, θ is the incidence angle and ε is the dielectric constant of the soil.

For non-homogeneous soils, radiative transfer models that predict emission at the soil surface can be classified as either coherent or non-coherent. Coherent models include the models developed by Wilheit (1978) and Njoku and Kong (1977) who developed radiative transfer models based on similar theoretical assumptions. This class of model solves a differential equation to obtain the fraction of energy absorbed at different depths within the medium, with

flux conservation at soil/air interface used as a boundary condition. Schmugge and Choudhury (1981) and Costes et al. (1994) compared these two coherent models and concluded that both models are in good agreement, but the Wilheit model is simpler and therefore preferred (Raju et al., 1995; Schmugge and choudhury, 1981). The Wilheit (1978) model (summarized in section 2.3.1) has been found to be in good agreement with experimental observations (Wang, 1987; Laguerre et al., 1994, Raju et al., 1995; Burke et al, 1997; 1998). In addition, Raju et al. (1995) compared the Wilheit (1978) model with the (single-layer) Fresnel model. They concluded that, in terms of estimating T_B, the two models perform similarly at low frequencies providing the Fresnel model is implemented with an optimal sampling depth.

It should be noted that interference effects can occur in a coherent model. Schmugge et al., (1981) observed them during a field experiment at the University of California, Davis, when they monitored the downward progression of a wetting front. However, these phenomena are unlikely to occur commonly in nature because of surface roughness effects and the horizontal inhomogeneity of soils (Schmugge, 1982).

In non-coherent models, emissivity is determined by the dielectric constant at the air/soil interface and so depends on the layer thickness used, especially when near-surface soil moisture is strongly depth-dependent (Schmugge, 1982). Burke et al. (1979) developed a non-coherent radiative transfer model in which the soil was treated as homogeneous layers of dielectric of arbitrary thickness. This model is not directly applicable to soil moisture remote sensing because only the upper layers of the soil moisture profile contributes to the effective temperature calculation (Raju et al., 1995).

2.1.3.1. Wilheit (1978) model

The model discussed in detail in this thesis is the Wilheit (1978) microwave emission model. In the Wilheit (1978) model, the soil is described as a semi-infinite layered dielectric medium with each layer characterized by a dielectric constant that is assumed to be homogeneous within the layer. The model uses Maxwell's equations and boundary condition at the interface to calculate the electric field in each layer assuming (1) the soil is a semi-infinite medium with a smooth air-soil boundary; (2) boundaries between the layers are planar and parallel; and (3) each layers is in thermal equilibrium and each layer emits the same energy as it absorbs. With these assumptions, the microwave brightness temperature is given by:

$$T_B = \sum_{i=1}^{n} f_i T_i \qquad (2.3)$$

where T_i is the physical temperature of the i th layer, and f_i is the fraction of the energy of the incident wave, E_i, absorbed by the i th layer, and n is the number of layers. Conservation of energy at the air/soil interface determines the reflectivity of the soil surface, r_s, as:

$$r_s = 1 - \sum_{i=1}^{n} f_i \tag{2.4}$$

The thermal sampling depth is given by:

$$\delta_T = \frac{\sum x_i f_i}{\sum f_i} \tag{2.5}$$

Where X_i is the depth of the i_{th} layer. The average soil temperature over this thermal sampling depth, referred to as the effective radiating temperature, is given by:

$$T_{eff} = \frac{\sum T_j f_j}{\sum f_i} \tag{2.6}$$

The ratio of T_B to T_{eff} is the effective emissivity for the soil.

2.1.4 Model of soil dielectric

At microwave frequencies, the dielectric behavior of the soil medium is a function of the nature of the soil particles and the soil water, which exists as free water

and water molecules that are bound to soil particles. Free water molecules can readily align themselves with an applied electric field but water molecules bound to soil particles cannot. Consequently, bound water is usually treated like ice in models and has a significantly lower dielectric constant (~4, for L-band) than free water (~80, at L- band). The relative proportions of bound and free water depend on soil particle size distribution, which is therefore an important factor controlling the dielectric constant of soil. Water binds more easily to the smaller clay particles and hence clay soils have a higher fraction of bound water than sandy soil. There are two models that are commonly used to predict the dielectric of the soil in passive microwave remote sensing (Wang and Schmugge, 1980; Dobson et al., 1985).

Wang and Schmugge (1980) developed a simple mixture model for the soil dielectric that is a straightforward combination of the dielectric constants of ice, water, air, and soil particles. This is applicable for frequency range of 1.4 GHz and 5 GHz. Schmugge (1980) distinguish between cases where the volumetric water content (W_s) is either smaller than or equal to the transition water content or grater than the transition water content (W_t). This is the value at which the maximum possible amount of water is bound. The dielectric constant is given by:

$$\varepsilon = W_s \varepsilon_x + (P - W_s)\varepsilon_a + (1 - P)\varepsilon_r \qquad W_c \le W_t \qquad (2.7)$$

with

$$\varepsilon_x = \varepsilon_i + (\varepsilon_w - \varepsilon_i)\frac{W_s}{W_t} \cdot \gamma \tag{2.8}$$

and

$$\varepsilon = W_t \varepsilon_x + (W_s - W_t)\varepsilon_w + (P - W_s)\varepsilon_a + (1 - P)\varepsilon_r \qquad W_s \geq W_t \tag{2.9}$$

with

$$\varepsilon_x = \varepsilon_i + (\varepsilon_w - \varepsilon_i) \cdot \gamma \tag{2.10}$$

In the above equations; P is the porosity of the dry soil; ε_a is the dielectric constant of air; ε_w is the dielectric of the water; ε_r is the dielectric of rock; ε_i is the dielectric of ice; ε_x is the dielectric of the initially absorbed water; and γ is a fitting parameter. See Wang and Schmugge (1980) for details.

Dobson et al. (1985) developed a four-component dielectric mixing model for the 1.4-18 GHz frequency range that treats the soil-water system as comprising a host medium of dry soil solids which contains randomly distributed, randomly oriented disc-shaped inclusions of bound water, bulk water, and air, and calculates the dielectric as:

$$\varepsilon_m^{\alpha} = 1 + \frac{\rho_b}{\rho_s}(\varepsilon_s - 1) + W_s^{\beta}\,\varepsilon_{fw}^{\alpha} - W_s \qquad (2.11)$$

$$\varepsilon_s = (1.01 + 0.44\rho_s)^2 - 0.062$$

This equation is based on the Birchak et al. (1974) refractive volumetric mixing model. The parameter $\alpha = 0.65$, while β depends on the textural composition of the soil. The soil particle dielectric constant, ε_s, and the free water dielectric constant, ε_{fw} are considered to approximate the dielectric of the soil-water mixture in the model because the complex dielectric constant of bound water is poorly known and its volume fraction is available only after lengthy calculations. ρ_b is a bulk density of soil and ρ_s is a specific density of soil and m_v is volumetric soil moisture. (Dobson et al., 1985).

2.1.5 Effect of vegetation on microwave emission from the soil

A vegetation canopy overlying soil reflects, transmits, and absorbs the radiation emitted from the soil, while the vegetation itself emits its own radiation that adds to the total radiative flux (scattering of the radiation from the soil by the vegetation is negligible at L-band and C-band). Basharinov and Shutko (1975) presented a fairly simple model for the microwave brightness temperature of an interface comprising a semi-infinite soil layer with physical temperature, T_s (in

$^{\circ}K$) and air-soil reflectivity $r(\theta,p)$ with overlying vegetation with a physical temperature T_v (in $^{\circ}K$), that has the following :

$$T_B(\theta,p) = [1 + r_s(\theta,p)\Gamma(\theta)][1 - \Gamma(\theta)](1-\alpha)T_v + [1 - r_s(\theta,p)]\Gamma(\theta)T_s \qquad (2.12)$$

where α is the single-scattering albedo and $\Gamma(\theta)$ the transmissivity of the vegetation layer, respectively. This model is based on the following assumptions:

i. the single-scattering albedo (assumed independent of θ and p) is small ($0.04 \le \alpha \le 0.12$);

ii. the air-vegetation reflectivity is zero;

iii. r_s (assumed independent of p) is set to the air-soil reflectivity rather than the vegetation-soil reflectivity because the average index of refraction of vegetation layer is only slightly larger than that of air (Ulaby et al., 1986).

In this model, the brightness temperature, T_B (in $^{\circ}K$), of the two-layers (soil and vegetation), neglecting atmospheric effects, is a combination of three components:

i. the radiation emitted by the canopy itself, given by:

$$T_{B1} = (1 - \Gamma)(1 - \alpha)T_v \qquad (2.13)$$

ii. the radiation emitted by the canopy in the downwards direction which is reflected by the soil surface and subsequently travels upwards through the canopy, given by:

$$T_{B2} = \Gamma(1 - r_s)(1 - \Gamma)(1 - \alpha)T_v \qquad (2.14)$$

iii. and the radiation emitted by the soil surface and attenuated by vegetation, given by:

$$T_{B3} = (1 - r_s)\Gamma T_s \qquad (2.15)$$

The two parameters describing the vegetation canopy that is required as input by this model are the transmissivity and the single scattering albedo. The single scattering albedo is determined by the distribution of water within the canopy and is impacted by the canopy structure. It is of the order zero especially at the lower frequencies. In many examples where measurements were made at L-band it has been assumed to be zero (Shutko, 1986; Jackson and O'Neill, 1990; Jackson, 1991; van de Griend and Owe, 1993; van de Griend et al. 1994). However, at C-band its value becomes more significant (Jackson and Schmugge, 1991). There are few examples where the single scattering albedo has been estimated (Jackson and Schmugge, 1991) and the dependence of the single scattering albedo on the properties of the vegetation, polarization and frequency of detection are largely unknown.

The other required parameter is the transmissivity of the vegetation helps to quantify the amount of absorption and emission by the vegetation. At each frequency and polarization, it is mainly a function of look angle and vegetation water content, although the structure and type of canopy can also affect its value. The transmissivity of the vegetation can be expressed as:

$$\Gamma(\theta) = \exp(-\tau \sec\theta) \tag{2.16}$$

where τ is the optical depth and θ is the look-angle. The optical depth is theoretically related to the extinction coefficient of the canopy, K_e:

$$\tau = \kappa_e h \tag{2.17}$$

where h is the height of the canopy.

Kirdyashev et al. (1979) explored the quantitative effect of vegetation on microwave emission using measured data. They derived optical depth as a function of the dielectric properties and water content of the vegetation, plant shape and structure, wavelength, and look angle (Kirdyashev et al., 1979; Jackson and Schmugge, 1991), as follows:

$$\tau = k\frac{2\pi u}{3\lambda}\cdot 10^{-5}\cdot W_v \cdot \varepsilon'' \tag{2.18}$$

where u = 1 and u = 2 for cylinders and disks, respectively; λ is the wavelength; ϑ is the look angle; k is a unit conversion factor (Kirdyashev (1979) suggested that vegetation water content is $Q \cdot C$ where Q is the mass of vegetation per unit area (the fresh weight of the vegetation per unit area, in 100 kg/ha), m is the moisture content by weight, in (g/g); W_v is vegetation water content in kg/m^2

ε'' is the imaginary part of the complex dielectric constant of water .[Note: strictly, it is necessary to consider the effect of the portion of the biomass with quasi-random orientation (leaves) and well-defined orientation (trunks and stems)

separately when interpreting the microwave signal because these components depend strongly on the polarization.] Another, similar formulation for the optical depth was derived by (Schmugge and Jackson, 1992; Ulaby et al., 1986):

$$\tau = 4\pi \cdot (h/\lambda) \cdot \sqrt{\varepsilon''} \qquad (2.19)$$

Hence, the optical depth can be calculated using equation (2.19) or (2.21) given knowledge of the imaginary part of the dielectric constant of the canopy.

Jackson and Schmugge (1991) simplified the above approaches and proposed a simple empirical model for the effect of vegetation on microwave emission with the form:

$$\tau = b \cdot W_v \qquad (2.20)$$

where b is a opacity coefficient .

Where the dependence of optical depth on all factors other than the depth integrated water content are assumed to be adequately represented by the opacity coefficient, *b*. The opacity coefficient has been shown to be a function of canopy type and structure, as well as the polarization and wavelength of the radiation (Jackson and Schmugge, 1991). In addition, recent studies suggest that *b* depends on the gravimetric water content of vegetation (Wigneron et al., 2000; Wigneron et al., 1996; Le Vine and Karam, 1996). The value of *b* may even vary with soil wetness because the dielectric constant of water is temperature-dependent and the temperatures of the vegetation and soil are often assumed

equal, even though the vegetation temperature may be higher if the soil is dry (Wigneron et al., 2000).

Van de Griend and Owe (1993) determined the single scattering albedo and optical depth of typical savanna vegetation in Botswana (Africa) by inverse modeling. They based their model on the theory described above and used 6.6 and 37 GHz, dual polarization, satellite microwave signatures from Nimbus/SMMR along with in field measurements of surface soil moisture data. They showed a significant correlation between optical depth and NDVI values derived from NOAA/AVHRR. Van de Griend and Owe (1994) further studied the influence of polarization on canopy effects in large-scale soil moisture monitoring using the same data and found that the effects of the ratio of horizontal to vertical polarization on canopy effect are independent of seasonal variation. More recently, van de Griend and Owe (1996) developed a measurement procedure to determine these vegetation parameters at horizontal and vertical polarization. They concluded that both measurements and calculations suggest that these parameters are slightly dependent on view angle but that there was no discernable dependence of the ratio of horizontal to vertical polarization canopy effect on biomass density.

The dielectric constant of the vegetation canopy is key when modeling the effect of vegetation in microwave remote sensing. Ulaby and El-Rays (1987) developed a dielectric model for corn leaves by combining the dielectric of the

dry matter component and free and bound water for the frequency range 0.2-20 GHz, based on measurements of sucrose water solutions of known volume ratios. They assumed that the dielectric constant of a single leaf, ε_v can be expressed as a simple additive function of three components: (1) ε_r, a nondispersive residual component; (2) $V_{fw}\varepsilon_f$, a free-water component, where V_{fw} is the volume fraction of three water and ε_f is its dielectric constant, and (3) $V_b\varepsilon_b$, a bulk bound water component, where V_b is the volume fraction of the bound water in the vegetation and ε_b is its dielectric constant. Thus:

$$\begin{aligned}
\varepsilon_v &= \varepsilon_r + V_{fw}\varepsilon_f + V_b\varepsilon_b \\
\varepsilon_f &= 4.9 + \frac{75}{1 + jf/18} - j\frac{18\alpha}{f} \\
\varepsilon_b &= 2.9 + \frac{55}{1 + (jf/0.18)^{0.5}} \\
\varepsilon_r &= 1.7 - 0.74 m_g + 6.16 m_g^2 \\
V_{fw} &= m_g(0.55 m_g - 0.076) \\
V_b &= 4.64 m_g^2/(1 + 7.36 m_g^2) \\
\alpha &= 1.27
\end{aligned} \tag{2.21}$$

where m_g is the gravimetric vegetation water content (water content based on fresh weight in kg/kg. An example calculation using this approach is given in Table 2.1.

Matzler (1994) developed a semi-empirical formula for the complex dielectric constant of a single leaf for the frequency range from 1 to 100 GHz. This model assumes linearity with m_d in the range 0.1-0.5.

$$\varepsilon_v = 0.522(1 - 1.32m_d)\varepsilon_{fw} + 0.51 + 3.84m_d \qquad (2.22)$$

where:

$$m_d = 1 - m_g = {}^{dry\,mass}/_{fresh\,mass} \qquad (2.23)$$

Table2.1 Changes in water content of leaves during a day (from Kramer (1983), adapted from Curis and Clark (1950) and other sources.)

Plant	Water content maximum as fraction of fresh weight	Water content minimum as fraction of fresh weight
Amaranthus	0.86	0.79
Nicotiana	0.85	0.80
Physalis	0.90	0.87
Euphorbia	0.85	0.81
Helianthus	0.83	0.78
Zea mays	0.72	0.67

The dielectric constant of water, ε_w, is governed by the wavelength, the physical temperature, and the salinity. A typical salinity range of the fluid contained in vegetation material is 6 to 15 parts per thousand (ppt). Salinity exercises a negligible influence on ε_w at frequencies above about 5 GHz (Ulaby et al., 1986).

The vegetation canopy as a whole consists of the mixture of air, vegetation material, and vegetation water. Because attenuation of the microwave signal by a vegetation canopy is directly proportional to the imaginary part of the vegetation's dielectric constant, the dielectric constant of the canopy as a whole is very sensitive to the form of mixing model used to represent the combination of vegetation and air, as well as to the dielectric of individual leaves. Ulaby et al., (1986) states that due to the shortage of available measurements, it is not possible to specify precisely which mixing model to apply in a specific canopy. Schmugge (1992) used the Birchak (1974) mixing model (Ulaby et al, 1986). He concluded the refractive mixing model is better than a linear mixing model, however, the gravimetric vegetation water content, m_g in kg/kg is used as if it were the volumetric vegetation water content, m_w in kg/m^3 and plant height and vegetation volume fraction are assumed in his calculations. If the dielectric constant of individual leaves is known, the total canopy dielectric constant can be calculated from a generalized mixing model (Ulaby et al., 1986).

$$\varepsilon_c^a = \varepsilon_a^a (1 - v_f) + \varepsilon_v^a v_f \qquad (2.24)$$

where α is an empirical mixing coefficient and v_f is the vegetation volume fraction and can be given by:

$$v_f = \frac{LAI \cdot t}{h} \tag{2.25}$$

where LAI is the leaf area index, and t is the leaf thickness, and h is the canopy height. The vegetation volume fraction can also be calculated from:

$$v_f = \frac{W_v \cdot [1 + (1 - m_g)\, m_g \cdot \rho_w]}{h} \tag{2.26}$$

where ρ_v is the vegetation density in g / cm^3, which is typically 0.33 (Ulaby et al., 1986). Typically, the vegetation volume fraction in the vegetation/air mixture is less than 1% of the total canopy volume. The vegetation volume fraction is, for instance, 0.51% when V_{WC}=2.57 kg/m$_2$, m_g=0.8 kg/kg, ρ=0.33 g/cm^3, and h=0.89 m in the so-called "Drydown2" dataset collect in Beltsville in 1985.

2.1.6 Soil surface roughness

A rough soil surface increases the emissivity of the soil because the emitting area is greater. Incident collimated radiation is reflected in many directions with such a rough surface, and this mixes the two polarization states, resulting in less difference between the emissivities for horizontal and vertical polarizations. The effect of roughness is greater for wet soils, when the difference between smooth and rough surfaces can be as great as $50^{\circ}K$ (Choudhury et al., 1979).

Choudhury et al. (1986) and Wang and Choudhury (1981) developed an empirical model with the form:.

$$r_H^R(\theta) = [(1-Q)r_H(\theta) + Qr_v(\theta)]\exp(-h_s\cos^2\theta) \qquad (2.27)$$

$$r_v^R(\theta) = [(1-Q)r_v(\theta) + Qr_H(\theta)]\exp(-h_s\cos^2\theta)$$

where $r_H(\vartheta)$ and $r_v(\vartheta)$ are the reflectivity for horizontal and vertically polarized radiation, the parameter Q represents the mixing of polarization states resulting from surface roughness, the superscript R denotes values for a rough soil surface, and h_S is a roughness parameter given by

$$h_s = 4\sigma^2\left(\frac{2\pi}{\lambda}\right)^2 \qquad (2.28)$$

where σ is the standard deviation of the roughness height. This two-parameter model is a modification of the soil reflectivity for a smooth soil surface used to calculate the brightness temperature of a rough soil surface.

2.1.7 Coupled land surface microwave emission models

Reliable large-scale soil moisture estimates are an essential for determining the regional and global water and energy balance and in climate related studies. Owe et al. (1992) used a physically based, daily time step soil moisture model to study the relation, in semiarid southern Africa, between soil moisture and satellite-derived passive microwave observations from Nimbus 7, a multi-channel

scanning microwave radiometer operating at 6.6GHz. They demonstrated that this radiometer had considerable potential for quantifying surface moisture in a semiarid savanna environment, but pointed out that the operating frequency was not optimum. Raju et al. (1995) coupled a mechanistic model of heat and water flows in the soil with the Wilheit (1978) model and compared it with a single-layer Fresnel model as stated in section (2.3). Liou and England (1996) developed a point-scale, a biophysically based Land Surface Process/Radio-brightness (LSP/R) model and applied it to bare soil. Liou et al. (1998; 1999) used the LSP/R to examine the radio-brightness signal in freezing/thawing soil and prairie grassland. While Judge et al. (1999) used an LSP/R model for an area of crop, compared the modeled values with field observations gathered during SGP'97, and showed good agreement. Liou et al. (2001) reanalyzed the L-band microwave brightness temperature predicted by an LSP/R model incorporating the effect of rough soil surface scattering, as determined by IEM model for prairie grassland. They used simulated brightness temperatures given by their LSP/R model to retrieve surface soil moisture using an artificial neural network.

Burke et al. (1997; 1998) developed MICRO-SWEAT to predict surface soil moisture and the associated microwave emission. Galantowicz et al. (1999) used sequential data assimilation techniques to retrieve soil moisture (profiles) and temperature from L-band microwave brightness temperature observations. Galantowicz et al. (2000) also used a modeling approach to estimate the effect of

heterogeneity in soil-type on estimates of near-surface soil moisture derived from microwave brightness temperatures using Fresnel reflectivity without surface roughness and vegetation effect. Crow et al. (2001) used a high-resolution hydrologic model and a land surface microwave emission model (LSMEM) to investigate the impact of large-scale land surface heterogeneity on AMSR-E soil moisture retrieval. Houser et al. (1998) assimilated push-broom microwave radiometer (PBMR) images gathered over the Walnut Gulch experimental watershed in southeast Arizona into the TOP Model based Land-Atmosphere Transfer Scheme (TOPLATS). They also assimilated Information on surface soil moisture into the subsurface using knowledge of the surface-subsurface correlation, and concluded that Newtonian nudging assimilation procedures are preferable. Burke et al. (2001) used MICRO-SWEAT to explore the potential use of low-resolution remotely sensed observation of the microwave brightness temperature for surface and deep soil moisture in a "mosaic" based land surface scheme.

2.1.8 Land surface model used in this study

To be used in microwave emission model, a land surface model should be able to predict the near-surface soil moisture and relevant (soil and vegetation) temperature successfully. In this study, exploratory studies were made with the SiB-2 model (Sellers et al., 1996) and NOAH model (ftp.ncep.noaa.gov), developed by NCEP. However, the description of the soil moisture and temperature given by these models is less detailed than with the Common Land Model (CLM: http://clm.gsfc.nasa.gov). Consequently, the latter was used, without modification, to estimate the profiles of soil-moisture content and soil-temperatures required for the calculation of microwave emission from the soil, and the canopy temperature, which is needed to calculate the microwave emission of the vegetation.

CLM is a one-dimensional land-surface model developed and supported by a group of scientists in the USA and intended to be freely available to the research and academic community. It can be used (http://clm.gsfc.nasa.gov) either as a land-surface parameterization in numerical models of the atmosphere or as a base model in which sub-models of component land-surface processes can be developed. CLM includes the best elements of some well-tested physical parameterizations and numerical schemes (e.g., LSM, Bonan, 1996; BATS, Dickinson et al., 1986; IAP, Dai and Zeng, 1997). It requires a set of parameters

that specify physical constants and aspects of the soil and vegetation and, given meteorological forcing variables, it then provides prognostic and diagnostic land-surface state variables and surface energy and water fluxes as output.

CLM describes the diffusion of soil heat and liquid water through several (typically ten) layers of soil using the finite difference form of the thermal diffusion equation and Richard's equation, respectively. The layer thickness and the number of layers can be changed (ten layers were represented in CLM during the present study). The model is typically set up with a very shallow layer of soil (~ few mm) at the soil surface, and it can represent an exponentially decreasing saturated hydraulic conductivity associated with soil compaction. CLM uses the fraction of sand and clay to specify the properties of the soil rather than defining soil classes: many other models (e.g., BATS) do the latter. In CLM, the vegetation covering the ground is assumed to belong to one of the 17 IGBP vegetation classes (Belward and Loveland, 1995) and an appropriate set of the vegetation-related parameters that control surface energy and water vapor exchange specified for each class. If vegetation is present, it is represented as though it is at a single level, at the height ($d + z_0$), where d is the zero plane displacement and z_0 is the aerodynamic roughness of the canopy. Turbulent transport between this level and a specified reference height above the canopy (the lowest modeled level in the atmosphere when CLM is used as a land-surface scheme) is described using the Monin-Obukhov similarity theory, with

allowance made for the effect of atmospheric stability. The whole canopy surface resistance is parameterized following the model introduced by Jarvis (1976). The temperature of the canopy is a prognostic variable in CLM.

2.2. PRODUCTS AND RESULTS OF THE RESEARCH

Detailed description of the specific methods, results, and conclusions of the research carried out in support of this degree are presented in the four papers which are attached as appendices. This chapter documents the candidate's contribution to these four papers (in Section 3.1), and the most important findings for each paper separately (in Sections 3.2, 3.3, 3.4, and 3.5), and for this doctoral program as a whole (in Section 3.5).

2.2.1 Statement of Candidate's Contribution to Papers

The two papers given as Appendices A and B, which are summarized in Sections 3.2 and 3.3, respectively, are those to which the candidate made most contribution. In each case, the scientific research described was carried out by the candidate who also wrote the first draft of the papers. Contributions from the other authors were in the form of guidance and advice during the research and scientific editing of the paper. Overall, the candidate made an estimated 80% contribution to these two papers. In the case of the paper given in Appendix C and summarized in Section 3.4, the candidate's contribution was primarily in the form of the modeling studies with the CLM model and in scientific discussion of the results of the paper, and estimated contribution of approximately 20%. The candidate made only a minor, approximately ~5%, contribution to the paper given

in Appendix D and summarized in Section 3.5, primarily in the form of participating in the data collection for the reported field study.

2.2.2 Summary of Paper#1: A PLANE-STRATIFIED EMISSION MODEL FOR USE IN THE PREDICTION OF VEGETATION EFFECTS ON PASSIVE MICROWAVE RADIOMETRY, by Khil-ha Lee, R. Chawn Harlow, Eleanor J. Burke, and W. James Shuttleworth, *Hydrology and Earth System Sciences, 6(2): 139-151, 2002*

A vegetation canopy will scatter and absorb microwave emission from the soil and also contribute its own emission. Any downward emission from the canopy will be reflected by the soil surface and again scattered and absorbed by the canopy. The water held within the canopy is mainly responsible for this scattering, absorption, and emission.

This paper reports the development of a new approach to model the effect of vegetation on passive microwave emission, based on the coherent propagation of electromagnetic radiation through a stratified medium. The resulting multi-layer vegetation model is plausibly realistic in that it recognizes the dielectric permittivity of the vegetation matter, the mixing of the dielectric permittivities for vegetation and air in the canopy, and, in simplified terms, the overall vertical distribution of dielectric permittivity and temperature through the

canopy. Any sharp changes in the dielectric profile of the canopy resulted in interference effects manifested via oscillations in the microwave brightness temperature as a function of canopy height or look angle. However, when Gaussian broadening of the top and bottom of the canopy (reflecting the natural variability between plants) was included within the model these oscillations were eliminated. Soil surface roughness can be similarly modeled with a Gaussian broadening of the dielectric profile at the soil surface. The model parameters required to specify the effect of dielectric mixing between vegetation and air in the vegetation canopy are not usually available in typical field experiments. The feasibility of specifying these parameters using an advanced single-criterion, multiple-parameter optimization technique by minimizing the difference between the modeled and measured brightness temperatures was investigated. The results imply these parameters can be so determined, but only if other parameters that specify vegetation dry matter and water content are measured independently. The new model was then applied to investigate the sensitivity of microwave emission to specific vegetation parameters. The primary conclusions of this study are as follows.

- The Wilheit (1978) model for the coherent propagation of electromagnetic radiation through a stratified medium can be applied to provide a realistic
- simulation of the whole soil-vegetation-atmosphere interface, but this requires recognition of a gradual change in dielectric permittivity at the top

- and bottom of the vegetation canopy associated with natural variability between plants. If discrete changes in canopy dielectric are assumed, multiple internal reflections can be generated within the canopy that result in an unrealistic simulation of constructive and destructive interference patterns in the modeled microwave emission. We suspect that failure to recognize the need for smooth canopy dielectric boundaries may have been the main reason why this Wilheit (1978) model-based approach has, to the author's knowledge, not been previously used in this particular application.
- Within the framework of a universal description of microwave emission from the soil-vegetation-atmosphere interface based on the Wilheit (1978) model, the effect of rough soil surfaces can also be included by simulating a gradual change in the dielectric permittivity of the soil near the surface by introducing Gaussian smoothing with a specified standard deviation. This approach yields results in the simulation of microwave emission from bare soil similar to that given by the approach of Choudhury et al. (1979), except for short periods immediately after rain, providing the standard

- deviation of the Gaussian smoothing is two-thirds of the surface roughness used in the Choudhury (1979) correction.
- Multi-parameter optimization methods were used to derive estimates of the parameters (used in the new model to describe in-canopy dielectric mixing) which are otherwise difficult to measure, from observed time series of microwave brightness temperature and model-forcing variables. However, because there is interaction between model parameters, the values of the parameters that represent the strength of in-canopy dielectric mixing can only be defined if the vegetation content parameters are directly measured.
- Sensitivity studies with this new coupled model show that the calculated microwave emission is insensitive to the values of parameters that specify the shape of the canopy, unless these imply a canopy with very rapid changes of dielectric permittivity at the canopy boundaries. The emission is , however,sensitive to parameters that specify the amount of free water in the vegetation and the extent of dielectric mixing in the canopy, which act together to change the whole-canopy dielectric permittivity.

On the basis of the above results, it is recommended that, in upcoming field activity for validating the SMOS mission, care be taken to make independent measurements of vegetation composition parameters in addition to measurements of microwave brightness. The new model, whose development and application is the main subject of this paper, could then be used to investigate in-canopy dielectric mixing effects within canopies and, in this way, the relationship between microwave optical depth and vegetation water content better understood.

2.2.3 Summary of Paper#2: INFLUENCE OF VEGETATION ON SMOS MISSION RETRIEVALS, by Khil-ha Lee, Eleanor J. Burke, W. James Shuttleworth, and R. Chawn Harlow, *Hydrology and Earth System Sciences, 6(2): 153-166, 2002*

Using the upcoming Soil Moisture and Ocean Salinity (SMOS) mission as a case study, this paper investigates how the presence and nature of vegetation cover influence the values of geophysical variables retrieved from multi-angle microwave radiometer observations. Synthetic microwave brightness temperatures were generated using the Wilheit (1978) model for the coherent propagation of electromagnetic radiation through a stratified medium applied to account simultaneously for the emission from both the soil and any vegetation canopy present. The synthetic data were calculated at the look-angles proposed

for the SMOS mission for three different soil-moisture states (wet, medium wet, and dry) and four different vegetation covers (nominally grass, crop, shrub, and forest). A retrieval mimicking that proposed for SMOS was then used to retrieve soil moisture, vegetation water content, and effective temperature for each set of synthetic observations. For the case of a bare soil with a uniform profile, the simpler Fresnel model proposed for use with SMOS gave identical estimates of brightness temperatures to the coherent model. However, in order to retrieve accurate geophysical parameters in the presence of vegetation, the opacity coefficient (one of two parameters used to describe the effect of vegetation on emission from the soil surface) used within the SMOS retrieval algorithm needed to be a function of look-angle, soil-moisture status, and vegetation cover. The effect of errors in the specification of the vegetation parameters within the extended Wilheit (1978) model was explored by imposing random errors in the values of these parameters before generating the synthetic data and evaluating the errors in the retrieved geophysical parameters. Random errors of 10% result in systematic errors (up to 0.5°K, 3%, and ~0.2 kg m^{-2} for temperature, soil moisture, and vegetation content, respectively) and random errors (up to ~2°K, ~8%, and ~2 kg m^{-2} for temperature, soil moisture, and vegetation content, respectively) that depend on vegetation cover and soil-moisture status. The primary conclusions of this study are as follows:

- When describing the microwave emission of bare soil, the simple two-source (Fresnel) model of microwave emission used in the proposed SMOS retrieval and the extended Wilheit (1978) model are consistent.
- When describing the microwave emission of vegetation-covered soil, the simple two-source model of microwave emission is not consistent in detail with the extended Wilheit (1978) model and cannot therefore be used to retrieve accurate values of near-surface soil moisture, vegetation water content, and effective temperature unless effective values of the opacity coefficient, *b*, that vary with look-angle, soil moisture status, and vegetation cover, are used.
- If effective values of the opacity coefficient are used, the proposed SMOS retrieval algorithm returns very good retrievals, with errors in soil moisture typically of the order 1%; in vegetation water content less than 0.5%; and with very small errors in effective temperature.
- With multi-angle microwave radiometers and a retrieval algorithm based on the simple two-source (Fresnel) model, heterogeneity within the vegetation cover (as represented by introducing 10% random error in vegetation parameters) can result in both systematic and random errors in retrieved values which are vegetation cover and soil-moisture status dependent.

]

- Systematic errors in retrieved variables induced by 10% random errors in vegetation parameters are up to 0.5°K for temperature (worst for grass cover and moist soil), up to 3% in soil moisture (worst for forest cover and moist soil), and up to ~0.2 kg m^{-2} for vegetation content (worst for shrub cover). Random errors so induced are up to ~2°K for temperature (worst for grass-cover and moist soil), up to ~8% in soil moisture (worst for forest
- cover and moist soil), and up to ~2 kg m^{-2} for vegetation content (worst for forest cover).
- The size of both systematic and random errors increases with the heterogeneity in vegetation cover (as represented by random error in vegetation parameters) for all cover types, the systematic error in the retrieved soil moisture increasing more significantly than in vegetation water content for forest cover, and vice-versa for the crop cover.

2.2.4 Summary of Paper#3: USING AREA-AVERAGE REMOTELY SENSED SURFACE SOIL MOISTURE IN MULTI-PATCH LAND DATA ASSIMILATION SYSTEMS, by Eleanor J. Burke, W. James Shuttleworth, Khil-ha Lee, and Luis A. Bastidas, in *IEEE Transactions on Geoscience and Remote Sensing,* 39(10): 2091-2100, 2001.

There is now ample evidence that, over continental areas, weather and climate are significantly influenced by the local and regional availability of soil

moisture that can reach the atmosphere by evapotransration from soil and plants status in large-scale forecast models. Currently, no reliable measurements of soil moisture are available to specify soil moisture in meteorological models and, as an interim measure pending the availability of remotely sensed estimates, modeling centers have begun to implement so-called Land Data Assimilation Systems (LDAS). LDAS are two-dimensional (2-D) arrays of the relevant land-surface model used in the forecast model that are forced with available observations of weather variables (especially precipitation and radiation), to estimate the current status of soil moisture.

In coming years, Land Data Assimilation Systems are likely to become the routine mechanism by which many predictive weather and climate models will be initiated. If this is so, it will be via assimilation into the LDAS that other data relevant to the land surface, such as remotely sensed estimates of soil moisture, will find value. This paper explores the potential for using low-resolution, remotely sensed observations of microwave brightness temperature to infer soil moisture in an LDAS with a "mosaic patch" representation of land-surface heterogeneity, by coupling the land-surface model in the LDAS to a physically realistic microwave emission model. The past description of soil water movement by the LDAS is proposed as the most appropriate, LDAS consistent basis for using remotely sensed estimates of surface soil moisture to infer soil moisture at depth, and the plausibility of this proposal is investigated. Three alternative methods are

explored for partitioning soil moisture between modeled patches while altering the area-average soil moisture to correspond to the observed, pixel-average microwave brightness temperature, namely, 1) altering the soil moisture by a factor, which is the same for all the patches in the pixel, 2) altering the soil moisture by adding an amount that is the same for all the patches in the pixel, and 3) altering the change in soil moisture since the last assimilation cycle by a factor which is the same for all the patches in the pixel. In each case, an iterative procedure is required to make the adjustment. Comparison is made between these alternative procedures for a hypothetical pixel that contains eight individual patches (three different vegetation types growing both in clay and sand, plus one patch of bare soil and one of open water) using a mosaic-patch version of the MICRO-SWEAT model. When the applied forcing variables are artificially degraded, all three methods provide similar, improved descriptions of the time-evolution of soil moisture in the pixel as a whole and of the deep soil moisture for each patch. However, in each case, the ability of the LDAS to correctly describe the separate evolution of surface soil moisture in each patch is imperfect. The primary findings of this study are as follows.

- The recent and/or time average history of the LDAS description of soil water movement represents a plausible, LDAS-consistent way to use remotely sensed estimates of surface soil moisture to infer soil moisture at depth

- If such a relationship is defined, it is possible to use the LDAS description of soil and vegetation processes and microwave emission to allow approximate allocation of area-average soil moisture between the modeled patches using iterative techniques, which results in good area-average correction to soil moisture (and evaporation); good patch-specific deep soil moisture; but the patch-specific corrections to surface soil moisture are not as good
- The three iterative methods for allocating single area-average microwave brightness temperature between patches tested in the present study gave similar results, but Method 2 was arguably preferable, primarily because it was best in estimating deep soil moisture.

Notwithstanding the significant and general improvement in the area-average simulations when area-average microwave brightness temperature is assimilated for a multipatch LDAS grid square described in this paper, the fact remains that the patch specificity of the soil moisture, especially that of the surface soil moisture, is less than perfectly captured. Presumably, this is because there is not enough remotely sensed information to accurately assign the microwave brightness temperature between patches, and the mosaic-patch representation of individual patches is not sufficiently powerful to fully compensate for this. It is possible that, given measurements of area-average microwave brightness temperatures at a range of look angles and with vertical

and horizontal polarizations, it may be possible to disaggregate the area-average signal more effectively. The upcoming soil moisture ocean salinity (SMOS) L-band mission will, for example, provide this type of additional information, and detailed investigation of the potential value of SMOS observations for LDAS is the subject of our ongoing research.

2.2.5 Summary of Paper #4: ESTIMATION OF AREA-AVERAGE SENSIBLE HEAT FLUX USING A LARGE APERTURE SCINTILLOMETER DURING THE SEMI-ARID LAND-SURFACE-ATMOSPHERE (SALSA) EXPERIMENT, by A. Chehbouni, Y.H. Kerr, C. Watts, O. Hartogensis, D. Goodrich, R. Scott, J. Schieldge, K. Lee, W.J. Shuttleworth, G. Dedieu, and H.A.R. De Bruin, in *Water Resources Research,* 35(8): 2505-2511, 1999.

This paper reports the feasibility of using a large-aperture scintillometer to measure the area-average sensible heat flux from heterogeneous land surfaces. During the 1997 Semi-Arid Land-Surface-Atmosphere (Salsa) field campaign, the area-average measurements provided by a scintillometer over two adjacent and contrasting vegetation patches were compared with independent measurements for the two patches using the eddy correlation technique. There was good agreement between the two and this suggests that use of the scintillometer approach may be a simple way to make adequately reliable measurements of

area-average sensible heat flux at spatial scales compatible with meteorological models and remote sensing estimates. The primary findings of this study are as follows:

- There was good agreement between the area-average measurements made with the scintillometer and the average measurements made using eddy correlation techniques weighted by the area of the two patches. The correlation coefficient between these two estimates of area-average sensible heat flux was around 0.95.
- This result suggests that the scintillometer, which is a reliable instrument that is easy to operate and maintain, can be used to measure area-average sensible heat flux over heterogeneous (multi-patch) land surface to validate model-calculated or remotely sensed estimates of surface fluxes at corresponding spatial scale.

2.2.6 Primary Results and Conclusions of this Doctoral Research Program

This thesis describes the candidate's contribution in several related areas of research. In parallel with the main research activity, the candidate participated in two research studies which were somewhat independent from the main theme of the research and whose conclusions have already been given in Sections 3.4 and 3.5. The most important, general conclusions that can be drawn from the main research activity undertaken during the graduate study program, that are described in Appendices A and B and summarized in Sections 3.4 and 3.5, are as follows.

- Multi-layer model of vegetation canopies of intermediate complexity developed as an extension of the Wilheit (1978) model, such as that developed and applied in this research, successfully represent the most important influences of vegetation on the L-band microwave emission from the soil-vegetation-atmosphere interface.
- To achieve realistic simulation using a coherent multi-layer emission model to represent vegetation it is necessary to assume, and to introduce into the model, a gradual change in the canopy dielectric at the top and bottom of the canopy similar to that which would, in practice, occur in nature due to the natural variability between plants.

- Those vegetation parameters required by the new multi-layer microwave emission model that are difficult to measure can be estimated from field observations of microwave emission using automatic calibration procedures providing some other important, measurable parameters (notably the vegetation water content of the canopy) are independently determined.
- The microwave emission from the soil-vegetation-atmosphere interface calculated by the new multi-layer microwave emission model is sensitive to the amount of free water in the vegetation and the extent of dielectric mixing in the canopy, but it is comparatively insensitive to the detailed structure of the canopy.
- By using the new multi-layer microwave emission model to evaluate the accuracy of the simpler model to be used in SMOS retrievals, it was shown that, in order to make accurate retrievals, the opacity coefficient, b, used in the SMOS retrieval algorithm must be specified as a function of the look-angle, vegetation cover, soil moisture status. Fortunately, the form of these required functions can be estimated using the new multi-layer microwave emission model.
- When the required variation in opacity coefficient is accurately specified (see above), using the simpler model adopted in the retrieval algorithm proposed for SMOS (with advanced parameter estimation techniques and simulated

SMOS data) results in very good retrieval of surface soil moisture, vegetation water content, and surface temperature.

- However, imprecision in the (area-average) vegetation-related parameter parameters that influence microwave emission results in errors in retrieved values for SMOS, especially in the retrieved values of vegetation water content, that will need to be recognized in any data-assimilation process that uses these data. Fortunately, the size of these errors can be estimated using the new multi-layer model given estimates of the variability in vegetation-related parameters across the footprint of the sensor.

REFERENCES

Belward, A. S. and T. Loveland, 1995, The IGBP-DIS 1-km land cover project: remote sensing in action, *Proceedings of the 21st Annual Conference of the Remote Sensing Society*, Southampton, UK, pp1099-1106.

Birchak, J.R., C.G.Gardner, J.E.Hipp, and J.M. Victor, 1974, High dielectric constant microwave probes for sensing soil moisture, *Proceedings of the IEEE*, 62:93-98.

Bonan, G.B., 1996, A land surface model (LSM version 1.0) for ecological, hydrological, and atmospheric studies: technical description and user's guide, NCAR Technical Note, NCAR/TN-417+STR, Boulder, CO.

Burke E. J., R. J. Gurney, L. P. Simmonds, and T. J. Jackson, 1997, Calibrating a soil water and energy budget model with remotely sensed data to obtain quantitative information about the soil, *Water Resources Research*, 33:1689-1697.

Burke E. J., R. J. Gurney, L. P. Simmonds, and P. E. O'Neill, 1998, Using a modeling approach to predict soil hydraulic properties from passive microwave measurements, *IEEE Transactions on Geoscience and Remote Sensing*, 36: 454-462.

Burke, E.J., W.J. Shuttleworth, K. Lee, and L.A. Bastidas, 2001, Using area average remotely sensed surface soil moisture in multi-patch Land Data Assimilation Systems, *IEEE Transactions on Geoscience and Remote Sensing*, 39(18):2091-2100.

Burke, W. J., T. J. Schmugge, J. F. Paris, 1979, Comparison of 2.8 and 21 cm microwave radiometer observations over soils with emission model calculations, *Journal of Geophysical Research, 84*:287-294.

Calvet, J.C., J.P. Wigneron, A. Chanzy, and D. Haboudane, 1995, "Retrieval of surface parameters from microwave radiometry over open canopies at high frequencies", *Remote Sensing of the Environment*, 53:46-60.

Chanzy, A., T.J. Schmugge, J.C. Calvet, Y. Kerr, P. van Oevelen, O. Grosjean, and J.R. Wang, 1997, "Airborn microwave radiometry on a semi-arid area during Hapex-Sahel", *Journal of Hydrology,* 188/189:285-309.

Choudhury, B. J., T. J. Schmugge, A. Chang, and R. W. Newton, 1979, Effect of surface roughness on the microwave emissivity from soils, *Journal of eophysical Research*, 84:5699-5706.

Costes, F., S. Raju, A. Chanzy, I. Chenerie, and J. Lemorton, 1994, Microwave radiometry on bare soils:comparison of various emission models of layered media with measurements, *Proceeding of Geosciences and Remote Sensing Symposium (IGARSS 94),* Vol.3, IEEE, Seabrooke, TX, pp.1579-1581.

Crow WT, Drusch M, Wood EF, 2001, An observation system simulation experiment for the impact of land surface heterogeneity on AMSR-E soil moisture retrieval, *IEEE Transaction on Geoscience and Remote Sensing*, 39 (8): 1622-1631.

Dai, Y.J. and Q.C. Zeng, 1997, A land surface model (IAP94) for climate studies, I: formulation and validation in off-line experiments, *Advances in Atmospheric Science*, 14:433-460.

Dickinson, R.E., A. Henderson-Sellers, P.J. Kennedy, and M.F. Wilson, 1986, Biosphere-Atmosphere Transfer Scheme (BATS) for the NCAR Community Climate Model, Technical Note, NCAR/TN-275+STR, National Center for Atmospheric Research, Boulder, CO.

Dobson, M.C., F.T. Ulaby, M.T. Hallikainen, and M.A. El-Rays, 1985, Microwave dielectric behavior of wet soil-part2: Dielectric mixing models, *IEEE Transaction on Geoscience and Remote Sensing*, 23(1):35-46.

Galantowicz, J.F., D. Entekhabi, and E.G. Njoku, 1999, Tests of sequential data assimilation for retrieving profile soil moisture and temperature from observed L-band radiobrightness, *IEEE Transaction on Geoscience and Remote Sensing*, 37:1860-1870.

Galantowicz, J.F., D. Entekhabi, E.G. Njoku, 2000, Estimation of soil-type heterogeneity effects in the retrieval of soil moisture from radiobrightness, *IEEE Transaction on Geoscience and Remote Sensing,* 38 (1):312-316.

Houser, P.J., W.J. Shuttleworth, J.S. Famiglietti, H.V. Gupta, K.H. Syed, and D.C. Coodrich, 1998, Integration of soil moisture remote sensing and hydrological modeling using data assimilation, *Water Resources Research*, 34:3405-3420.

Jackson, T.J. and P.E. O'Neill, 1990, Attenuation of soil microwave emissivity by corn and soybeans at 1.4 and 5 GHz,, *IEEE Transactions on Geoscience and Remote Sensing,* 28:978-980.

Jackson, T.J., and T.J. Schmugge, 1991, Vegetation effects on the microwave emission of soils. *Remote Sensing of the Environment*, 36:203-212.

Jackson, T.J., T.J. Schmugge, and R.J. Wang, 1982, Passive microwave sensing of soil-moisture under vegetation canopies, *Water Resources Research*, 18(4):1137-1142.

Jackson, T.J., D.M. Le vine, C.T. Swift, T.J. Schmugge, and F.R. Schiebe, 1995, "Large area mapping of soil moisture using the ESTAR passive microwave radiometer in Washita '92", *Remote Sensing of the Environment*, 53:27-37.

Jackson, T.J., D.M. Le Vine, A.Y. Hsu, A. Oldak, P.J. Starks, C.T. Swift, J.D. Isham, and M. Kaken, 1999, Soil Moisture Mapping at Regional Scales using Microwave Radiometry: The Southern Great Plains Hydrology Experiment, *IEEE Transaction on Geoscience and Remote Sensing*, 37(5):2136-2151.

Jarvis, P. G., 1976,The interpretation of the variations in leaf water potential and stomatal conductance found in canopies in the field, *Philosophical Transactions of the Royal Society of London*, 273B:593-610.

Judge J, A.W. England, W.L. Crosson et al., 1999, A growing season Land Surface Process/Radiobrightness model for wheat-stubble in the Southern Great Plains, *IEEE Transaction on Geoscience and Remote Sensing*, 37(5): 2152-2158.

Kerr, Y.H., P. Waldteufel , J.P. Wigneron, J.M. Martinuzzi, J. Font, and M. Berger, 2001, Soil moisture Retrieval from Space: the soil Moisture and Ocean Salinity (SMOS) Mission, *IEEE Transaction on Geoscience and Remote Sensing*, 39(8):1729-1735.

Kidayashev, K.P.,A.A.Chukhlantsev, and A.M. Shutko, 1979, Microwave Radiation of the earth's surface in the presence of a vegetation cover, *Radio Engineering and Electronic Physics*, 24:256-264 (English Translation).

Kramer, P.J., 1983, Water relations of plants, Academic Press, Inc., Orlando, Florida, pp352.

Laguerre, L.,S. Raju, A. Chanzy, Y.H. Kerr, J.C. Calvet, and J.P. Wigneron, 1994, Physical modeling of microwave emission from bare soils. Inter comparison of models and ground data", *Proceedings of the 6th International Symposium on Physical Measurements, Signatures, and Remote Sensing*, CNES, Paris, pp527-534.

Le vine, D.M., and M.A. Karam, 1996, Dependence of attenuation in a vegetation canopy on frequency and plant water content, *IEEE Transaction on Geoscience and Remote Sensing*, 34:1090-1096.

Lee K, R.C. Chawn, E.J. Burke, and W.J. Shuttleworth, 2002, Application of a plane-stratified emission model to predict the effects of vegetation in passive microwave radiometry, *Hydrology and Earth System Sciences, 6(2):139-151*

Liou YA, A.W. England, 1996, Annual Temperature and Radiobrightness Signature for Bare soils, *IEEE Transaction on Geoscience and Remote Sensing*, 34(4):981-990.

Liou YA, A.W. England, 1998, A land surface process radiobrightness model with coupled heat and moisture transport in soil, *IEEE Transaction on Geoscience and Remote Sensing*, 36(1):273-286.

Liou Y.A., J.F. Galantowicz, A.W. England, 1999, A land surface process radiobrightness model with coupled heat and moisture transport for prairie grassland, *IEEE Transaction on Geoscience and Remote Sensing,* 37(4):1848-1859.

Liou Y.A., K.S. Chen, T.D. Wu, 2001, Reanalysis of L-band brightness predicted by the LSP/R model for prairie grassland: Incorporation of rough surface scattering, *IEEE Transaction on Geoscience and Remote Sensing,* 39(1):129-135.

Matzler, C., 1994, Microwave(1-100 GHz) Dielectric Model of leaves, *IEEE Transaction on Geoscience and Remote Sensing*, 32(5):947-949.

Njoku, E.G. and J.A. Kong, 1977, Theory for passive microwave sensing of near surface soil moisture, Journal of Geophysical Research, 82:3108-3118.

Nojku, E.G., and L. Li, 1999, Retrieval of land surface parameters using passive microwave measurements at 6-18 GHz, *IEEE Transaction on Geoscience and Remote Sensing,* 37(1):79-93.

Owe, M., A.A. Van De Griend, and A.T.C. Chang, 1992, Surface Moisture and satellite microwave observations in semiarid southern Africa, *Water Resources Research*, 28(3):829-839.

Raju S, A. Chanzy, J.P. Wigneron, Calvet, Y. Kerr and L. Laguerre, 1995, Soil moisture and temperature profile effects on microwave emission at low frequencies, *Remote Sensing of the Environment,* 54(2):85-97.

Reichle R.H., D.B. Mclaughlin, and D. Entekhabi, 2001, Variational data assimilation of microwave radiobrightness observations for land surface hydrology application, *IEEE Transaction on Geoscience and Remote Sensing, 39(8):1708-1718*

Schmugge, T.J., 1998, Application of passive microwave observations of surface soil moisture, *Journal of Hydrology*, 212/213:188-197.

Schmugge, T.J., and B.J. Choudhury, 1981, A comparison of radiative transfer models for predicting the microwave emission from soils, *Radio Science*, 16(5):927-938.

Schmugge, T. J. and T. J. Jackson, 1992, A dielectric model of the vegetation effects on the microwave emission from soils, *IEEE Transaction on Geoscience and Remote Sensing*, 30:757-760.

Sellers, P.J., S.O. Los, C.J. Tucker, C.O. Justice, D.A. Dazlich, G.J. Collatz, and D.A. Randall, 1996, A revised land surface parameterization (SiB2) for atmospheric GCMs. Part2: The generation of global fields of terrestrial biophysical parameters from satellite data, *Journal of Climate*, 9:706-737.

Shutko, A.M., 1986, Microwave Radiometry of Water surface and Grounds, Nauka, Moscow, pp192 (English Translation).

Teng, W.L., J.R. Wang, and Doraiswamy, P.C., 1993, "Relationship between satellite microwave radiometric data, antecedent precipitation index, and regional soil moisture. *IEEE Transaction on Geoscience and Remote Sensing*, 14:2483-2500.

Ulaby, F.T., R. K. Moore, and A. K. Fung, 1986, Microwave Remote Sensing: Active and Passive Volume 3, Artech House, Inc., 610 Washington St., Dedham, MA.

Ulaby, F. T. and M. A. El Rayes, 1987, Microwave dielectric spectrum of vegetation, 2, Dual dispersion model, *IEEE Transaction on Geoscience and Remote Sensing*, 25:550-557.

Van de Griend, A.A.and M. Owe, 1993, Determination of microwave vegetation optical depth and signal scattering albedo from large scale soil moisture and Nimbus/SMMR satellite observations, *International Journal of Remote Sensing*, 14(10):1875-1886.

Van de Griend, A.A.and M. Owe, 1994, The influence of polarization on canopy transmission properties at 6.6 GHz and implications for large scale soil

moisture monitoring in semi-arid environments, *IEEE Transactions on Geoscience and Remote Sensing,* 32(2):409-415.

Van de Griend, A.A.and M. Owe, 1996, Measurement and behavior of dual-polarization vegetation optical depth and single scattering albedo at 1.4 and 5 GHz microwave frequencies, *IEEE Transactions on Geoscience and Remote Sensing,* 34(4):957-965.

Wang, J.R., 1987, Microwave emission from smooth bare fields and soil moisture sampling depth, *IEEE Transactions on Geoscience and Electronics,* 25:616-622.

Wang, J.R. and T.J. Schmugge, 1980, An Empirical model for the complex dielectric permittivity of soils as a function of water content, *IEEE Transaction on Geoscience and Remote Sensing*, 18(4):288-294.

Wang, J.R., B.J. Choudhury, 1981, Remote sensing of soil moisture content over bare field at 1.4 GHz frequency, *Journal of Geophysical Research*, 86(c6):5277-5282.

Wang, J.R., J.C., Shiue, T.J., Schmugge, and E.T., Engman, 1990, The L-band PBMR measurements of surface soil moisture in FIFE, *IEEE Transaction on Geoscience and Remote Sensing, 28:906-913*

Wigneron, J.P., J.C. Calvet, and Y. Kerr, 1996a, Monitoring water interception by crop fields from passive microwave observations, *Agricultural and Forest Meteorology*, 80:177-194.

Wigneron, J. -P., J. -C. Calvet, Y. H. Kerr, A. C. Chanzy, and A. Lopes, 1993, Microwave emission of vegetation, sensitivity to leaf characteristics, *IEEE Transactions on Geoscience and Remote Sensing, 31*:716-726

Wigneron, J-P, T.J. Schmugge, A. Chanzy, J.C. Calvet, and Y. Kerr, 1998, Use of Passive Microwave Remote Sensing to Monitor Soil Moisture, *Agronomy*, 18(1):27-43.

Wigneron, J-P, P. Waldteufel, A. Chanzy, J.C. Calvet, and Y. Kerr, 2000, "Two-Dimensional Microwave Interferometer Retrieval Capabilities over Land Surfaces (SMOS) Mission", *Remote Sensing of the Environment*, 73:270-282.

Wilheit T. T., 1978, Radiative transfer in a plane-stratified dielectric, *IEEE Transactions on Geoscience and Electronics*, 16:138-143.

APPENDIX A: APPLICATION OF A PLANE-STRATIFIED EMISSION MODEL TO PREDICT THE EFFECTS OF VEGETATION IN PASSIVE MICROWAVE RADIOMETRY, by Khil-ha Lee, R. Chawn Harlow, Eleanor J. Burke, and W. James Shuttleworth, ***Hydrology and Earth System Science, 6(2): 149-151, 2002***

Hydrology and Earth System Sciences, 6(2), *139–151* (2002) © EGS

Hydrology & Earth System Sciences

Application of a plane-stratified emission model to predict the effects of vegetation in passive microwave radiometry

Khil-ha Lee, R. Chawn Harlow, Eleanor J. Burke and W. James Shuttleworth

Department of Hydrology and Water Resources, University of Arizona, Tucson, AZ, USA

E-mail of corresponding author: eleanor@hwr.arizona.edu

Abstract

This paper reports the application to vegetation canopies of a coherent model for the propagation of electromagnetic radiation through a stratified medium. The resulting multi-layer vegetation model is plausibly realistic in that it recognises the dielectric permittivity of the vegetation matter, the mixing of the dielectric permittivities for vegetation and air within the canopy and, in simplified terms, the overall vertical distribution of dielectric permittivity and temperature through the canopy. Any sharp changes in the dielectric profile of the canopy resulted in interference effects manifested as oscillations in the microwave brightness temperature as a function of canopy height or look angle. However, when Gaussian broadening of the top and bottom of the canopy (reflecting the natural variability between plants) was included within the model, these oscillations were eliminated. The model parameters required to specify the dielectric profile within the canopy, particularly the parameters that quantify the dielectric mixing between vegetation and air in the canopy, are not usually available in typical field experiments. Thus, the feasibility of specifying these parameters using an advanced single-criterion, multiple-parameter optimisation technique was investigated by automatically minimizing the difference between the modelled and measured brightness temperatures. The results imply that the mixing parameters can be so determined but only if other parameters that specify vegetation dry matter and water content are measured independently. The new model was then applied to investigate the sensitivity of microwave emission to specific vegetation parameters.

Keywords: passive microwave, soil moisture, vegetation, SMOS, retrieval.

Introduction

Passive microwave radiometers operating at L-band (21 cm, 1.4 GHz) frequencies have promise as tools to measure the moisture of the surface layer of the soil over large areas (Jackson *et al.*, 1999). It is well recognised that the relationship between microwave brightness temperature and soil moisture can be influenced significantly by several factors, including soil properties and - especially significant in the context of the present paper - the nature and form of any overlying vegetation (Wigneron *et al.*, 1998).

A vegetative canopy will scatter and absorb the emission from the soil. It will also contribute its own emission that will be scattered and absorbed by the canopy it passes through. Any downward emission will be reflected by the soil surface and again scattered and absorbed by the canopy. The water held within the canopy is mainly responsible for this scattering, absorption and emission. The two main approaches to account for the effect of vegetation on the microwave emission from the soil are based on solutions of the radiative transfer equation (Kerr and Wigneron, 1994). The simpler, more common approach is valid only at the lower frequencies, where any scattering effects can be assumed to be small. The vegetation is treated as a homogeneous uniform layer and uses two semi-empirical parameters: the optical depth and the single scattering albedo (Ulaby *et al.*, 1986). At L-band, the single-scattering albedo is assumed to be zero (Jackson and Schmugge, 1991) and the optical depth is proportional to the vegetation water content, where the value of the constant of proportionality, the opacity coefficient, is an uncertain function of the canopy type and structure, wavelength, polarisation and, possibly, also vegetation water content (Jackson and Schmugge, 1991; Wigneron *et al.*, 1996, 2000; Le Vine and Karam, 1996). An alternative approach is to create a complex model that

includes a detailed description of all of the components of the canopy (Wigneron *et al.*, 1993; Burke *et al.*, 1999), where all the required input parameters are measured properties of the canopy. However, this model requires a very detailed description of the vegetative canopy. This paper discusses an alternative approach — the development of a realistic model of intermediate complexity that captures the more important features of a vegetative canopy, but requires fewer input parameters. This type of model might prove to be highly appropriate for in-field validation studies and for evaluating the reliability of satellite retrieval algorithms that necessarily make simplifying assumptions concerning the vegetation, e.g., ESA's Soil Moisture and Ocean Salinity (SMOS) upcoming L-band mission (Wigneron *et al.*, 2000).

The model evaluated in this paper is an extension of the Wilheit (1978) model for the coherent propagation of electromagnetic radiation through a stratified medium; it is applied frequently to model microwave emission from soils (Burke *et al.*, 1997, 1998). However, in this paper, it is used to describe the combined emission from both the soil and vegetation. This application is highly suitable for use in coupled land surface and microwave emission models such as that used by Burke *et al.* (1997, 1998). In fact, in this example, the Common Land Model (CLM, 2000) land surface scheme is used to provide soil profile information required by the Wilheit (1978) model.

Unfortunately, in no field experiments to date have all the vegetation parameters required as input by the extended Wilheit (1978) model been measured. However, multi-parameter optimisation techniques have been shown (Bastidas *et al.*, 1999; Burke *et al.*, 2002; Sen *et al.*, 2001) to be very powerful tools in the estimation of model parameters. This paper discusses the potential of using multi-parameter, single-criterion techniques to evaluate the values of the parameters required by the extended Wilheit (1978) model. A companion paper (Lee *et al.*, 2002) uses this extended Wilheit (1978) model to provide a realistic description of the vegetation canopy when creating synthetic microwave brightness temperatures for the SMOS mission. It then examines the ability of the proposed SMOS retrieval to obtain the soil water content, vegetation water content and effective temperature from these data.

Modelling approach

Two types of models are used to predict microwave emission from soils: coherent (Wilheit, 1978; Njoku and Kong, 1977; England, 1976) and non-coherent (Burke *et al.*, 1979; England, 1975). Both Schmugge and Choudhury (1981) and Ulaby *et al.* (1986) compared coherent and non-coherent emission models and their results are summarised below. Non-coherent models estimate emissivity using the dielectric contrast at the air/soil interface and are accurate only when the (variable) sampling depth within the soil is well known. In coherent models, the value of the emissivity at the surface is coupled to the dielectric properties below the surface; hence, they provide better estimates of the emissivity when the soil water content profile is non-uniform. One disadvantage of coherent models is that interference effects can occur. However, these have been witnessed only rarely in nature (Schmugge *et al.*, 1998). The Wilheit (1978) model was selected for this study because of its accuracy in non-uniform conditions and it was configured to minimise the impact of interference. Because it does not include scattering effects, it can be used only in conditions where scattering is negligible, i.e. at L-band.

The Wilheit (1978) model assumes that the medium under consideration consists of a layered dielectric of semi-infinite extent, that the boundaries between the layers are planar and parallel and that each layer is homogenous. To calculate the instantaneous microwave emission, it is also assumed that each layer is in thermal equilibrium, so that each layer of dielectric emits the same amount of energy as it absorbs. The microwave brightness temperature, T_B, can then be expressed as:

$$T_B = \sum_{i=1}^{N} f_i T_i \qquad (1)$$

where T_i is the temperature of the i^{th} layer, f_i is the fraction of energy absorbed from an incident microwave by the i^{th} layer (a function of the dielectric constant of the soil), and N is the number of layers in the semi-infinite medium.

The dielectric and temperature profiles of the soil, required as input by the Wilheit (1978) model, were predicted using results from the Common Land Model (CLM, 2000) land surface scheme. The CLM includes the best elements of some well-tested physical parameterisations and numerical schemes (e.g., LSM, Bonan, 1996; BATS, Dickinson *et al.*, 1986, and IAP, Dai and Zeng, 1997). It requires a set of parameters that specify physical constants and aspects of the soil and vegetation and, given meteorological forcing variables, it then provides prognostic and diagnostic land-surface state variables and surface energy and water fluxes as output. CLM describes the diffusion of soil heat and liquid water through several (typically ten) layers of soil using the finite difference form of the thermal diffusion equation and Richard's equation, respectively. CLM uses the fraction of sand and clay to specify the properties of the soil. If vegetation is present, it is represented as though it is at a single level, at the height ($d + z0$), where d is the zero plane displacement and $z0$ is the aerodynamic roughness of the

canopy. Turbulent transport between this level and a specified reference height above the canopy is described using the Monin-Obukhov similarity theory, with allowance made for the effect of atmospheric stability. The whole canopy surface resistance is parameterized following the model introduced by Jarvis (1976).

Following Burke *et al.* (1997) and Camillo *et al.* (1986), the soil component of the microwave emission model was run with 200 layers at the depths indicated: 0–1 cm, 10 layers at 1 mm; 1–3 cm, 10 layers at 2 mm; 3–6 cm, 10 layers at 3 mm; 6–10 cm, 10 layers at 4 mm; 1–20 cm, 20 layers at 5 mm; and 20–160 cm, 140 layers at 10 mm. The soil temperature and soil water content output by the CLM for the ten layers simulated in this study were linearly interpolated to the 200 soil layers required by the microwave emission model.

The Wilheit (1978) model calculates the depth below which the emission is negligible and neglects all layers below this depth. Because this depth is a function of soil type and soil water content profile, it may well change every time step. The Dobson *et al.* (1985) model is used to predict the profile of soil dielectric from knowledge of the profile of soil water content and soil particle size distribution. This is a simple non-linear dielectric-mixing model that takes into account the proportions of free water (dielectric ~ 80), bound water (dielectric ~4), soil solids (dielectric ~ 4) and air (dielectric ~1) within the soil medium. The soil particle size distribution determines the relative proportions of free and bound water.

The extended Wilheit (1978) model also requires the dielectric and temperature profile within the vegetation. Limited information is available in the literature about the dielectric permittivity of either the vegetative matter (El-Rayes and Ulaby, 1987; Ulaby and Jedlicka, 1984; Chuah *et al.*, 1997, Colpitts and Coleman, 1997; Franchois *et al.*, 1998; Ulaby *et al.*, 1986) or the canopy itself (Ulaby *et al.*, 1986; Ulaby and Jedlicka, 1984; Brunfeldt and Ulaby, 1984; Schmugge and Jackson, 1992). To model the dielectric properties of a vegetative canopy, two separate mixing effects must be taken into account. The first mixing is that between the constituents of the vegetation to get the dielectric of the vegetative matter itself. The approach to modelling the dielectric of the vegetative matter taken in this paper is analogous to a linear version of the Dobson *et al.* (1985) mixing model for soils:

$$\varepsilon_v = \varepsilon_{dry} V_{dry} + \varepsilon_{fw} V_{fw} + \varepsilon_{bw} V_{bw} \tag{2}$$

where ε_v is the dielectric permittivity for leaf material as a whole, ε_{dry}, ε_{fw}, and ε_{bw} are the dielectric permittivities, and V_{dry}, V_{fw}, and V_{bw} are the volume fractions of dry matter, free water and bounded water, respectively. It is assumed that ε_{dry}, ε_{fw}, and ε_{bw} are independent of the vegetation water content. The dielectric permittivity of the mixed vegetation matter and air making up a vegetation canopy (ε_{can}) is given by:

$$\varepsilon_{can}^{\alpha} = \varepsilon_v^{\alpha} V_V + \varepsilon_{air}^{\alpha} (1 - V_V) \tag{3}$$

where ε_{air} is the dielectric permittivity of air; V_v is the fractional volume of vegetation elements per unit volume canopy; and α is a so-called "shape factor". (In the case of the Dobson *et al.*, 1985 mixing model for soils, $\alpha = 0.65$.) Schmugge and Jackson (1992) suggested that the refractive model ($\alpha = 0.5$) provides a better representation of the dielectric properties of the canopy than a linear model ($\alpha = 1$). However, the dielectric permittivity of a canopy is very similar to air and very much lower than that of soil, and there is little additional evidence to indicate the value of α for such a sparse medium. One of the purposes of this present study was to investigate the feasibility of deriving values of this parameter from field data.

In initial studies, the profile of dielectric within the canopy was assumed to be uniform. However, despite the dielectric of the canopy being close to air, this resulted in interference effects. Interference occurs when discrete changes in dielectric permittivity are assumed at two or more surfaces, e.g. at the top or bottom of the canopy as well as at the soil surface. In this case, a portion of the microwaves incident on each surface will be reflected and add constructively or destructively. Consequently, the modelled radiometric temperature changes greatly, depending on the thickness of the canopy, the wavelength of the radiation and the angle of emission. This phenomenon has been observed only as a wetting front descends within the soil (Schmugge *et al.*, 1998) and is unlikely to be observed in vegetation because there is never a discrete and uniform change at the top or bottom of the vegetative canopy. The natural variability between the individual plants that make up the canopy results in a more gradual change. The effect of this natural variability was modelled using Gaussian broadening at the top and bottom of the canopy. The Gaussian broadening was introduced so that the total amount of dielectric within the canopy remained constant but it was redistributed over a slightly greater height. The Appendix describes in more detail how the vertical profiles of canopy dielectric permittivity are specified in the model. Figure 1 shows an example of the interference effects which occur in the modelled microwave brightness temperature as a function of look angle when assuming a discrete change at the canopy top (0.9 m) and bottom (0.09 m) rather than a more realistic canopy with Gaussian broadening of both the top and bottom

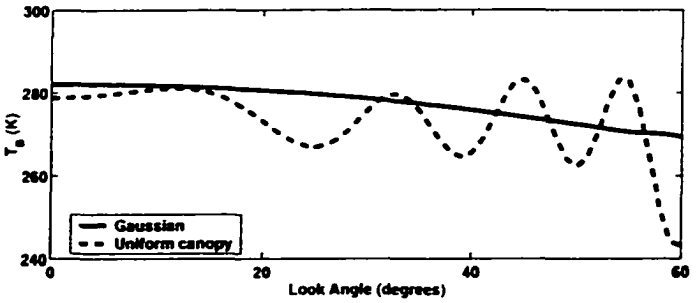

Fig. 1 *The modelled brightness temperature as a function of observation angle calculated at 11:30 a.m. on DOY 208 using the DRYDOWN2 data set with and without Gaussian smoothing of the top and bottom of the canopy.*

(with a standard deviation of 0.09 m in each case). In this example, the canopy was assumed to consist of 100 layers, each 1 cm thick. This amount of detail is required to smooth the interfaces at the top and bottom of the canopy sufficiently. For the range of look angles shown, it is evident that Gaussian broadening eliminates the effect of within-canopy internal reflections and interference. It should be noted that, even with gradual changes in dielectric permittivity, significant reflections may still occur at very shallow angles. However, for the observation angles normally used by field and satellite systems, this reflection phenomenon and its associated interference are effectively suppressed.

The temperature of the canopy is a prognostic variable in CLM. In the present study, the temperature profile of the canopy used within the microwave emission model is estimated very simply. For canopy above $(d + z_o)$ — where d is the zero plane displacement and z_o is the aerodynamic roughness of the canopy — it is estimated by linear interpolation between the air temperature at the reference height and the simulated canopy temperature. For canopy below $(d + z_o)$, it is estimated by linear interpolation between the simulated canopy temperature and the simulated soil-surface temperature below. It is also assumed that the description of aerodynamic transfer assumed in CLM is insensitive to the detailed shape of the canopy dielectric profile specified in the microwave emission model.

Optimisation for evaluating model parameters

Bastidas *et al.* (1999) and Sen *et al.* (2001) provided a detailed discussion of the usefulness of multi-criteria optimisation methods for the evaluation and improvement of land-surface schemes. For example, they showed that the use of calibration procedures may lead to reductions of 20 to 30% in the root mean square error (RMSE) between model and measurements when compared to the traditional method of using lookup tables for model parameter estimation. In addition, they gained valuable insight into acceptable ranges of model parameters, the quality of the model physics and the complexity of the model required to describe a particular scenario. The present study uses a single-criterion optimisation technique to minimize the difference between time series of measured and modelled microwave brightness temperatures and explores the feasibility of estimating the values of the vegetation parameters in the extended Wilheit (1978) microwave emission model.

In general, a numerical model might have n parameters (in this case, the parameters describing the dielectric profile of the vegetation) to be calibrated using m observations (in this case, the time series of microwave brightness temperatures). The distance between the m model-simulated responses and the m observations is defined by an objective function (O) such as the root mean square error between the modelled responses and observations (RMSE). The goal of a model calibration is then to find the preferred value for the n parameters within the feasible set of parameters that minimise O. The Shuffled Complex Evolution algorithm (SCE-UA, Duan *et al.*, 1993, 1994) is a single-criterion, multi-parameter optimisation technique developed at the University of Arizona. It is a general-purpose global optimisation method designed to handle many of the response surface problems encountered in the calibration of nonlinear simulation models. It randomly samples the feasible parameter space to select a population of points. The population is then partitioned into several "complexes", each of which evolves independently in a manner based on the downhill simplex algorithm (Nelder and Mead, 1965).

The population is periodically "shuffled" and new complexes formed so that the information gained by previous complexes is shared. As the search progresses, the entire population tends to converge towards the neighbourhood of the global optimum value for the objective function. These steps are repeated until prescribed termination rules are satisfied (Duan *et al.*, 1993, 1994).

The SCE-UA has been used successfully to calibrate, against field observations, the values of the parameters in a hydrological model (Duan *et al.*, 1993, 1994). In addition, Burke *et al.* (2002) used it to retrieve near surface soil moisture and vegetation water content for several patches of different land-cover types within one pixel using a set of brightness temperatures measured simultaneously at a wide range of look angles. The new application discussed here explores the feasibility of estimating parameters within a microwave emission model.

Field data

The experimental data used in this paper were collected over a soybean canopy monitored during a field experiment carried out in 1985 at the USDA, ARS Beltsville Agricultural Research Center, Maryland, USA. (Burke *et al.*, 1998).

The site consisted of a 10 × 10 m controlled plot containing loamy sand soil. Half of the plot was left bare and half was covered with soybeans. Different periods of drying were monitored during the soybean growth, with the bare soil monitored at the same time. A dual-polarised L-band (21-

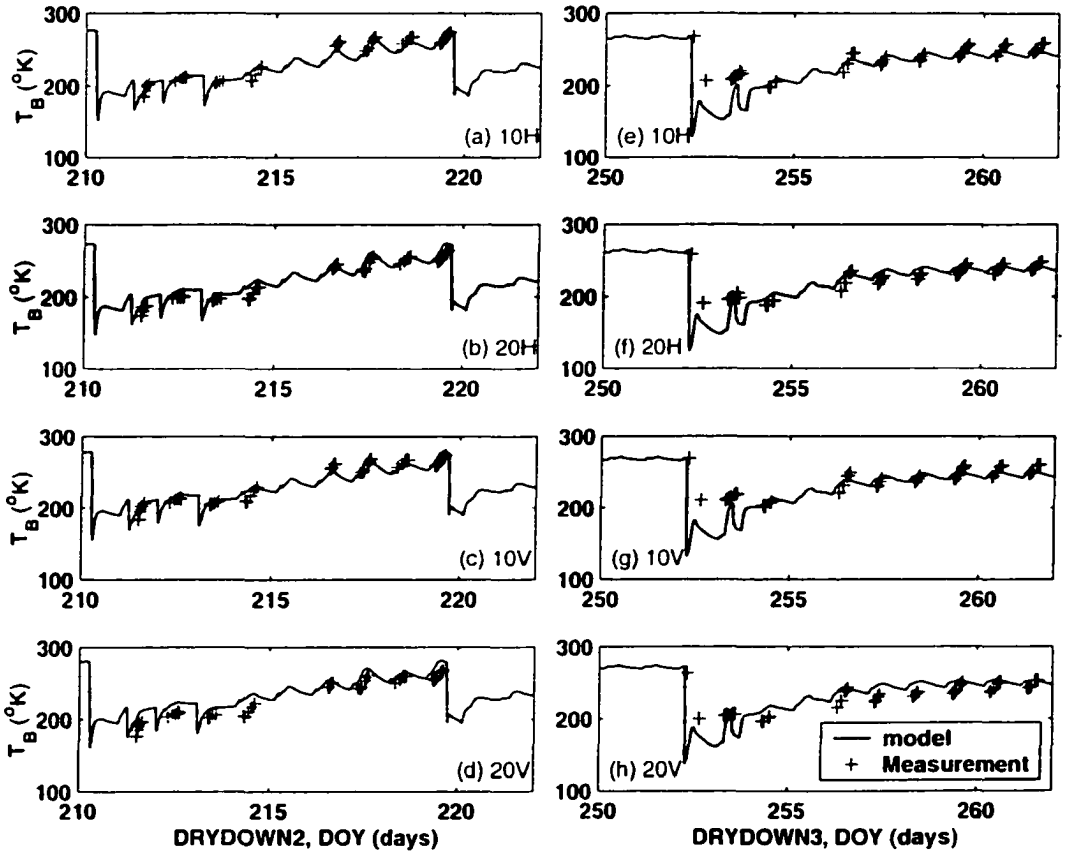

Fig. 2 *Time series of measured and modelled microwave brightness temperatures for a bare soil surface during DRYDOWN2 and DRYDOWN3. 10 and 20 denote 10° and 20° look angles, and H and V denote horizontal and vertical polarisation, respectively*

cm wavelength, 1.4 GHZ frequency) passive microwave radiometer measured the horizontally and vertically polarised microwave brightness temperatures at view angles of 10° and 20°. In addition to the radiometric measurement, soil and limited vegetation characteristics (including single-point volumetric soil-water content, soil temperature, the hydraulic properties of the soil, plant height, and the wet and dry matter weight of the vegetation) were measured. The data from the Beltsville site used in this study fall into two distinct periods that are hereafter referred to as DRYDOWN2, between Day of Year (DOY) 210 and 222, and DRYDOWN3, between DOY 252 and 262.

Model results

SOIL MICROWAVE EMISSION

One of the assumptions in using SCE-UA to optimise the vegetation parameters in the extended Wilheit (1978) model for soil and vegetation, is that there is a high level of agreement between the modelled and measured microwave brightness temperatures at the soil surface. CLM was used to simulate surface energy and water fluxes and the related changes in soil temperature and soil moisture for a bare soil and, hence, calculate the dielectric permittivity profile of the soil for input into the bare soil Wilheit (1978) model. Figure 2 shows the microwave brightness temperature predicted using the time series of profile soil water content and soil temperature predicted by CLM for DRYDOWN2 and DRYDOWN3 for a bare soil. There are some discrepancies on the days immediately after irrigation; however, as the soil dries out further, there is excellent agreement between the modelled and measured brightness temperatures.

The ability of CLM to describe relevant changes in near-surface soil temperature and soil moisture under a vegetation canopy was also evaluated. Figure 3 shows the soil temperature at 1-cm depth and the average soil moisture over the depth ranges 0-2 cm and 0-5 cm as modelled by CLM during DRYDOWN2 and DRYDOWN3 using the soil parameters measured at the site and vegetation parameters for IGBP vegetation cover class 12 ["cropland"]. The equivalent measured values are also shown in this figure when available. The RMSE for DRYDOWN2 is 2.1°C for temperature at 1 cm depth, 3.1% for 0–2 cm average soil

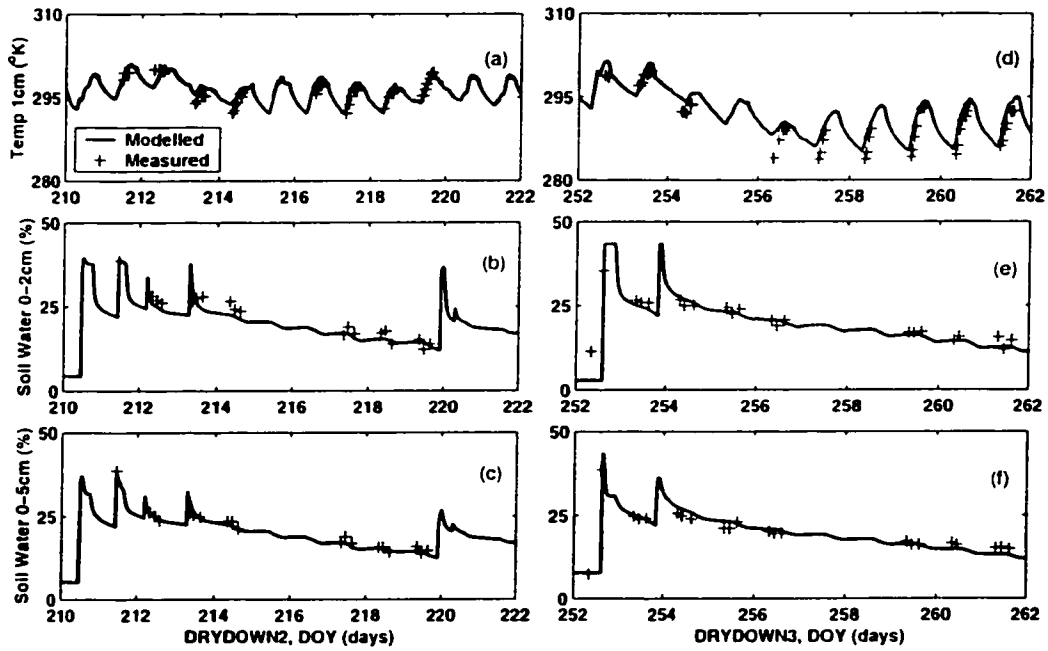

Fig 3. *CLM-calculated and observed values of soil temperature at 1 cm depth (a and d), average soil moisture over 0-2 cm depth (b and e), and 0-5 cm depth (c and f) for DRYDOWN2 (a, b, and c) and DRYDOWN3 (d, e, and f)*

moisture, and 2.1% for 0–5 cm average soil moisture. The RMSE for DRYDOWN3 is 2.6°C for temperature at 1 cm depth, 2% for 0-2 cm average soil moisture, and 1.9% for 0–5 cm average soil moisture. The time series of both the modelled temperature and soil moisture show good agreement with the measurements.

Given that CLM can model, accurately, the near surface soil water content and the near surface temperature under a vegetation canopy, and that the Wilheit (1978) model for bare soil predicts, accurately, the microwave brightness temperature for a bare soil, it can be assumed that the extended Wilheit (1978) model for soil and vegetation will predict, accurately, the microwave emission at the soil surface.

EXTENDED WILHEIT (1978) MODEL FOR SOIL AND VEGETATION

The extended Wilheit (1978) model for soil and vegetation was run within the SCE algorithm and the RMSE between the modelled and measured microwave brightness temperature minimised by optimising the parameters that describe the dielectric profile of the canopy. These parameters are salinity (S in ppt); canopy height (t in m); height of bottom of canopy (b in m); standard deviation of top height (σ_t in m); standard deviation of bottom height (σ_b in m); fresh weight of the canopy (V_w in kg m^{-2}); volume fraction of free water (V_{fw} in m^{3}m^{-3}); volume fraction of dry matter (V_{dry} in m^{3}m^{-3}) and dielectric mixing coefficients for vertical and horizontal polarisation (α_v and α_H). Optimum values were found for the DRYDOWN2 and DRYDOWN3 periods separately by minimising the RMSE between the observed and modelled microwave brightness temperature at L-band and both (10° and 20°) observation angles. It should be noted that, when operating in a complex parameter space, multi-parameter optimisation algorithms (including SCE) discover "local" minima of the objective function as well as the required "global" minimum. Therefore, the SCE-UA algorithm was randomly initiated and run 20 times for each example creating 20 different parameter sets. The parameter set that provides the minimum RMSE was then selected to be the "preferred parameter set". Figure 4 shows

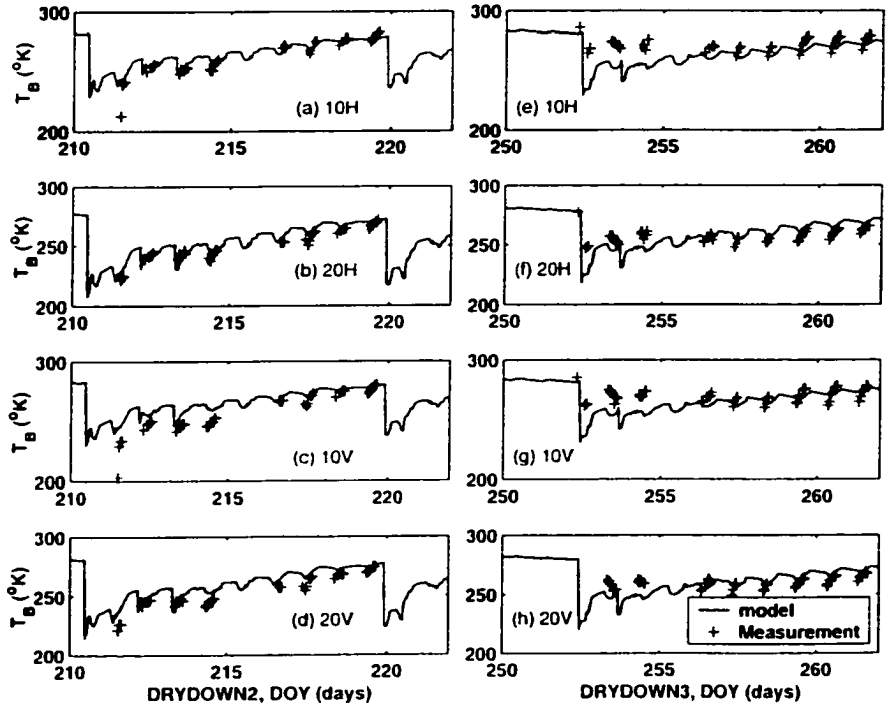

Fig 4 *Time series of measured and modelld microwave brightness temperatures in the presence of vegetation during DRYDOWN2 and DRYDOWN3. 10 and 20 denote 10° and 20° look angles, and H and V denote horizontal and vertical polarization, respectively*

an example of the excellent agreement between model and measured time series of microwave brightness temperatures.

Unfortunately, for this example, there is insufficient information in the available measured microwave brightness temperatures to use single-criterion multi-parameter optimisation techniques to determine the parameters that control the shape of the canopy (height of bottom (b) and the standard deviation of the Gaussian broadening of top (σ_t) and bottom (σ_b)). This may be partly because the observations were made at two angles fairly close to the zenith. However, it also implies that, at least for look angles near the nadir, the microwave brightness temperature predicted by this model is insensitive to canopy structure. (Note: from the standpoint of retrieving estimates of soil moisture and vegetation optical depth from remotely sensed observations, it is helpful that the canopy structure is modelled to have only a limited influence on microwave surface brightness temperature because precise knowledge of canopy structure will usually not be available for use in the retrieval process.)

In the next example, the values of these three parameters, b, σ_t and σ_b were arbitrarily set to be 15% of the height of the canopy, this being a plausible value that avoids the model-generated interference effects at observation angles of 10° and 20°, and the simulations repeated. Despite the lack of sensitivity of the model to these canopy shape parameters (and hence the high likelihood of SCE-UA generating any value of these parameters within the allowed range), it was reassuring to see that the optimised values of the other parameters in this new simulation were very similar to those found previously. However, there was also interaction between some pairs of vegetation-related parameters that have opposing influence on the overall microwave emission by a vegetation canopy. This made it difficult to obtain independent estimates of these parameters merely from a time series of observations of microwave brightness temperature at just two look angles. Fortunately, some of the relevant parameters were measured during the field experiment, specifically: the fresh weight of the vegetation (3.42 and 4.41 kg m^{-2} during DRYDOWN2 and DRYDOWN3, respectively) and the crop height (0.89 and 1.15 m during DRYDOWN2 and DRYDOWN3, respectively). The volume fraction of dry matter (V_{dv}) was calculated (0.38 and 0.5 during DRYDOWN2 and DRYDOWN3 respectively) from the mass fraction of dry matter by assuming a dry matter density of 0.3 g cm^{-3} (Ulaby *et al.*, 1986). The parameters remaining to be determined by multi-parameter optimisation are the volume fraction of free water (V_{fw}), salinity of the water in the vegetation (S), and the mixing coefficient (α) defined in Eqn. (3). Since α may well be a function of polarisation, different values were assumed for the vertically and horizontally polarised brightness temperature data (α_H and α_v).

Table 1 lists the optimised values of vegetation-related parameters for the soybean canopy at the Beltsville site during DRYDOWN2 and DRYDOWN3. The values shown

Table 1. Parameters used in the coupled model and their values for the Beltsville site as given by multi-parameter optimisation (unless pre-set to fixed values prior to optimisation).

Parameter	*Symbol name*	*Range of optimisation*	*Values during DRYDOWN2*		*Values during DRYDOWN3*		*Values during DRYDOWN2*		*Values during DRYDOWN3*	
Fractional free water volume in vegetation (m^3 m^{-3})	V_{fw}	0 – 1 accurately optimised)	0 041	0 040	0 048	0 047	0 5 (fixed)	0 5 (fixed)	0 5 (fixed)	0 5 (fixed)
Salinity of water in vegetation (ppt)	S	0 – 15 (when optimised)	0 (fixed)	0 00	0 (fixed)	0 00	0 (fixed)	0 94	0 (fixed)	0 73
Mixing parameter for L-band with horizontal polarisation (dimensionless)	α_L	0 – 3	1 98	1.98	1.94	1 93	1 24	1 12	1.17	1.09
Mixing parameter for L-band with vertical polarisation dimensionless	α_H	0 – 3	2 07	2.07	2.19	2.18	1 29	1 16	1 31	1.22

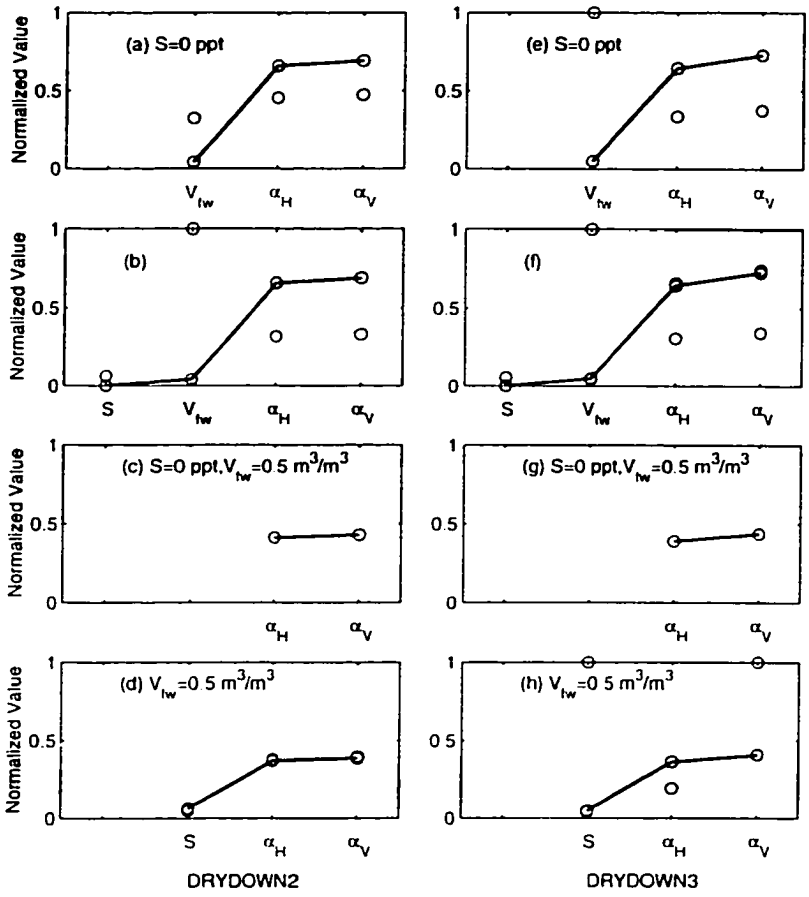

Fig 5 *Estimated parameter values for the 20 replicate optimisations. In each case, parameter values are normalised by the predefined range of each parameter over which optimisation was made, and the set of parameters corresponding to the lowest error in modelled microwave brightness temperature are linked by a line. Results are shown for S set to 0 ppt (a and e), all parameters optimised (b and f), S set to 0 ppt and V_{fw} set 0.5 m³m⁻³ (c and g), and V_{fw} set 0.5 m³m⁻³ (d and h), for DRYDOWN2 (a-d) and DRYDOWN3 (e-h)*

are the sets of parameters that produce the minimum RMSE in brightness temperatures from 20 randomly initiated replications: this is assumed to be the global minimum parameter set. Also shown is the predefined allowed range of each parameter. Eight optimisation runs were made. In the first four, the fractional free water volume, V_{fw}, was optimised along with other parameters. Because this resulted in optimised values for V_{fw} that were unexpectedly low when compared to the typically cited value, the value of V_{fw} in the second four optimisations was (arbitrarily) set to the more typical value of 0.5. In each group of four optimisation runs, two optimisations were made for DRYDOWN2 and two for DRYDOWN3, with the value of salinity optimised in one and set to 0 parts per thousant (ppt) in the other. Figure 5 demonstrates the potential range of these optimised parameters by showing the optimised parameter values normalised by the predefined allowed range of each optimised parameter for the 20-member sample of local minima identified by the SCE algorithm during the optimisation runs. In each figure, the normalised values for the parameter set with the smallest objective function (assumed to be the global minimum) are linked. In general, SCE-UA repeatedly sampled a single parameter set which corresponded to a well-defined global minimum value for

the RMSE. In all cases, the parameter set with minimum RMSE fell within the predefined range of selection. However, in a few cases (Figs. 5b, e, f, h), the multi-parameter optimisation process became trapped in subsidiary minimum and defined parameter sets with an RMSE significantly greater than that of the global minimum and with one or more parameters at the limit of the allowed range.

Some features of the optimisation results are obvious and consistent. All of the optimisation runs in which the salinity, S, of the water in the vegetation was optimised gave values for this parameter that were very close to 0 ppt. The four runs in which the fractional fresh water volume, V_{fw}, was not prescribed resulted in similar, low, optimised values (~0.04–0.05) for this parameter, and the values of α_H and α_V simultaneously estimated by multi-parameter optimisation were markedly different and larger than the corresponding values found when V_{fw} was set to (the more plausible) value of 0.5 during optimisation. It is clear that there is a strong correlation between the value of V_{fw} and the apparent strength of in-canopy dielectric mixing as expressed in the optimised values of the a parameters. This point is discussed further in the context of the single-parameter sensitivity described in the next section. Notwithstanding the interdependence of parameters just mentioned, for a given value of V_{fw}, whether optimised or prescribed, it is reassuring that the preferred values of a_H and a_V are fairly similar in DRYDOWN2 and DRYDOWN3. The values of α_H and α_V are slightly different, with the value for vertical polarisation higher in all cases, suggesting some differences between the effect of the canopy at horizontal and vertical polarisation. It should be noted that the values of α retrieved by the optimisation procedure are higher than the values found by Schmugge and Jackson (1992). However, little other information is available on the realistic range of α. One possible error in the determination of α could be that some of the other parameters were set to slightly wrong values and the optimisation procedure adjusted itself accordingly.

SENSITIVITY TO INDIVIDUAL MODEL PARAMETERS

It is of interest to investigate the sensitivity of microwave brightness temperature to the assigned values of parameters in the extended Wilheit (1978) model. To illustrate this, Fig. 6 shows how the calculated brightness temperature viewed at an angle of 20° at 11:30 p.m. on DOY 224 varies for a range of parameter values around the optimised values for

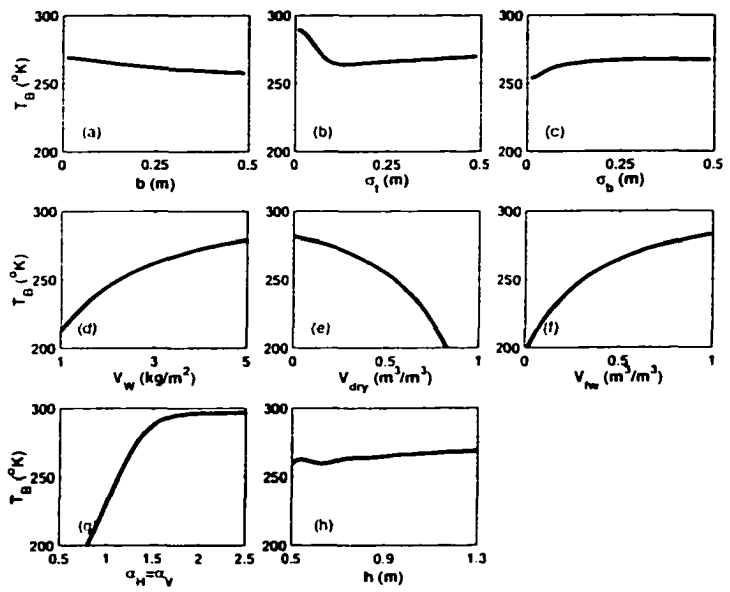

Fig 6. *Modelled microwave brightness temperature for a range of values of individual parameters around their optimised value (parameter specified in the x-axis), with the salinity of in-canopy water set to zero. The calculations are made at 11:30 p.m. on DOY 224*

L-band microwave radiation. The calculations are made using the optimised values for DRYDOWN2, with the fractional free water volume and salinity of the vegetation fixed at 0.5 and 0 ppt, respectively (Fig. 5c). The sensitivity to three groups of model parameters, those controlling the shape of the canopy, the composition of the vegetation, and the extent of in-canopy dielectric mixing, are shown in Fig. 6 for dry soil conditions.

Figures 6a–c demonstrate the expected result that calculated microwave emission is only weakly related to the value of the model parameters that control the shape of the canopy over a broad range of values. However, at very low values of σ_t and σ_b, there is evidence of higher sensitivity. This is because, when the transition in dielectric permittivity at the top/bottom of the canopy becomes very sharp, some modelled within-canopy internal reflection (and constructive/destructive interference) occurs even for a view angle of 20°. Figures 6d–f show, as expected, that the fresh weight of the canopy (V_w) can have a significant impact on modelled microwave brightness temperatures. The extent of in-canopy dielectric mixing, as represented by the value of a, directly influences the overall value of the canopy dielectric permittivity. Consequently, the sensitivity to the value of a shown in Fig. 5g is to be anticipated.

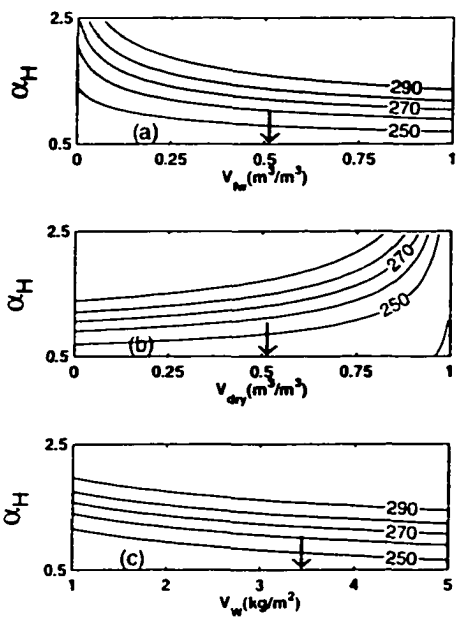

Fig 7. *Contours of the horizontally polarised modelled microwave brightness temperature at nadir at 11:30 p.m. on DOY 224 using the optimised parameter given in column 8 of Table 1. Calculations are made for combinations of α_H and V_{fw} (a). α_H and V_{dry} (b), and α_H and V_w (c)*

Because non-linear dielectric mixing (i.e., the values of α) and vegetation composition parameters (especially V_w and V_{fw}) together determine the overall canopy dielectric permittivity, it will always be difficult and perhaps impossible to determine their values in the model by multi-parameter optimisation methods from a time series of the observed microwave brightness temperature. Figure 7 illustrates this point by showing contours of the modelled microwave brightness temperature, T_B, at a look angle of 20° at the Beltsville site calculated at 11:30 p.m. on DOY 224 using the optimised parameter given in column 8 of Table 1, but for a range of values of a and a range of values of V_{fw}, V_{dry}, or V_w.

In the context of field studies of the microwave emission of vegetation in general and in future field validation studies associated with the SMOS and Advanced Microwave Scaning Radiometer (AMSR) missions in particular, it is strongly recommended that these key vegetation composition parameters be measured directly. Doing so will allow an opportunity to investigate the significance of in-canopy dielectric mixing for the vegetation under study. This, in turn, will allow more detailed investigation of the relationship between the optical depth at microwave frequencies of sampled canopies and their vegetation water content, the latter being a potentially more valuable geophysical variable.

Discussion and conclusions

This paper describes the application of the Wilheit (1978) model for the coherent propagation of electromagnetic radiation through a stratified medium to predict the effect of a vegetation canopy on the microwave emission from the soil surface. The model produced a realistic simulation of the microwave emission, provided there was a gradual change in the dielectric at the top and bottom of the canopy as would be associated with the natural variability between plants.

The Common Land Model was used to predict the profiles of soil temperature and water content and vegetation temperature for use within the extended Wilheit (1978) model. These predictions compared favourably with available measurements. However, not all of the relevant vegetation parameters required by the extended Wilheit (1978) model were measured. Therefore, an evaluation of the ability of automatic calibration procedures to predict the required vegetation parameters was performed. Unfortunately, there was not sufficient information in the available range of microwave brightness temperatures to predict all of the required vegetation parameters using multi-parameter optimisation methods; this was either because the

brightness temperature was insensitive to a particular parameter or because there were interactions between parameters such that a high value of one combined with a low value of another produced the same answer as a low value of the former combined with a high value of the latter. However, when any available measurements were included to limit the number of parameters to be determined, and the canopy shape parameters (parameters to which the modelled microwave brightness temperatures are insensitive) set to plausible values, multi-parameter optimisation techniques provided estimates of the remaining parameters–those which would be difficult to measure in any future field experiment. This is particularly relevant for the mixing coefficient (α) between vegetation matter and air used to calculate the dielectric of the vegetation canopy.

Sensitivity studies with the extended Wilheit (1978) model showed that the calculated microwave emission is insensitive to the values of parameters that specify the shape of the canopy, unless these imply a canopy with very rapid changes of dielectric permittivity at the canopy boundaries. Microwave emission is sensitive to parameters that specify the amount of free water in the vegetation and the extent of dielectric mixing in the canopy, which act together to change the whole-canopy dielectric permittivity.

On the basis of the above results, it is recommended that, future field activity for validating the SMOS mission, care be taken to make independent measurements of vegetation composition parameters in addition to measurements of microwave brightness and forcing variables. The extended Wilheit (1978) model, whose development and application is the main subject of this paper, could then be used to investigate in-canopy dielectric mixing effects within canopies and, in this way, the relationship between microwave brightness temperature and vegetation water content could be understood better.

Acknowledgements

Primary support for Khil-ha Lee and Dr. Eleanor Burke while preparing this paper was provided from NOAA project NA96GP0412. Additional support for Dr. James Shuttleworth was provided from NASA project NAG8-1531. The editorial assistance provided by Corrie Thies is appreciated.

References

Bastidas, L.A., Gupta, H.V., Sorooshian, S., Shuttleworth, W.J. and Yang, Z.L., 1999. Sensitivity analysis of a land surface scheme using multicriteria methods. *J. Geophys. Res.-Atmos.*, **104**, 19481–19490

Bonan, G.B., 1996. *A land surface model [LSM version 1.0] for ecological, hydrological, and atmospheric studies: technical description and user's guide.* NCAR Technical Note, NCAR/TN-417+STR, Boulder, CO.

Brunfeldt, D.R. and Ulaby, F.T., 1984. Measured microwave emission and scattering in vegetation canopies. *IEEE Trans. Geosci. Remote Sens.*, **22**, 520–524.

Burke, E.J., Gurney, R.J., Simmonds, L.P. and O'Neill, P.E., 1998. Using a modeling approach to predict soil hydraulic properties from passive microwave measurements. *IEEE Trans. Geosci. Remote Sens.*, **36**, 454–462.

Burke, E.J., Bastidas, L.A. and Shuttleworth, W.J., Multi-patch retrieval for the SMOS mission. *IEEE Trans Geosci. Remote Sens.* In press.

Burke, E.J., Gurney, R.J., Simmonds, L.P. and Jackson, T.J., 1997. Calibrating a soil water and energy budget model with remotely sensed data to obtain quantitative information about the soil. *Water Resour. Res.*, **33**, 1689–1697.

Burke, E.J., Wigneron, J.-P. and Gurney, R.J., 1999. The comparison of two models that determine the effects of a vegetation canopy on passive microwave emission. *Hydrol. Earth Syst. Sci.*, **3**, 439–444.

Burke, W.J., Schmugge, T.J. and Paris, J.F., 1979. Comparison of 2.8 and 21 cm microwave radiometer observations over soils with emission model calculations. *J. Geophys. Res.*, **84**, 287–294.

Camillo, P.J., O'Neill, P.E. and Gurney, R.J., 1986. Estimating soil hydraulic parameters using passive microwave data. *IEEE Trans. Geosci. Remote Sens.*, **24**, 930–936.

Chuah, H.T., Kam, S.W. and Chye, Y.H., 1997. Microwave dielectric properties of rubber and oil palm leaf samples: measurement and modelling. *Int. J. Remote Sens.*, **18**, 2623–2639.

Colpitts, B.G. and Coleman, W.K., 1997. Complex permittivity of the potato leaf during imposed drought stress. *IEEE Trans. Geosci. Remote Sens.*, **35**, 1059–1064.

Common Land Model, 2000. http://clm.gsfc.nasa.gov.

Dai, Y.J. and Zeng, Q.C., 1997. A land surface model [IAP94] for climate studies, I: formulation and validation in off-line experiments. *Adv. Atmos.Sci.*, **14**, 433–460.

Dickinson, R.E., Henderson-Sellers, A., Kennedy, P.J. and Wilson, M.F., 1986. *Biosphere-Atmosphere Transfer Scheme [BATS] for the NCAR Community Climate Model. Technical Note*, NCAR/TN-275+STR, National Center for Atmospheric Research, Boulder, CO.

Dobson, M.C., Ulaby, F.T., Hallikainen, M.T. and El-Rayes, M.A., 1985. Microwave behavior of wet soil, 2: dielectric mixing models. *IEEE Trans. Geosci. Remote Sens.*, **23**, 35–46.

Duan, Q.Y., Gupta, V.K. and Sorooshian, S., 1993. Shuffled Complex Evolution approach for effective and efficient global minimization. *J. Optimiz. Theor. Appl.*, **76**, 501–521.

Duan, Q.Y., Sorooshian, S. and Gupta, V.K., 1994. Optimal use of the SCE-UA global optimization method for calibrating watershed models. *J. Hydrol.*, **158**, 265–284.

El-Rayes, M.A. and Ulaby, F.T., 1987. Microwave dielectric spectrum of vegetation, I: experimental observations. *IEEE Trans. Geosci. Remote Sens.*, **25**, 541–549.

England, A.W., 1975. Thermal microwave emission from a scattering layer. *J.Geophys. Res.*, **32**, 4484–4496.

England, A.W., 1976. Relative influence upon microwave emissivity of fine-scale stratigraphy. *Pure Appl.Geophys.*, **114**, 287–299.

Franchois, A., Pineiro, Y. and Lang, R.H., 1998. Microwave permittivity measurements of two conifers. *IEEE Trans. Geosci..Remote Sens.*, **36**, 1384–1395.

Jackson, T.J. and Schmugge, T.J., 1991. Vegetation effects on the microwave emission of soils. *Remote Sens. Environ.*, **36**, 203–212.

Jackson, T.J., Le Vine, D.M., Hsu, A.Y., Oldak, A., Starks, P.J., Swift, C.T., Isham, J.D. and Haken, M., 1999. Soil moisture mapping at regional scales using microwave radiometry: the Southern Great Plains hydrology experiment. *IEEE Trans. Geosci. Remote Sens.*, **37**, 2136–2151.

Jarvis, P.G., 1976. Interpretation of variations in leaf water potential and stomatal conductance found in canopies in field. *Phil. Trans. Roy. Soc., London*, Series B, **273**, 593–601.

Kerr, Y.H. and Wigneron, J.P., 1994. Vegetation models and observations: a review. In: *ESA/NASA International Workshop on Passive Microwave Remote Sensing Research Related to Land-Atmosphere Interaction*, B.J. Choudhury, Y.H. Kerr, E.G. Njoku and P. Pampaloni (Eds.), 317–344.

Le Vine, D.M. and Karam, M.A., 1996. Dependence of attenuation in a vegetation canopy on frequency and plant water content. *IEEE Trans. Geosci. Remote Sens.*, **34**, 1090–1096.

Lee, K.H., Burke, E.J., Shuttleworth, W.J. and Harlow, R.C., 2002. Influence of vegetation on SMOS mission retrievals. *Hydrol. Earth System Sci.*, **6**, 15–28.

Nelder, J.A. and Mead, R.A., 1965. A simplex method for function minimization. *Comput. J.*, **7**, 308–313..

Njoku, E.G. and Kong, J.A., 1977. Theory for passive microwave sensing of near surface soil moisture. *J. Geophys. Res.*, **82**, 3108–3118.

Schmugge, T.J., and Choudhury, B.J., 1981. A comparison of radiative transfer models for predicting the microwave emission from soils. *Radio Sci.*, **16**, 927–938.

Schmugge, T.J. and Jackson, T.J., 1992. A dielectric model of the vegetation effects on the microwave emission from soils. *IEEE Trans. Geosci. Remote Sens.*, **30**, 757–760

Schmugge, T.J., Jackson, T.J., O'Neill, P.E. and Parlange, M.B., 1998. Observations of coherent emissions from soils. *Radio Sci.*, **33**, 267–272.

Sen, O.L., Bastidas, L.A., Shuttleworth, W.J., Yang, Z.L., Gupta, H.V. and Sorooshian, S., 2001. Impact of field-calibrated vegetation parameters on GCM climate simulations. *Quart. J. Roy Meteorol. Soc.*, **127**, 1199–1223.

Ulaby, F.T., and Jedlicka, R.P., 1984. Microwave dielectric-properties of plant materials. *IEEE Trans. Geosci. Remote Sens.*, **22**, 406–415.

Ulaby, F.T., Moore, R.K. and Fung, A.K., 1986. *Microwave Remote Sensing: Active and Passive, Volume 3.* Artech House, Inc., 610 Washington St., Dedham, MA.

Wigneron, J.-P., Calvet, J.-C., Kerr, Y.H., Chanzy, A.C. and Lopes, A., 1993. Microwave emission of vegetation, sensitivity to leaf characteristics. *IEEE Trans.Geosci.Remote Sens.*, **31**, 716–726.

Wigneron, J.-P., Calvet, J.-C. and Kerr, Y.H., 1996. Monitoring water interception by crop fields from passive microwave observations. *Agr. Forest Meteorol.* **80**, 177–194

Wigneron, J.-P., Schmugge, T.J., Chanzy, A.C., Calvet, J.-C. and Kerr, Y.H., 1998. Use of passive microwave remote sensing to monitor soil moisture. *Agronomy*, **18**, 27–43.

Wigneron, J.-P., Waldteufel, P., Chanzy, A.C. and Calvet, J.-C., 2000. Two-dimensional microwave interferometer retrieval capabilities over land surfaces. *Remote Sens. Environ.*, **73**, 270–282.

Wilheit, T.T., 1978. Radiative transfer in a plane stratified dielectric. *IEEE Trans.Geosci. Electron.*, **16**, 138–143

APPENDIX

SPECIFICATION OF SMOOTHED DIELECTRIC PROFILES

The better to represent natural variability in the height of the top and bottom of vegetation canopies, a smooth transition is introduced using Gaussian smoothing. If t and b are the height of top and bottom of the canopy, respectively, and the natural variability in t and b are σ_t and σ_b, respectively, then the normalised through-canopy profile of dielectric permittivity used in the microwave emission model, $\varepsilon_c(z)$, is calculated from the function:

$$\varepsilon_c(z) = \varepsilon_{canopy} \cdot \frac{W_b(z) \cdot W_t(z)}{\int_0^z [W_b(z) \cdot W_t(z)]dz} \qquad \text{(A.1)}]$$

where ε_{canopy} is the dielectric permittivity of all the leaf material present in the canopy, and the weighting functions, $W_b(z)$ and $W_t(z)$, are zero for $z < 0$ but, for values of $z \geq 0$, are given by:

$$W_b(z) = \frac{\int_0^z \exp(-(z'-b)^2 / 2\sigma_b^2)dz'}{\int_0^z \exp(-(z'-b)^2 / 2\sigma_b^2)dz'} \qquad \text{(A.2)}$$

and

$$W_t(z) = 1 - \frac{\int_0^z \exp(-(z'-t)^2 / 2\sigma_t^2)dz'}{\int_0^z \exp(-(z'-t)^2 / 2\sigma_t^2)dz'} \qquad \text{(A.3)}$$

APPENDIX B: INFLUENCE OF VEGETATION ON SMOS MISSION RETRIEVALS, by Khil-ha Lee, Eleanor J. Burke, W. James Shuttleworth, and R. Chawn Harlow, *Hydrology and Earth System Science, 6(2): 153-166, 2002*

Hydrology and Earth System Sciences, 6(2), *153–166* (2002) © EGS

Hydrology & Earth System Sciences

Influence of vegetation on SMOS mission retrievals

Khil-ha Lee, Eleanor J. Burke, W. James Shuttleworth and R. Chawn Harlow

Department of Hydrology and Water Resources University of Arizona, Tucson, AZ 85721, USA

Email for corresponding author: shuttle@hwr.arizona.edu

Abstract

Using the proposed Soil Moisture and Ocean Salinity (SMOS) mission as a case study, this paper investigates how the presence and nature of vegetation influence the values of geophysical variables retrieved from multi-angle microwave radiometer observations. Synthetic microwave brightness temperatures were generated using a model for the coherent propagation of electromagnetic radiation through a stratified medium applied to account simultaneously for the emission from both the soil and any vegetation canopy present. The synthetic data were calculated at the look-angles proposed for the SMOS mission for three different soil-moisture states (wet, medium wet and dry) and four different vegetation covers (nominally grass, crop, shrub and forest). A retrieval mimicking that proposed for SMOS was then used to retrieve soil moisture, vegetation water content and effective temperature for each set of synthetic observations. For the case of a bare soil with a uniform profile, the simpler Fresnel model proposed for use with SMOS gave identical estimates of brightness temperatures to the coherent model. However, to retrieve accurate geophysical parameters in the presence of vegetation, the opacity coefficient (one of two parameters used to describe the effect of vegetation on emission from the soil surface) used within the SMOS retrieval algorithm needed to be a function of look-angle, soil-moisture status, and vegetation cover. The effect of errors in the initial specification of the vegetation parameters within the coherent model was explored by imposing random errors in the values of these parameters before generating synthetic data and evaluating the errors in the geophysical parameters retrieved. Random errors of 10% result in systematic errors (up to 0.5°K, 3%, and ~0.2 kg m^{-2} for temperature, soil moisture, and vegetation content, respectively) and random errors (up to ~2°K, ~8%, and ~2 kg m^{-2} for temperature, soil moisture and vegetation content, respectively) that depend on vegetation cover and soil-moisture status.

Keywords: passive microwave, soil moisture, vegetation, SMOS, retrieval

Introduction

Evaporation from bare soil or from soil beneath vegetation, infiltration into the soil and, thus, surface runoff, are important aspects of the land-surface water and energy balance that are controlled by near-surface soil moisture (often defined to be that present in the uppermost 5 cm). Moreover, the uptake of soil water by vegetation for transpiration is, in part, controlled by soil moisture in the plants' rooting zone. Consequently, water and energy fluxes at the land surface/atmosphere interface depend strongly on soil-moisture status (Kerr *et al.*, 2001). Weather and climate are, in turn, influenced significantly by the local and regional availability of soil moisture *via* the evaporation and transpiration processes.

Many observational and modelling studies have shown the potential of passive microwave remote sensing, particularly L-band (1.4 GHz frequency), for estimating near-surface soil moisture (Calvet *et al.*, 1995; Chanzy *et al.*, 1997; Jackson *et al.*, 1999; Teng *et al.*, 1993; Wang *et al.*, 1990; Wigneron *et al.*, 2000). The development of robust retrieval algorithms for use with microwave brightness temperature measurements (e.g. Kerr *et al.*, 2001; Njoku and Li, 1999; Wigneron *et al.*, 2000) is essential if the retrieved soil moisture is to be used in, for example, climate analysis and prediction. Of particular uncertainty is the detailed effect of vegetation on the microwave emission from the soil surface. This is usually described by a single empirical parameter (Jackson and Schmugge, 1991), the optical depth of the vegetation (i.e. the opacity coefficient multiplied by the vegetation water content).

The European Space Agency (ESA) has selected the Soil Moisture Ocean Salinity (SMOS) mission (http://www.cesbio.upstlse.fr/indexsmos.html), with a proposed launch date in the 2003-2005 time frame. The SMOS

mission will be based on a dual polarisation, L-band radiometer with an innovative aperture synthesis concept (a two-dimensional interferometer) that can achieve an on-the-ground resolution of ~50 km near the edge of the swath, coupled with multi-angular acquisition designed to deliver several key land-surface variables, namely, near-surface soil moisture, vegetation water content and effective temperature (Kerr *et al.*, 2001; Wigneron *et al.*, 2000). Wigneron *et al.* (2000) used simulated SMOS observations created by adding random and systematic errors to the same model proposed for the SMOS retrieval algorithm to test the accuracy of that algorithm. This model assumes that the optical depth of the vegetation does not depend on either the polarisation of the radiation or the look-angle of the sensor. It also assumes that the opacity coefficient is independent of temperature and vegetation water content.

Recent work has, however, shown that the opacity coefficient depends on both the gravimetric water content of vegetation (Wigneron *et al.*, 1996, 2000; Le Vine and Karam, 1996) and the temperature (Wigneron *et al.*, 2000). In addition, the canopy type and structure (Jackson and Schmugge, 1991), the polarisation (van de Griend and Owe, 1996) and wavelength of the radiation (Jackson and Schmugge, 1991) and the look-angle of the sensor (van de Griend and Owe, 1996) may also influence the opacity coefficient. Because the influence of these factors on the accuracy of the retrieval algorithm is currently uncertain, an accurate description of the role of vegetation is a significant need if near-surface soil moisture is to be estimated reliably. Moreover, in the context of the SMOS mission, understanding the role of vegetation on overall microwave emission is particularly important because the water content of the vegetation is one of the geophysical variables to be retrieved and the large (~50 km) footprint of the sensor means that vegetation cover will rarely be homogeneous across the area sampled.

Lee *et al.* (2002) extended an existing coherent radiative transfer model (Wilheit, 1978) to create what is, in effect, a new approach to modelling the effect of vegetation on passive microwave emission and explored the ability of their model to describe field data. This approach results in a plausibly realistic model of intermediate complexity that captures, adequately, most of the important features of the microwave emission of vegetation, such as the influence of canopy type/structure, polarisation and wavelength of the radiation, look-angle of the sensor and temperature and water content of vegetation. In the present study, the modelling approach of Lee *et al.* (2002) was adopted and used to simulate synthetic, multi-angle, L-band microwave brightness temperatures of different soil-vegetation-atmosphere systems to investigate (a) the retrieval capability of the proposed SMOS retrieval algorithm; and (b) the effect of heterogeneity in vegetation parameters on retrievals made with the proposed SMOS retrieval algorithm.

Models and methods

As outlined above, the strategy adopted in this study was to use the extended Wilheit (1978) model for a linked soil and vegetation system to generate synthetic microwave observations equivalent to those that (it is proposed) the SMOS mission will make for a range of soil wetness states and vegetation covers. These synthetic data were then regarded as the "true" observations and the accuracy of retrievals made using a retrieval algorithm similar to that proposed for SMOS was assessed. This retrieval algorithm optimises a simple representation of the effect of vegetation on microwave emission against the synthetic observations of surface brightness temperatures at each position in the footprint of the sensor.

MULTI-LAYER MICROWAVE EMISSION MODEL

The Wilheit (1978) model for the coherent propagation of electromagnetic radiation through a stratified medium relates the microwave brightness temperatures transmitted through the surface-air interface of the medium to the dielectric properties and temperature of the underlying layers. Lee *et al.* (2002) extended the application of the original Wilheit (1978) microwave emission model upwards through the vegetation canopy to create a model of the microwave emission that represents both the soil and the vegetation together. Thus, in this extended Wilheit (1978) model, the vegetation canopy is assumed to be infinite in horizontal extent and to be made up of homogeneous, planar layers of dielectric medium, which lie above similar homogeneous, planar layers of dielectric medium representing the soil.

In the Lee *et al.* (2002) model, the dielectric of the vegetation matter itself (ε_v) is calculated assuming a linear version of the Dobson *et al.* (1985) mixing model (hitherto used for soils), i.e. from:

$$\varepsilon_v = \varepsilon_{dry} V_{dry} + \varepsilon_{fw} V_{fw} + \varepsilon_{bw} V_{bw} \quad (1)$$

where ε_{dry}, ε_{fw}, and ε_{bw} are the dielectric permittivities, and V_{dry}, V_{fw}, and V_{bw} are the volume fractions of dry matter, free water and bounded water, respectively. It is assumed that ε_{dry}, ε_{fw}, and ε_{bw} are independent of the vegetation water content because they are the permittivities of a pure sample of the dry matter, free water and bounded water if such an ideal, pure sample were physically available. The dielectric permittivity of the mixed vegetation matter and air that

makes up the vegetation canopy (ε_{can}) is assumed to be given by:

$$\varepsilon_{can}^{\alpha} = \varepsilon_{v}^{\alpha} V_V + \varepsilon_{air}^{\alpha} (1 - V_V) \quad (2)$$

where ε_{air} is the dielectric permittivity of air, V_v is the fractional volume of vegetation elements per unit volume canopy and α is a "shape factor" (Note: In the case of the Dobson *et al.* (1985) mixing model for soils, $\alpha = 0.65$.)

Equations (1) and (2) together calculate the dielectric constant for the canopy as a whole, and this amount of dielectric is then distributed vertically among the plane parallel layers above the soil. The heights of the top and bottom of the canopy, h_t and h_b, respectively, are specified but gradual changes in dielectric permittivity are simulated around these levels by introducing broadening that follows a Gaussian distribution with standard deviations σ_t and σ_b, respectively. This broadening reflects the natural variability between the individual plants that make up the canopy but its presence is also critical to the reliable operation of this coherent emission model. Avoiding sharp transitions in dielectric at canopy boundaries suppresses internal reflections within the canopy and the associated interference patterns in microwave emission. Lee *et al.* (2002) give a more detailed description of this phenomenon.

For the purpose of the present study and in the absence of any better information, the canopy dielectric permittivities ε_{dry}, ε_{fw} and ε_{bw} in Eqn. (1) were set arbitrarily to the plausibly realistic values of (2.0, 0.1*j*), (77.2, 4.9*j*) and (4.0, 1.0*j*), respectively, while V_{dry}, V_{fw} and V_{bw} were selected to represent a canopy which was 38% dry matter, the remainder being water assumed bound and free in equal amounts ($V_{dry} = 0.38$, $V_{fw} = V_{bw} = 0.31$). The volume fraction of vegetation in the canopy, V_v, and the shape factor, α, are required to calculate ε_{can} from Eqn. (2). In this study, the vegetation volume fraction was estimated from the fresh weight of the vegetation per unit area of canopy, W_{fresh}, and vegetation canopy structure parameters using the equation:

$$V_V = f_r \left(\frac{W_{fresh}}{(h_t - h_b)\rho_c} \right) \quad (3)$$

where ρ_c is the density of the (fresh) vegetation in the canopy, estimated as $[\rho_{dry} V_{dry} + 1000(1 - V_{dry})]$ kg m^{-3}, with ρ_{dry} = 330 kg m^{-3} (Ulaby and El-Rayes, 1987) the density of dry vegetation. (Note: in Eqn. (3), the re-normalisation factor, f_r (usually close to unity), is included as a correction to allow for the possibility that (Gaussian) smoothing of the top and/or bottom of the profile (unrealistically) distributes some of the canopy dielectric below ground level.) It is difficult to define the shape factor, α, used in Eqn. (2) on the basis of existing field data. However, using parameter optimisation techniques and the same values for ε_{dry}, ε_{fw}, and ε_{bw} as in this study, Lee *et al.* (2002) obtained values of around 1.24 for a soybean canopy and, for the purpose or this exploratory study and in the absence of better information, this value was adopted for both horizontal and vertically polarised microwave radiation.

SIMULATION OF SYNTHETIC SMOS DATA

Synthetic microwave observations that correspond to those that will be provided during the SMOS mission were calculated using the extended Wilheit (1978) model (Lee *et al.*, 2002) for a range of canopies and soil-moisture conditions. The calculations showed only limited sensitivity to the assumed nature of the soil and a soil particle size distribution of 75% sand and 5% clay was selected arbitrarily.

For the purpose of this modeling study, the temperature profiles in the soil and canopy were assumed uniform and set to 300 K, and the soil moisture profile was also assumed to be uniform, with calculations made for soil moisture contents (θ_s) of 30%, 18%, and 8%, these being respectively referred to as "wet", "medium wet" and "dry". Calculations were made for four different types of vegetation broadly corresponding to "grass", "crop", "shrub" and "tree": the values of h_t and the vegetation water content, W_{vc}, for these crops are given in Table 1. A simple canopy structure was assumed with, in each case, σ_t set to 35% of h_t and σ_b and h_b set to zero. The brightness temperature of the complete soil-vegetation profile for both horizontal and vertical polarised L-band microwave radiation was then calculated using the extended Wilheit (1978) model (Lee *et al.*, 2002) for swath angle dependent ranges of look-angles (Table 2) corresponding to those proposed for the SMOS mission.

PROPOSED SMOS RETRIEVAL ALGORITHM

The retrieval algorithm used in this study mimics that proposed for the SMOS mission and delivers three variables over land surfaces, namely, near-surface soil moisture, the optical depth of the vegetation cover (or, by implication, vegetation water content) and the effective temperature of the land surface (assumed to be the same for the vegetation and the soil surface). The retrieval is based on the Fresnel model for microwave emission and assumes two distinct sources, a single, thin layer of vegetation and the surface of the soil beneath.

Thus, in the retrieval algorithm, the microwave emissivity of the soil surface, e_s (which is equal to $(1 - r_s)$, where r_s is the reflectivity of the soil surface) relates the microwave

Table 1. **Surface conditions used when calculating the synthetic SMOS data. The soil effective temperature and the vegetation temperature were set to 300 deg K.**

	Soil Wetness	θ_s *(% vol.)*	*Temp. (deg K)*	*Height (m)*	W_c *(kg/m²)*	*Optical Depth at Nadir (τ)*
Grass	Wet	30	300	0.3	1.25	0.228
	Mid	18				0.251
	Dry	8				0.303
Crop	Wet	30	300	1.0	2.68	0.414
	Mid	18				0.431
	Dry	8				0.463
Shrub	Wet	30	300	3.0	4.17	0.627
	Mid	18				0.636
	Dry	8				0.652
Tree	Wet	30	300	5.0	7.50	1.121
	Mid	18				1.127
	Dry	8				1.138

Table 2. The available look-angles as a function of the half-swath angle proposed for the SMOS mission. The synthetic observations were simulated using these look-angles at each half-swath angle (Wigneron *et al.*, 1999)

Swath angle (degrees)	*Look-angle (degrees)*
0.0	51.7 49.1 46.4 44.3 41.2 38.7 37.0 34.2 31.4 29.4 27.3 24.1 21.9 19.6 17.3 14 9 12.5 5 1 2.5 0.0
3.4	51.7 49.2 46.5 44.3 41.3 38.8 37.1 34.4 31.5 29.6 27.5 24.4 22.2 20.0 17.7 15.4 13.1 6.3 4.6 3.8
9.0	51.4 48.9 46.2 43.4 41.0 38.6 36.1 34.3 31.6 29.7 26.8 24.8 22.8 20.8 17.8 15.9 14.1 10.4 10.1
11.2	49.8 47.2 44.4 42.2 39.9 37.4 34.9 33.1 30.4 28.5 25.7 23.8 22.0 20.1 17.5 15.9 14.5 12.5
12.3	48.7 46.7 43.9 41.6 39.3 36.9 34.3 31.7 29.9 28.1 25.3 23.5 21.7 20.0 17.6 16.2 15.0 14.0
14.4	47.7 45.7 42.9 40.6 38.3 35.9 33.4 31.7 29.1 27.4 24.8 23.1 21.6 20.1 18.2 17.2 16.5
15.5	47.3 45.2 42.4 40.2 37.8 35.4 33.8 31.3 28.8 27,1 25.5 23.1 21.7 20.4 19.2 18.0 17.5
16.6	47.5 44.8 42.0 39.7 37.4 35.9 33.5 31.0 29.4 27.0 25.4 24.0 22.0 20.8 19.8 18.8 18.5
18.6	46.7 44.0 41.9 39.7 37.5 35.2 32.9 31.4 29.1 27.0 25.6 24.4 22.8 21.9 21.1 20.8
19.6	46.3 43.6 41.6 39.4 37.2 35.0 32.8 31.3 29.1 27.8 25.9 24.8 23.4 22.7 22.0 21.9
20.6	45.9 44.0 41.2 39.1 37.0 34.8 32.7 31.3 29.2 28.0 26.2 25.2 24.0 23.5 23.1
22.6	46.0 43.4 41.4 39.4 37.3 35.3 33.3 31.4 30.2 28.6 27.6 26.4 25.6 25.3 25.2
23.6	5.7 43.8 41.2 39.2 37.2 35.3 33.4 31.6 30.5 29.0 27.8 27.1 26.5 26.3
25.4	45.8 43.4 41.5 39.6 37.8 36.0 34.2 32.6 31.2 30.0 29.1 28.7 28.4
26.4	45.6 43.2 41.4 39.6 37.8 36.1 34.5 33.0 31.7 30.6 29.9 29.5 29.4
28.1	46.5 44.2 41.9 40.2 38.6 37.0 35.1 33.8 32.8 32.0 31.5 31.4
29.9	46.2 44.,6 42.5 40.4 38.9 37.5 36.3 34.9 34.1 33.6 33.3
31.6	46.7 44.6 43.1 41.2 39.4 38.2 37.2 36.1 35.5 35.2
33.2	47.6 45.7 43.8 42.1 40.5 37.0

brightness temperature of the soil, $T_B(\varphi p)$ (in deg K), to the effective physical temperature of the soil, T_s (in deg K) thus:

$$T_B(\varphi,p) = e_s(\varphi,p)T_s \tag{4}$$

where $e_s(\varphi,p)$ ($1 \geq e_s \geq 0$) is the polarised specular emissivity of the soil medium at angle φ for polarisation state p and is related to the soil dielectric constant via the Fresnel equations. The soil dielectric constant is calculated from the soil-moisture content and soil particle size distribution using Dobson's (1985) model. The simple model of Jackson and Schmugge (1991) is used to describe the effect of vegetation overlying the soil surface in terms of an equivalent optical depth, τ, with:

$$\tau = bW_{vc} \tag{5}$$

where b is the opacity coefficient, and W_{vc} is the vegetation water content in kg m^{-2}.

By combining these simple concepts, Basharinov and Shutko (1975) presented a model for the microwave brightness temperature of an interface comprising a semi-infinite soil layer with physical temperature, T_s (in °K) and air-soil reflectivity $r_s(\varphi,p)$ with overlying vegetation with a physical temperature T_v (in °K),. This model is the basis for the algorithm, and the microwave brightness temperature is estimated as:

$$T_B(\varphi,p) = [1+r_s(\varphi,p)\Gamma(\varphi)][1-\Gamma(\varphi)](1-\alpha)T_v + [1-r_s(\varphi,p)]\Gamma(\varphi)T_s \tag{6}$$

where α is the single-scattering albedo of the soil surface, and $\Gamma(\varphi)$ is the transmissivity of the vegetation layer. This simple model is based on the following assumptions (Ulaby *et al.*, 1986):

(a) the single-scattering albedo is assumed to be independent of φ and p and small ($0.04 \leq \alpha \leq 0.12$);
(b) the air-vegetation reflectivity is assumed to be zero; and
(c) r_s is set to the air-soil reflectivity rather than the vegetation-soil reflectivity because the average index of refraction of the vegetation layer is only slightly larger than that of air.

For simplicity, in the proposed SMOS retrieval algorithm, the soil temperature and vegetation temperature are assumed to be identical. Typically, the vegetation temperature drops below the soil temperature at night but, soon after sunrise, these temperatures are more similar: this assumption will influence the proposed timing of SMOS mission observations.

The SMOS mission will provide observations of surface brightness temperatures at several angles for each point on the ground, the number and selection of angles depending on the location of the point within the sensor footprint (Table 2). Over land surfaces, the mission will provide three geophysical variables, near-surface soil moisture, vegetation optical depth (assumed related to vegetation water content via Eqn. (5)) and an effective land-surface temperature (assumed equal for soil and vegetation). An optimisation technique will be used to deliver these geophysical variables from the multi-angle measurements of microwave brightness temperatures. The present paper seeks insight on the capability to retrieve these variables and the dependence of this on the nature of the vegetation overlying the soil independent of any possible shortcoming in the particular optimization technique that is ultimately adopted for the SMOS retrieval. For this reason, the best multi-parameter optimisation algorithm available, the Shuffled Complex Evolution algorithm (SCE-UA; Duan *et al.*, 1993) has been used in this study.

The SCE-UA is a global optimisation strategy designed to be effective and efficient for a broad class of complex global optimisation problems. It combines the strengths of the simplex procedure of Nelder and Mead (1965) with the concepts of controlled random search (Price, 1987), competitive evolution (Holland, 1975) and complex shuffling (Duan *et al.*, 1993). All of these help to ensure that the information contained in a data sample is efficiently and thoroughly exploited in the attempt to find a global optimum. Hence, the SCE-UA algorithm has good convergence properties over a broad range of problems and a high probability of succeeding in its objective of finding the global optimum (Duan *et al.*, 1993). The algorithm requires specification of a range of allowed values for each optimised variable. In this study, the range of values used in SCE-UA was 0–50% for soil moisture content (implicitly assumed constant with depth in the retrieval algorithm), 273–320 K for effective temperature (assumed equal for vegetation and soil in the retrieval algorithm) and 0–10 kg m^{-2} for vegetation water content.

It is possible to match the estimates of microwave emission given by the simple two-source model used in the SMOS retrieval algorithm and estimates given by the (assumed to be more realistic) extended Wilheit (1978) model (Lee *et al.*, 2002) by selecting an appropriate value of the optical depth, τ, or (for a specified value of vegetation water content) the opacity coefficient, b. Details of the derivation of the equivalent value of τ or b are given in the Appendix. In practice, it proved necessary to derive and use look-angle dependent effective values of b to achieve accurate retrieval of the geophysical variables when using the simple two-source model.

Results

MODEL EQUIVALENCE

The central goal of the present study is to use the presumably better representation of the effect of vegetation on microwave emission in the extended Wilheit (1978) model to evaluate the simpler representation of vegetation in the two-source model that is the basis of the proposed SMOS retrieval algorithm. It is first necessary to ensure that these two models give equivalent representation of the microwave emission from bare soil when no vegetation is present. Figure 1 shows a comparison of the microwave brightness temperature for bare soil and the soil reflectivity calculated by the two models for three different conditions of soil moisture (i.e. 30%, 18% and 8%). The agreement is excellent: the calculated values given by the two models are indistinguishable.

Figure 2 shows a comparison between the microwave brightness temperature for the combined soil-vegetation system calculated by the extended Wilheit (1978) model and the two-source model used in the SMOS retrieval for the three different soil moisture levels and for four different vegetation covers representing grass, crops, shrub and forest, with the vegetation parameters given in Table 1. In this comparison, the value of the opacity coefficient, b, was determined using the approach given in the Appendix to ensure equivalence at the nadir. In general, using this value at greater look-angles in the Fresnel model results in increased estimates of microwave brightness temperatures for all of the simulated canopies and for both polarisation states. These differences are larger at greater look-angles for canopies with lower vegetation water content (the difference is greatest for grass and least for forest) and for vertically polarised radiation.

Clearly, it is possible to use the approach described in the Appendix to ensure equivalence between the two different models by modifying the value of b at angles other than the nadir. In this way, it is possible to derive look-angle

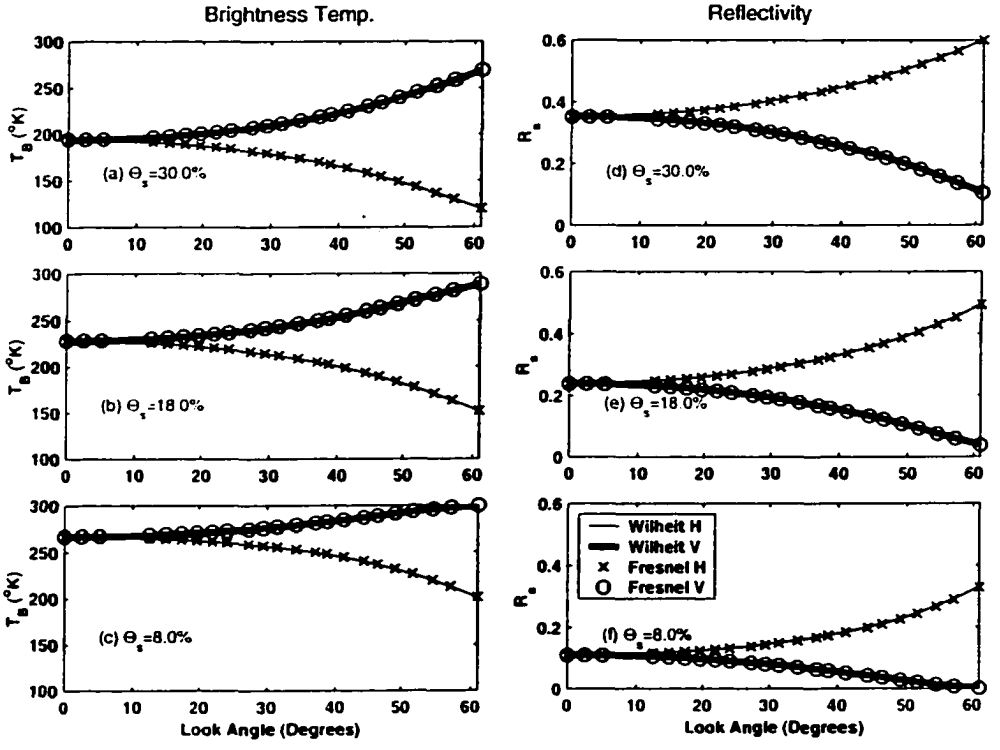

Fig 1 *Comparison of the microwave brightness temperature (°K) and soil reflectivity (no units) calculated for bare soil using the extended Wilheit (1978) model and the two-source Fresnel model for three different soil wetness conditions.*

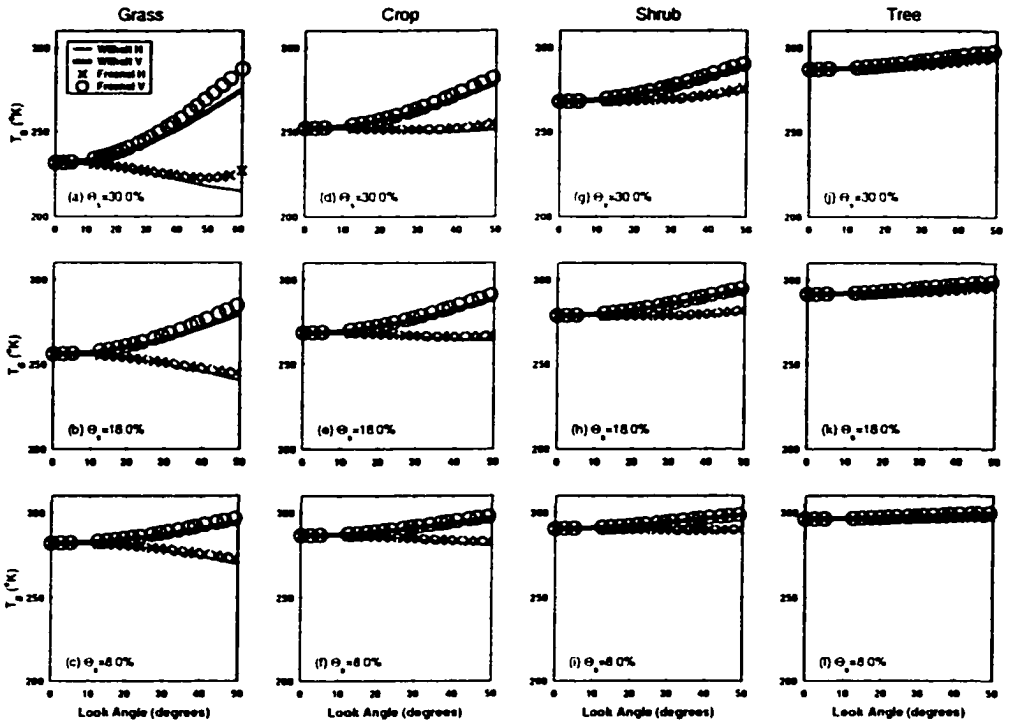

Fig 2. *Microwave brightness temperature (°K) as a function of look-angle (°) for three different conditions of soil wetness (8, 18, and 30%) and four different vegetation covers specified in Table 1 using a constant opacity coefficient, b, the value being specified to ensure equality between the two models at the nadir.*

dependent functions specifying the value of b needed to give accurate retrieval with the proposed SMOS retrieval algorithm for each of the selected soil-moisture levels and for each specified vegetation cover. Figure 3 shows the required equivalent value of b needed for accurate retrieval as a function of look-angle and for both polarisation states. Consistent with Fig. 2, the variation in the required value of b with look-angle is greater for vertically polarised radiation and for canopies with lower vegetation water content.

RETRIEVAL ACCURACY FOR HOMOGENEOUS VEGETATION

On the basis of these results, it is clear that to obtain truly accurate recovery using a retrieval algorithm based on the two-source Fresnel model in the presence of vegetation, it is necessary to allow for look-angle dependency in the effective value of b that changes with the vegetation cover and soil-moisture status. The mechanics of making such an allowance is peripheral to the present study and, for the remainder of this paper, it is assumed that corrections for this systematic effect have been made and that the appropriate value of b is being used in the retrieval. (In practice, perhaps these would be obtained from "look-up" tables applied in an iterative system). Outstanding issues are the accuracy of the retrieval of soil moisture, optical depth, and effective temperature from multi-angle data when using (in this study, state-of-the-art) optimisation techniques and the impact on that retrieval accuracy of having heterogeneous vegetation within a pixel.

The process of retrieval involves searching for that combination of soil moisture, optical depth and effective temperature which, when used in the Fresnel model, calculates microwave brightness temperatures (with appropriate, effective value of b) at the set of look-angles corresponding to a specified position in the footprint of SMOS that most nearly corresponds to the simulated observations calculated by the extended Wilheit (1978) model. In this study, searching for the preferred combination of variables involved randomly initiating the SCE-UA

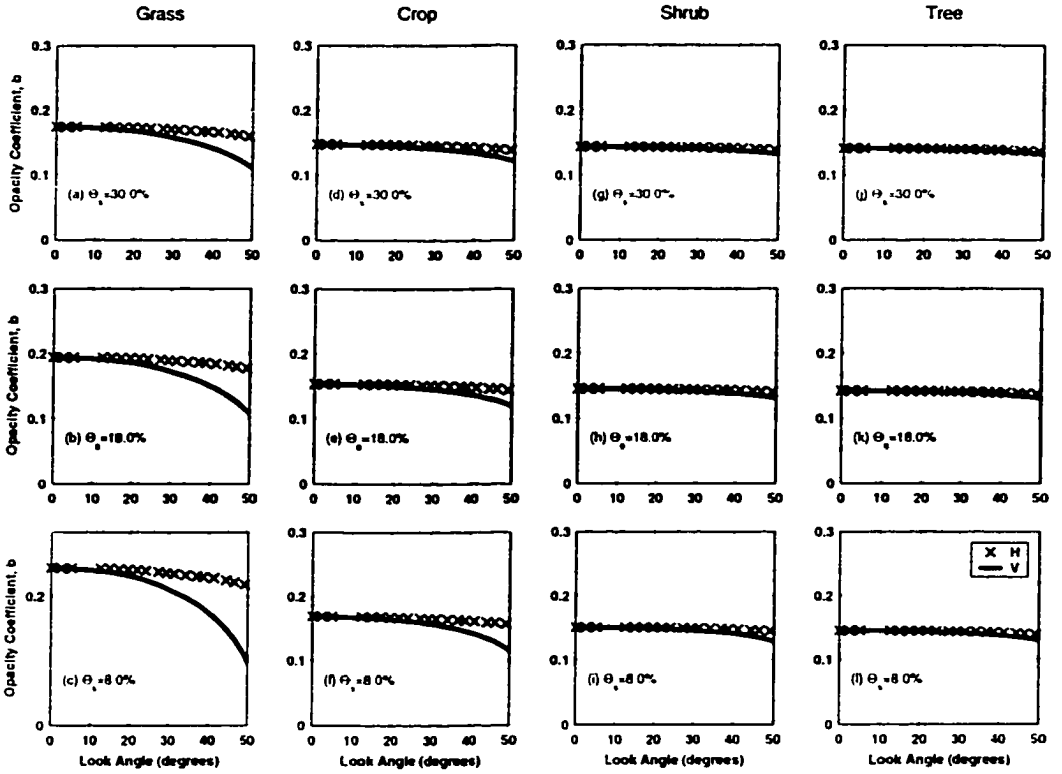

Fig. 3 *The effective value of the opacity coefficient, b, required to make accurate retrievals with the two-source Fresnel model as a function of look-angle for three different soil wetness conditions and four different vegetation covers*

optimisation procedure within the allowed range of the required variables and allowing it to find that combination with minimum root mean square error (RMSE) between the brightness temperature calculated with the Fresnel model and the synthetic observations. In general, different random initiations of the SCE-UA algorithm resulted in the same set of values for the three required variables.

Figure 4 shows the results of applying the retrieval process with different vegetation covers and with different soil moisture states. In Fig. 4, the location of the sampled point within the SMOS footprint is specified on the horizontal axis as a function of the half-swath angle. Errors are given relative to the fixed equivalent values used in the forward calculations made with the extended Wilheit (1978) model, in percent, 10^{-1} kg m^{-2} and °K for soil moisture, vegetation water content and effective temperature, respectively. The retrieval results in very small errors in the retrieved values shown in Fig. 4; the errors are apparently haphazard and most obvious in the case of retrieved soil moisture. The presence of such "noise" confuses an interpretation of Fig. 4 but some general features are evident.

When changes in the effective value of b are taken into account, the retrieval is very successful with errors in soil moisture typically less than 0.5%, in vegetation water content less than 0.1 kg m^{-2} and with very small errors (0.1 K) in effective temperature. There is a tendency for the errors in the retrieved values, especially those in soil moisture, to be greater for bigger half-swath angles. This is, presumably, a consequence of the fact that the number of angles for which observations will be made in the SMOS mission reduces with half-swath angle. There is little evidence that retrieval errors change significantly with soil moisture status. However, there is some suggestion that the retrieval errors, at least for surface soil moisture, are greater for forest vegetation than for the other vegetation classes.

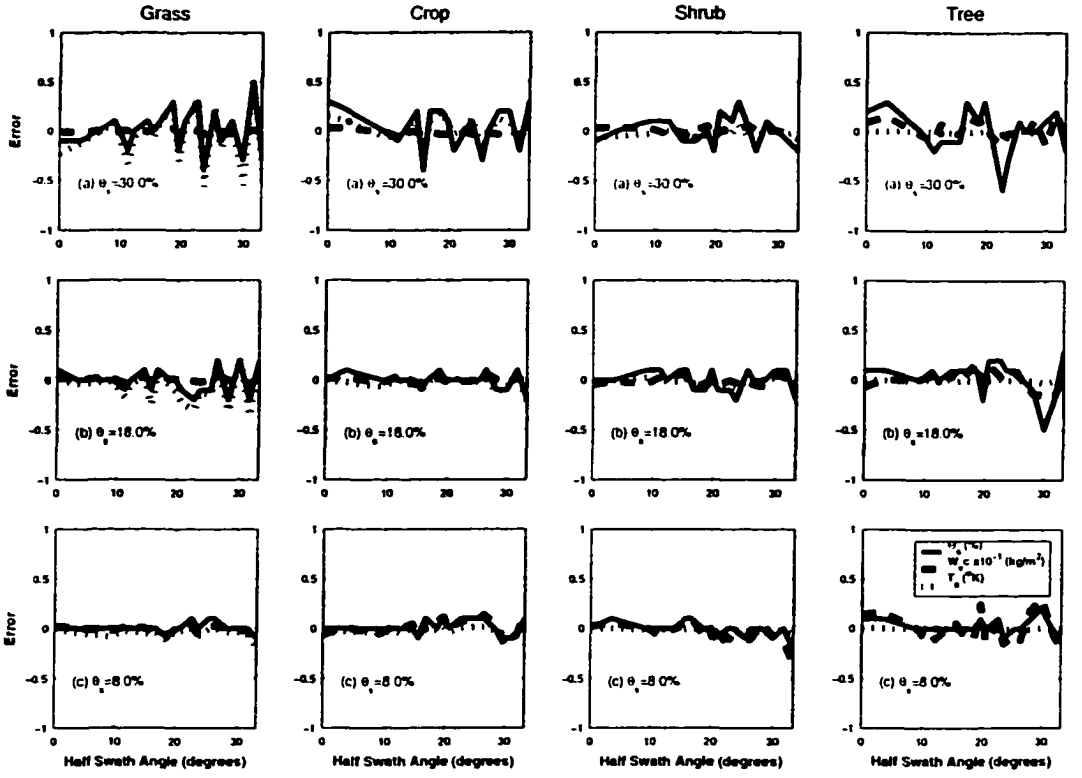

Fig. 4. Retrieved values of near-surface soil moisture, vegetation water content, and effective temperature obtained by optimising the two-source Fresnel model with the effective values of opacity coefficient given in Fig. 3, expressed as a function of half-swath angle for three different soil wetness conditions and four different vegetation covers.

RETRIEVAL ACCURACY FOR HETEROGENEOUS VEGETATION

The accuracy of the retrievals depends on the nature of the overlying vegetation and requires appropriate specification of vegetation-related parameters. However, in practice, even within one land-cover type and particularly for pixel sizes ~ 50 km, there will be a large variation in the nature of the vegetation and hence the vegetation-related parameters. To explore the impact of realistic variability in the vegetation on the quality of retrieval, one thousand forward calculations of synthetic SMOS observations were made for selected half-swath angles, soil moisture states and vegetation covers, as before, with the vegetation parameters in the extended Wilheit (1978) model randomly selected around the values previously used following a Gaussian distribution with a standard deviation equal to 10% of their (previously fixed) value. Retrievals were then made in each case using the SCE-UA optimisation procedure and the mean and standard deviation of the retrieved geophysical variables calculated.

Figure 5 shows the mean of the retrieved variables obtained using the procedure just outlined. In this figure, the location of the sampled point within the SMOS footprint is again specified on the horizontal axis in terms of the half-swath angle, and errors are again given relative to the fixed equivalent values used in the forward calculations in percent for soil moisture, 10^{-1} kg m^{-2} for vegetation water content and °K for temperature, respectively. The most noticeable and significant result demonstrated by Fig. 5 is that random errors in the parameters used to specify the nature of the vegetation can result in systematic offsets in the retrieved values of soil moisture and vegetation water content but they have less impact on the retrieved value of effective temperature. The induced systematic errors are broadly similar for grass-, crop- and shrub-covered surfaces (less than ~0.5% reduction in retrieved soil moisture and up to ~0.2 kg m^{-2} increase in retrieved vegetation water content,

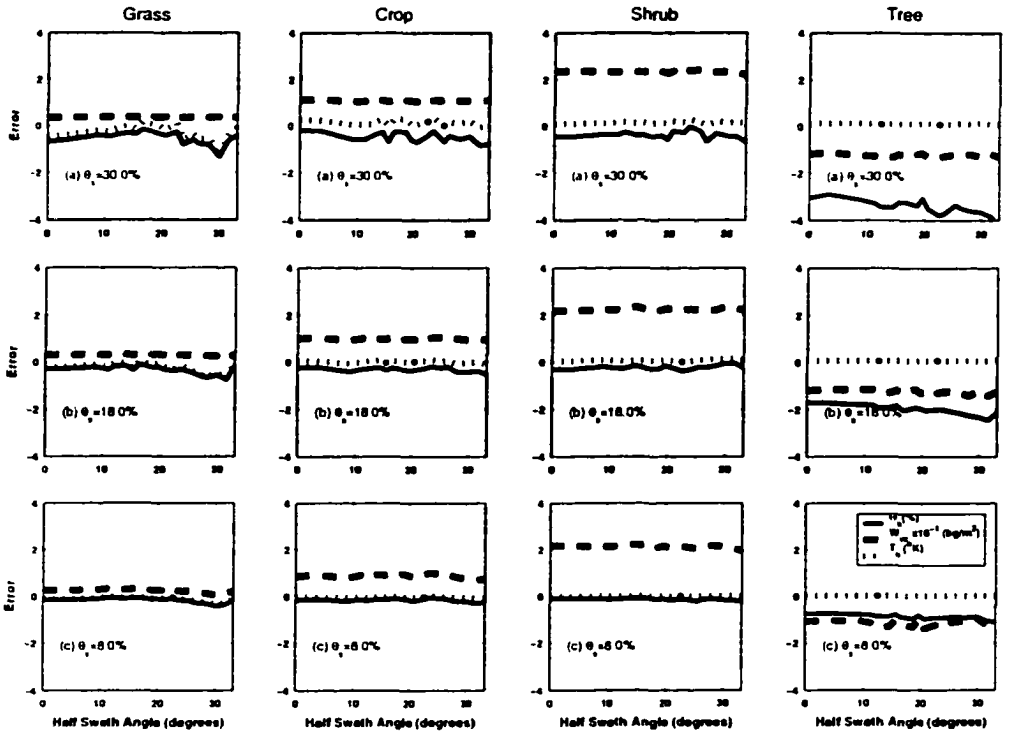

Fig. 5. *Systematic error in retrieved values of near-surface soil moisture, vegetation water content, and effective temperature as a function of half-swath angle for three different soil wetness conditions and four different vegetation covers when 10% random errors are introduced into the specification of the vegetation-related parameters used when calculating the synthetic observations with the extended Wilheit (1978) model.*

depending on the vegetation cover), but are noticeably different in the case of forest cover (~1–4% reduction in retrieved soil moisture, depending on the wetness of the soil, and a ~0.15 kg m^{-2} decrease in vegetation water content). In the case of forest cover, there is also some tendency for the systematic error in retrieved soil moisture to increase with half-swath angle, presumably because the sampled range of look-angles changes and, on average, the absolute values increase as the half-swath angle increases.

Imposing random errors in vegetation-related parameters generates both systematic and random errors in the retrieved variables. Table 3 gives the systematic bias and standard deviation of the retrieved values of soil moisture, vegetation water content and effective temperature at zero swath angle when 10% random errors are introduced into the vegetation-related parameters used to calculate the synthetic observations using the extended Wilheit model. In general, the absolute values of the systematic errors are small and less than 1% by volume in soil water content (but up to 3% for forest cover over moist soil), less than 0.1 kg m^{-2} in vegetation water content (but up to 0.1 kg m^{-2} for shrub cover over moist soil) and typically ~0.1 K in temperature (but up to ~0.5 K for grass cover over moist soil). The random errors in retrieved variables (here in all cases expressed in terms of the standard deviation of retrieved values) differ with the retrieved variable. The random error in soil moisture increases with soil wetness, being typically ~1–3% for grass, crop and shrub cover but is much larger both in absolute terms (up to 8%) and as a fraction of soil-water content for forest cover. Perhaps not surprisingly, the random error in vegetation water content generated by introducing 10% errors in vegetation parameters (largest in absolute terms for forest cover) is high in percentage terms (25—40%) for all cover types and soil-moisture conditions. While the random error in retrieved temperature is small for forest cover, it increases to ~2 K for grass cover over moist soil.

It is interesting to see how the systematic errors and the

Table 3. **Bias and standard deviation (SD) of retrieved surface variables at zero-swath angle when vegetation-related parameters are randomly selected following a Gaussian distribution with standard deviation of 10%.**

V_{wc} (kg m^{-2})	θ_s (%)	Bias in θ_s (%)	SD in θ_s (%)	Bias in W_{wc} (kg m^{-2})	SD in W_{wc} (kg m^{-2})	Bias in T_s (°K)	SD in T_s (°K)
Grass	30	−0.7	2.5	0.04	0.394	−0.49	2.17
1.25	18	−0.3	1.3	0.03	0.380	−0.20	1.08
	8	−0.1	0.6	0.03	0.367	−0.10	0.32
Crop	30	−0.2	2.5	0.11	0.965	0.25	1.05
2.68	18	−0.2	1.3	0.10	0.936	0.04	0.49
	8	−0.2	0.6	0.08	0.903	−0.03	0.13
Shrub	30	−0.4	2.2	0.23	1.700	0.10	0.38
4.17	18	−0.3	1.2	0.22	1.673	0.05	0.18
	8	−0.1	0.5	0.21	1.647	−0.00	0.05
Tree	30	−3.0	8.3	−0.11	2.092	0.13	0.25
7.50	18	−1.7	4.8	−0.12	2.075	0.08	0.13
	8	−0.8	2.2	−0.10	2.059	0.02	0.04

associated random errors in retrieved values change with the size of random errors introduced into the vegetation-related parameters. Recognizing that the systematic errors for grass-, crop- and shrub-covered surfaces are similar and also broadly similar for different soil moisture states, Fig. 6 shows the error in the retrieved variables for crop and forest cover for medium soil moisture status (18%) as a function of the standard deviation of the random error added to the vegetation parameters in the extended Wilheit (1978) model. The mean temperature is always retrieved very accurately,

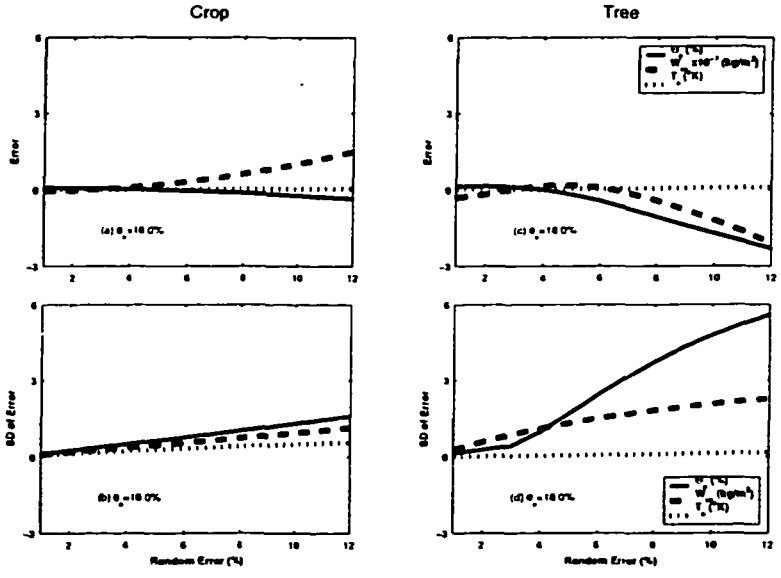

Fig 6 *Systematic error (given as a percentage for soil moisture and vegetation water content and absolute value for effective temperature) and random error (given as a percentage of the mean value) in retrieved values of near-surface soil moisture, vegetation water content, and effective temperature as a function of the random errors in the specification of vegetation-related parameters when calculating synthetic observations with extended Wilheit (1978) model. Results are given for crop cover and forest cover and for a soil-moisture status of 18%.*

regardless of the imposed errors in vegetation parameters. However, as the standard deviation of the random errors increases, the systematic error in the retrieved soil moisture and vegetation water content increases. The systematic error in the retrieved soil moisture increases more significantly than in vegetation water content for forest cover, and vice-versa for the crop cover. This might be expected because of the greater sensitivity of the microwave brightness temperature to the soil moisture when covered with vegetation with less water content. The random errors in soil moisture and vegetation water content also increase as the random error in vegetation parameter increases, and become large, particularly in the case of forest cover.

Summary and conclusions

This study investigated the potential sensitivity of the values of near-surface soil moisture, vegetation water content and effective temperature retrieved from multi-angle microwave radiometer observations to the presence and nature of vegetation cover, with the proposed SMOS mission used as a case study. The strategy adopted was, firstly, to simulate the range of observations of microwave brightness temperature that (it is proposed) SMOS will make using an extended version of the Wilheit (1978) model (Lee *et al.*, 2002) for three different soil moisture states (wet, medium and dry) and four different vegetation covers (grass, crop, shrub and forest). Then, the required values were found using a retrieval approach that mimicked that proposed for the SMOS mission in that it assumed a two-source Fresnel representation of microwave emission and used advanced optimization techniques.

The primary conclusions of the present study are as follows:

- When describing the microwave emission of bare soil, the simple two-source (Fresnel) model of microwave emission used in the proposed SMOS retrieval and the extended Wilheit (1978) model are consistent.
- When describing the microwave emission of vegetation-covered soil, the simple two-source model of microwave emission is not consistent in detail with the extended Wilheit (1978) model and cannot therefore be used to retrieve accurate values of near-surface soil moisture, vegetation water content and effective temperature unless effective values of the opacity coefficient, b, that vary with look-angle, soil moisture status and vegetation cover are used.
- If effective values of the opacity coefficient are used, the proposed SMOS retrieval algorithm gives very good retrievals, with errors in soil moisture typically of the order of 1%; in vegetation water content less than 0.5%; and with very small errors in effective temperature.
- With multi-angle microwave radiometers and a retrieval algorithm based on the simple two-source (Fresnel) model, heterogeneity within the vegetation cover (as represented by introducing 10% random error in vegetation parameters) can result in both systematic and random errors in retrieved values which are vegetation cover and soil-moisture status dependent.
- Systematic errors in retrieved variables induced by 10% random errors in vegetation parameters are up to 0.5 K for temperature (worst for grass cover and moist soil), up to 3% in soil moisture (worst for forest cover and moist soil), and up to ~0.2 kg m^{-2} for vegetation content (worst for shrub cover). Random errors so induced are up to ~2°K for temperature (worst for grass cover and moist soil), up to ~8% in soil moisture (worst for forest cover and moist soil), and up to ~2 kg m^{-2} for vegetation content (worst for forest cover).
- The size of both systematic and random errors increases with the heterogeneity in vegetation cover (as represented by random error in vegetation parameters) for all cover types; the systematic error in the retrieved soil moisture increases more significantly than in vegetation water content for forest cover, and vice-versa for the crop cover.

Acknowledgements

Primary support for Khil-ha Lee and Dr. Eleanor J. Burke while preparing this paper was provided from NOAA project NA96GP0412. Additional support for Dr. W. James Shuttleworth was provided from NASA project NAG8-1531. The editorial assistance provided by Corrie Thies is appreciated.

References

Basharinov, A.E. and Shutko, A., 1975. Simulation studies of the SHF radiation of soils under moist conditions. *NASA Tech. Translation TT F-16.*

Calvet, J.-C., Wigneron, J.-P., Chanzy, A. and Haboudane, D., 1995. Retrieval of surface parameters from microwave radiometry over open canopies at high frequencies. *Remote Sens. Environ.*, **53**, 46–60.

Chanzy, A., Schmugge, T.J., Calvet, J.-C., Kerr, Y., van Oevelen, P., Grosjean, O. and Wang, J.R., 1997. Airborne microwave radiometry on a semi-arid area during Hapex-Sahel. *J. Hydrol.*, **188–189**, 285–309.

Dobson, M.C., Ulaby, F.T., Hallikainen, M.T. and El-Rayes, M.A., 1985. Microwave behavior of wet soil, 2: dielectric mixing models. *IEEE Trans. Geosci. Remote Sens.*, **23**, 35–46.

Duan, Q.Y., Gupta, V.K. and Sorooshian, S., 1993. Shuffled Complex Evolution approach for effective and efficient global minimization. *J. Optimiz. Theor. Appl.*, **76**, 501–521

Holland, J.H., 1975. *Adaptation in Natural and Artificial Systems*. University of Michigan Press, Ann Arbor, Michigan.

Jackson, T.J. and Schmugge, T.J., 1991. Vegetation effects on the microwave emission of soils. *Remote Sens. Environ.*, **36**, 203–212.

Jackson, T.J., Le Vine, D.M., Hsu, A.Y., Oldak, A., Stark, P.J., Swift, C.T., Isham, J.D. and Haken, M., 1999. Soil moisture mapping at regional scales using microwave radiometry: the Southern Great Plains Hydrology Experiment. *IEEE Trans Geosci. Remote Sens.*, **37**, 2136–2151.

Kerr, Y.H., Waldteufel, P., Wigneron, J.-P., Martinuzzi, J.-M., Font, J. and Berger, M., 2001. Soil moisture retrieval from space: the Soil Moisture and Ocean Salinity (SMOS). *IEEE Trans. Geosci. Remote Sens.*, **39**, 1729–1735.

Kirdyashev, K.P., Chukhlantsev, A.A. and Shutko, A.M., 1979. Microwave Radiation of the earth's surface in the presence of a vegetation cover. *Radiotekhnika I Elektronika*, **24**, 256–264 (Engl Transl.)

Le Vine, D.M. and Karam, M.A., 1996. Dependence of attenuation in a vegetation canopy on frequency and plant water content. *IEEE Trans.Geosci. Remote Sens.*, **34**, 1090–1096.

Lee, K.H., Harlow, R.C., Burke, E.J. and Shuttleworth, W.J., 2002. Application of a plane-stratified emission model to predict the effects of vegetation in passive microwave radiometry. *Hydrol. Earth System Sci.*, **6**, 1–13.

Nelder, J.A. and Mead, R.A., 1965. A simplex method for function minimization. *Comput. J.*, **7**, 308–313.

Njoku, E.G. and Li, L., 1999. Retrieval of land surface parameters using passive microwave measurements at 6-18 GHz. *IEEE Trans. Geosci. Remote Sens.*, **37**, 79–93.

Price, W.L., 1987. Global optimization algorithms for a CAD workstation. *J. Optimiz. Theor. Appl.*, **55**, 133–146.

Teng, W.L., Wang, J.R. and Doraiswamy, P.C., 1993. Relationship between satellite microwave radiometric data, antecedent precipitation index, and regional soil moisture. *Int. J. Remote Sens.*, **14**, 2483–2500.

Ulaby, F.T. and El-Rayes, M.A., 1987. Microwave dielectric spectrum of vegetation. 2, dual dispersion. *IEEE Trans. Geosci. Remote Sens.*, **25**, 550–557.

Ulaby, F.T., Moore, R.K. and Fung, A.K., 1986. *Microwave Remote Sensing - Active and Passive*. Addison-Wesley, Reading, MA.

van de Griend, A.A. and Owe, M., 1996. Measurement and behavior of dual-polarization vegetation optical depth and single scattering albedo at 1.4 and 5 GHz microwave frequencies *IEEE Trans. Geosci. Remote Sens.*, **34**, 957–965.

Wang, J.R., Shiue, J.C., Schmugge, T.J. and Engman, E.T., 1990 The L-band PBMR measurements of surface of soil moisture *IEEE Trans. Geosci. Remote Sens.* **28**, 906–913.

Wigneron, J.-P., Calvet, J.-C. and Kerr, Y.H., 1996. Monitoring water interception by crop fields from passive microwave observations *Agr. Forest Meteorol.*, **80**, 177–194.

Wigneron, J.-P., Waldteufel, P., Chanzy, A., Calvet, J.-C., Marloie, O., Hanocq, J.-F. and Kerr, Y.H., 1999 Retrieval capabilities of L-band 2-D interferometric radiometry over land surfaces (SMOS mission). In: *Microwave Radiometry and Remote Sensing of the Earth's Surface and Atmosphere*, VSP, The Netherlands, 552 pp.

Wigneron, J.-P., Waldteufel, P., Chanzy, A., Calvet, J.-C. and Kerr, Y., 2000 Two-dimensional microwave interferometer retrieval capabilities over land surfaces (SMOS mission) *Remote Sens Environ.*, **73**, 270–282

Wilheit, T.T., 1978. Radiative transfer in a plane stratified dielectric. *IEEE Trans. Geosci. Electron.*, **16**, 138–143.

APPENDIX

DERIVATION OF EQUIVALENT OPTICAL DEPTH

The extended Wilheit (1978) model (Lee *et al.*, 2002) calculates the microwave brightness temperature, $T_{B,all}$, of the complete soil-vegetation-atmosphere interface as:

$$T_{B,all} = \sum_{i=1}^{N} f_i \cdot T_i \tag{A1}$$

where T_i is the temperature of the i^{th} layer, f_i is the fraction of energy absorbed from an incident microwave by the i^{th} layer of dielectric represented in the model and N is the number of the layers in the semi-infinite medium. A number, N_s, of these layers of dielectric represent the underlying soil. Hence, the effective reflectivity, r_s, and emissivity, e_s, of the soil surface within the overall description of the Lee *et al.* (2002) model are given by:

$$r_s = (1 - e_s) = 1 - \sum_{i=1}^{N_s} f_i \tag{A2}$$

while the effective microwave brightness temperature of the soil surface is:

$$T_{B,soil} = \sum_{i=1}^{N_s} f_i \cdot T_i \tag{A3}$$

In the simpler, two-layer Fresnel model of the soil-vegetation-atmosphere interface, vegetation is treated as an absorbing layer with a transmissivity, Γ, which is described in terms of an optical depth, τ, (Kirdyashev *et al.*, 1979) that depends on the vegetation dielectric properties, the plant shape or structure, the wavelength and polarisation of the radiation, and the look angle, φ, (Jackson and Schmugge, 1991). Thus:

$$\Gamma = \exp(-\tau \sec\varphi) \tag{A4}$$

In this expression, τ is often written (see, for instance, Jackson and Schmugge, 1991) as:

$$\tau = bW_c \tag{A5}$$

where W_c is the vegetation water content (kg m^{-2}) and b, the opacity coefficient, is a parameter that represents all of the other influences of vegetation on optical depth.

Assuming there is no scattering of radiation at long wavelengths, the two-layer model gives the overall microwave brightness temperature of the soil-vegetation-atmosphere interface as:

$$T_{B,eff} = (1+r_s\Gamma)(1-\Gamma)(1-\alpha)T_v + (1-r_s)\Gamma T_s \qquad \text{(A6)}$$

where α is the single scattering albedo, and T_v is the temperature of the vegetation canopy. Equation (A6) can be rearranged to give:

$$\Gamma^2 + \frac{[(1-r_s)(1-\alpha)T_v - (1-r_s)T_s]}{(1-\alpha)r_sT_v}\Gamma - \frac{[T_{B,eff} - (1-\alpha)T_v]}{(1-\alpha)r_sT_v} = 0 \qquad \text{(A7)}$$

Hence, if the value of α is known or assumed, Γ can be found for known values of temperatures and r_s as the (real) solution of the quadratic Eqn. (A7). The effective value of the optical depth, τ, and the opacity coeficient, b, in the two-level model can then be calculated from Eqns. (A4) and (A5), respectively. In this way, the dependence of τ and b in the simpler two-source model can be investigated in terms of vegetation characteristics, as specified by parameters in the extended Wilheit (1978) model (Lee *et al*., 2002).

APPENDIX C: USING AREA-AVERAGE REMOTELY SENSED SURFACE SOIL MOISTURE IN MULTI-PATCH LAND DATA ASSIMILATION SYSTEMS, by Eleanor J. Burke, W. James Shuttleworth, Khil-ha Lee, and Luis A. Bastidas, in *IEEE Transactions on Geoscience and Remote Sensing,* 39(10): 2091-2100, 2001.

IEEE TRANSACTIONS ON GEOSCIENCE AND REMOTE SENSING, VOL. 39, NO. 10, OCTOBER 2001

Using Area-Average Remotely Sensed Surface Soil Moisture in Multipatch Land Data Assimilation Systems

Eleanor J. Burke, W. James Shuttleworth, Khil-ha Lee, and Luis A. Bastidas

Abstract—In coming years, Land Data Assimilation Systems (LDAS) two-dimensional (2-D) arrays of the relevant land-surface model) are likely to become the routine mechanism by which many predictive weather and climate models will be initiated. If this is so, it will be via assimilation into the LDAS that other data relevant to the land surface, such as remotely sensed estimates of soil moisture, will find value. This paper explores the potential for using low-resolution, remotely sensed observations of microwave brightness temperature to infer soil moisture in an LDAS with a "mosaic-patch" representation of land-surface heterogeneity, by coupling the land-surface model in the LDAS to a physically realistic microwave emission model. The past description of soil water movement by the LDAS is proposed as the most appropriate, LDAS-consistent basis for using remotely sensed estimates of surface soil moisture to infer soil moisture at depth, and the plausibility of this proposal is investigated. Three alternative methods are explored for partitioning soil moisture between modeled patches while altering the area-average soil moisture to correspond to the observed, pixel-average microwave brightness temperature, namely, 1) altering the soil moisture by a factor, which is the same for all the patches in the pixel, 2) altering the soil moisture by adding an amount that is the same for all the patches in the pixel, and 3) altering the change in soil moisture since the last assimilation cycle by a factor which is the same for all the patches in the pixel. In each case, an iterative procedure is required to make the adjustment. Comparison is made between these alternative procedures for a hypothetical pixel that contains eight individual patches (three different vegetation types growing both in clay and sand, plus one patch of bare soil and one of open water) using a mosaic-patch version of the MICRO-SWEAT model. When the applied forcing variables are artificially degraded, all three methods provide similar, improved descriptions of the time-evolution of soil moisture in the pixel as a whole and of the deep soil moisture for each patch. However, in each case, the ability of the LDAS to correctly describe the separate evolution of surface soil moisture in each patch is imperfect.

Index Terms—Hydrology, microwave radiometry, remote sensing, soil moisture.

I. Introduction

THERE is now ample evidence that, over continental areas, weather and climate are significantly influenced by the local and regional availability of soil moisture that can reach the atmosphere by evaporation from soil or by transpiration from plants, e.g., [1]–[7]. At least at midlatitudes, and at least during the warm season, weather and climate forecasts can be improved by providing better initiation and description of the subsequent evolution of soil-moisture status in forecast models. At present, the most practical method is via the use of land data assimilation systems (LDAS). LDAS are two-dimensional (2-D) arrays of the land-surface scheme of the relevant weather or climate forecast model. These land-surface schemes are forced mainly by observations, so the soil moisture status is not biased by poor simulation of the near-surface atmospheric forcing, especially precipitation. Currently, most LDAS operate with resolutions on the order of 10–30 km, and many make use of remotely sensed information on land cover by including the separate representation of several patches of vegetation within each grid square using the "mosaic" approach [8]. In the "mosaic" approach, the fluxes of heat and moisture are calculated for each patch of vegetation present within a grid-square and then an area-weighted average is calculated for the entire grid-square.

An example of an LDAS running in near real-time can be found at [9]. This consists of several physically-based land-surface models running on a common 0.125°-resolution grid covering the contiguous United States, driven by common surface forcing fields. Observed hourly, gauge/radar precipitation and observed GOES-based satellite-derived surface solar insolation are used [10]. Presently underway is the extension of this LDAS to the entire globe [9].

It is possible that LDAS such as this will become the routine mechanism by which many predictive weather and climate models will be initiated in coming years. Assuming this is so, it will be via assimilation into LDAS that other data relevant to the current status of the land surface, such as remotely sensed estimates of soil moisture, will find value for initiating predictive models. They can bring together remotely sensed and *in-situ* measurements in a balanced way, reduce uncertainty to poorly modeled variables, and can readily be used to calculate frequent and regular estimates of soil moisture with significant vertical resolution.

In the course of the next decade (while the LDAS approach to model initiation remains current), it is possible that remotely sensed measures of soil moisture will become available in the form of observations made with L-band, passive microwave radiometers. Such data potentially have great value. However, a way must be found to extract this value given that the observations of brightness temperature: a) will be made at low resolution (~50 km); b) are a measure of soil moisture in the top 5 cm only;

Manuscript received December 18, 2000; revised May 25, 2001. This work was supported in part by NOAA Project NA96GP0412, NASA Project NAG5-7554, and NOAA Project NA86GP0324.

The authors are with the Department of Hydrology and Water Resources, University of Arizona, Tucson, AZ 85721 USA (e-mail: shuttle@hwr.arizona.edu).

Publisher Item Identifier S 0196-2892(01)08123-2.

and c) are strongly affected by the (often heterogeneous) vegetation cover present at the surface. Therefore, there is a need to explore theoretical methods by which large-pixel-average, near-surface remotely sensed estimates of soil moisture can be used in an LDAS framework to improve estimates of both the surface and deep soil moisture. Ideally the area-average value is apportioned in a way that reflects its relevance to the component vegetation patches represented within the pixel. The purpose of this paper is to propose and explore theoretical methods to do this.

In the following, models that couple description of surface energy and water exchange with description of the microwave emission of the whole surface interface are first briefly discussed. Then the feasibility of using a coupled land-surface microwave emission model to provide patch-specific estimates of soil moisture from area-averaged microwave brightness temperatures measured over several vegetation patches is explored. It is implicitly assumed that the pixel observed by an L-band radiometer will have the same size and location as the grid-square of the LDAS and hence, the patches of different vegetation types will be the same within each one.

II. Models of Surface Water/Energy Exchange and Microwave Emission

Recently, models have been developed that merge a description of surface energy and water exchange with a description of the microwave emission of the whole soil-vegetation-atmosphere interface [11]–[14]. Burke *et al.* [13], [14] used MICRO-SWEAT, a soil water evaporation and transpiration (SWEAT) model [15] coupled with a microwave emission model (MICRO) to predict time courses of microwave brightness temperature. SWEAT is used to predict the temporal changes in profile soil-water status and profile soil temperature. These outputs are then passed into a microwave radiative transfer model that calculates the microwave brightness temperature. MICRO-SWEAT produces excellent simulations of time series of microwave brightness temperatures for a variety of bare and vegetated soils at both L-band and C-band and for a range of look angles [13], [14].

The radiative transfer model in MICRO-SWEAT is the Wilheit [16] model for the coherent propagation of electromagnetic radiation through a stratified medium, which relates the brightness temperature emergent at the soil surface to the dielectric properties and temperature of the underlying soil layers. The dielectric properties of the soil are related to the soil-water content via the Wang and Schmugge model [17]. The Wang and Choudhury model [18] is used to account for any increase in brightness temperature resulting from a rough soil surface. The effect of vegetation on the microwave emission from the soil surface was parameterized using the "optical depth" approach, where the optical depth represents the amount of water within the canopy [19].

The proposal that motivates this paper is that similar coupled land-surface and microwave emission models can be used to interface between LDAS and remotely sensed microwave brightness temperature. The development and application of such LDAS-relevant coupled models is the subject of a separate, parallel paper [20]. In this paper, one LDAS grid-square is under discussion with the SWEAT model being the land-surface model. MICRO-SWEAT is used to explore potential of assimilation of microwave brightness temperature measurements.

III. Methodology

This paper examines the difficult issue of extracting value from remotely sensed observations of brightness temperature via assimilation into the land-surface model. It is assumed that, for the foreseeable future, these measurements will be made at low resolution. In addition they are only a measure of near-surface soil moisture, which are strongly affected by the, often heterogeneous, vegetation cover present at the surface.

The proposed assimilation method is built on the realization that the representation of soil moisture status by remotely sensed data cannot be, and need not be, any more realistic than that already used in the LDAS itself. Further, the LDAS can provide the parameters needed to calculate microwave emission from patches of land cover (i.e., the nature and moisture status of the vegetation and soil). This paper uses the LDAS system as a basis for addressing the problem of estimating deep soil moisture from surface soil moisture and of allocating area-average, near-surface estimates of soil moisture between different land covers.

A. Assumptions

Our methods are based on the following assumptions.

1) The use of an LDAS with a "mosaic-patch" representation of the different vegetation classes present in each LDAS grid-square is an appropriate way to introduce soil-moisture estimates into weather and climate prediction models.
2) The proposed method can adopt assumptions already explicitly or implicitly made in the LDAS itself, such as:
   a) the forcing variables are uniform across each LDAS grid-square;
   b) the vertical profiles of soil moisture are adequately calculated by the LDAS for each patch of vegetation in the LDAS;
   c) within an LDAS grid-square, the surface can be classified into open water, bare soil, or one of several vegetation classes, and remotely sensed vegetation cover maps provide an adequate estimate of the relative proportion of the different vegetation classes present;
   d) for an individual LDAS grid square, the LDAS description of the relationship between the surface and deep soil moisture is the most LDAS-consistent way to estimate the moisture deep in the soil-moisture profile, given knowledge of the surface soil moisture.
3) Within the confines of the realism of the LDAS, for individual stands of vegetation, forward modeling of the microwave emission can be used to calculate the surface brightness temperature from the (near-surface and

deep) soil moisture and vegetation status calculated by the LDAS.

4) The microwave emission at L-band from a heterogeneous LDAS grid square is independent of the distribution of vegetation within that grid square and depends only on the relative proportions of each class of vegetation within the grid square [11].

B. Estimating Deep Soil Moisture From Surface Soil Moisture

Only soil moisture, within the top 5 cm of the soil, are amenable to L-band remote sensing, but studies suggest [21] that merely modifying surface soil moisture during data assimilation does not by itself provide a sufficiently strong updating of the deeper soil moisture profile. A method to propagate the surface layer information deeper into the profile is needed.

If an LDAS is being used to update soil moisture, an appropriate estimate of deep soil moisture with which to update is that consistent with the interrelationship between deep soil moisture and surface soil moisture derived for the specific patch within the specific LDAS (Assumption 3). Clearly, there are concerns when making Assumption 3 related to whether the modeled soil water profile, and hence the derived relationship, is realistic, but these are issues that are already present when using the LDAS itself and are not associated with the desire to assimilate remotely sensed soil moisture into the LDAS. Any improvement made in the simulation of the soil-moisture profile by the LDAS will mean that the definition of the relationship between deep soil and surface soil moisture will improve. Assumption 3 is important because it ensures that a reasonable, LDAS-consistent estimate of deep soil moisture is always available for assimilation into the LDAS whenever surface soil moisture estimates are available. However, to set against this, Assumption 3 also means that estimates of deep soil moisture are LDAS-dependent, making them less amenable for assimilation by other models or by other LDAS.

In this study, 5 cm is arbitrarily selected as the limit used to define deep and surface soil moisture. The surface soil moisture is that modeled in the LDAS above this level, and the deep soil moisture is that modeled by the LDAS below this level. The applicability of two possible relationships between surface and deep soil moisture is investigated, one very simple, the second more complex, both derived from the history of the MICRO-SWEAT model.

The simplest approach to estimating the deep soil moisture for the specific patch is to assume that the ratio of surface soil moisture to deep soil moisture remains the same before and after assimilation. Therefore, after assimilation, the deep soil moisture for each patch k in the LDAS is adjusted to correspond to the (remotely sensed) surface value using the equation

$$\theta_k^d(t_a) = \frac{\theta_k^s(t_a)\,\theta_k^d(t_b)}{\theta_k^s(t_b)} \tag{1}$$

where

$\theta_k^s(t_a)$ average soil moisture in the top 5 cm immediately after the assimilation at time t, for patch k;

$\theta_k^d(t_a)$ soil moisture in the underlying deep soil at that time;

TABLE I
SPECIFICATION OF THE CHARACTERISTICS OF EACH PATCH WITHIN THE GRID-SQUARE IN TERMS OF THE NATURE OF THE SOIL AND VEGETATION REPRESENTED IN THE MULTIPATCH VERSION OF MICRO-SWEAT

Patch	Soil	Vegetation	% Sand	% Clay	Optical depth
1	Sand	(None)	93	2	-
2	Water	(None)	-	-	-
3	Sand	Short grass	93	2	0.1
4	Clay	Short grass	15	55	0.1
5	Sand	Crop	93	2	0.3
6	Clay	Crop	15	55	0.3
7	Sand	Shrub	93	2	0.6
8	Clay	Shrub	15	55	0.6

$\theta_k^s(t_b)$ top 5 cm soil moisture before the assimilation cycle;

$\theta_k^d(t_b)$ deep soil moisture before the assimilation cycle.

A more complicated approach is to use the time-average historical description provided by the LDAS to derive an empirical equation that describes the interrelationship between surface soil moisture and deep soil moisture for each patch at each grid location. This approach was explored using soil-moisture profiles calculated by MICRO-SWEAT for seven example patches, i.e., three different vegetation types growing both in clay and sand plus one patch of bare soil (Table I). The nature of the modeled relationship between $\theta_k^s(t)$, the average soil moisture in the top 5 cm at time t, for patch k, and $\theta_k^d(t)$, the soil moisture in the underlying (1.2 m deep) soil layer at time t for patch k, was examined during a one-year period using forcing data from SGP97 [22]. Fig. 1 shows the relationship between (θ_k^s/θ_k^d) and θ_k^s for these seven patches. In each case, there is a significant relationship, but this is very noisy with more scatter in sandy soil and with denser vegetation covers. The interrelationship appears to be structured around several, separate linear correlations. However, it is encouraging that, for this LSM (MICRO-SWEAT), describing these patches, and subject to these forcing data, it is possible to find a simple relationship that efficiently describes the interrelationship between the surface and deep soil moisture, with the form

$$\left[\frac{\theta_k^s(t)}{\theta_k^d(t)}\right] = x_k\left(\theta_k^s(t) - \theta_k^s(t_p)\right) + \frac{\theta_k^s(t_p)}{\theta_k^d(t_p)} \tag{2}$$

where x_k is a constant derived from the historical predictions by SWEAT and t_p is the time immediately after the most recent precipitation event. At that time, the relationship likely depends strongly on the amount of precipitation and modeled runoff, i.e., a large precipitation event on a dry soil might penetrate to the deeper soil layers, whereas a small event will only dampen the soil at the surface. However, once the precipitation event is over, the relationship between (θ_k^s/θ_i^d) and θ_k^s changes mainly as a result of the surface soil drying. Fig. 2 shows the good agreement between the modeled values of (θ_k^s/θ_k^d) and the values calculated by (2) at hourly time intervals during the one-year simulation. A high ratio is likely to occur soon after a precipitation event, possibly after a relatively dry period. The relationship is not quite as good for the sandier soils with the denser vegetation. This may well be as a result of a combination of the faster movement of water in the sandy soils and the increased root extraction rate for the denser vegetation. Further exploration may yield additional

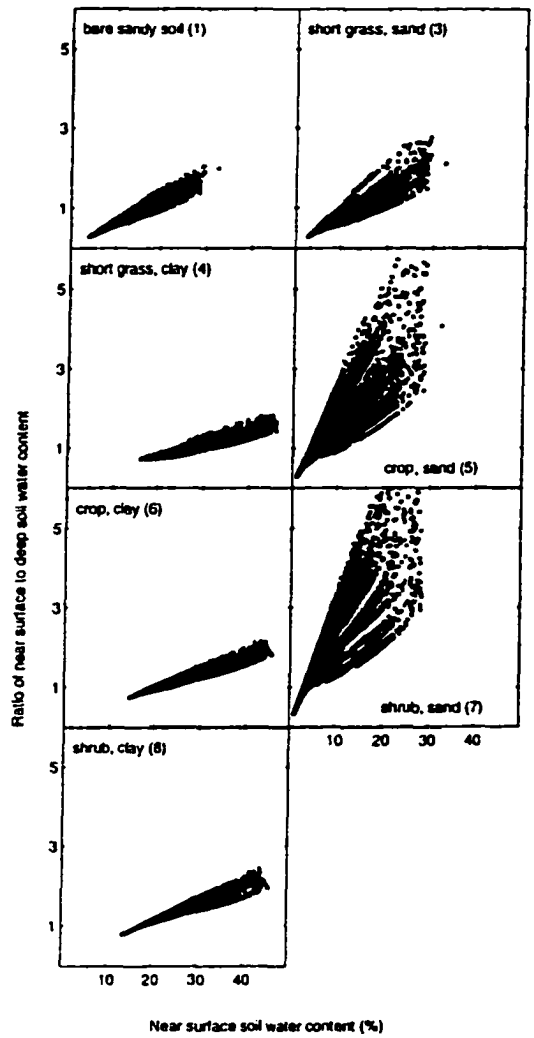

Fig. 1. MICRO-SWEAT modeled relationship between near surface soil moisture and deep soil moisture for the seven nonwater patches within the specified grid square.

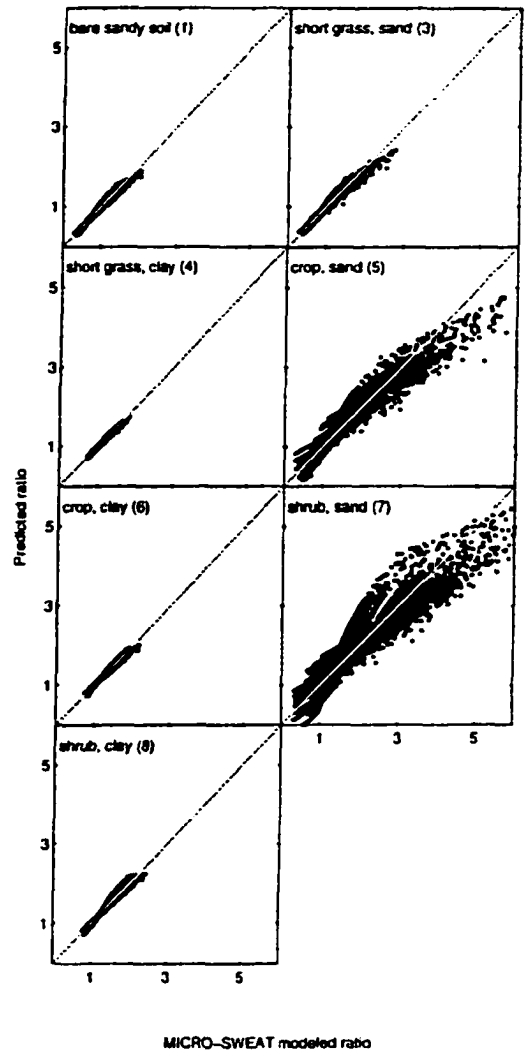

Fig. 2. Comparison of the predicted and modeled relationship between the ratio of near surface soil moisture to deep soil moisture for the seven nonwater patches within the specified grid square.

factors that need to be taken into account in addition to those included in (2). A simple artificial neural network (ANN) could be calibrated and applied for each patch, as a more general alternative approach. The main negative consequence of this LDAS history-based approach is that it requires the LDAS to be run for a substantial period to calculate the required relationship, in principle for every patch represented in each grid square. However, there should be some consistency between grid squares, because a common land-surface model is used for each.

Equations (1) and (2) are specific examples of the more general, LDAS-derived relationship between θ_k^d, the deep soil moisture for a patch k, and θ_k^s, the surface soil moisture for patch k used in the next section.

C. Assigning Area-Average Soil Moisture to Patches

It is assumed (Assumption 4) that the brightness temperature, $T_{B,k}$, for a patch of vegetation, k, can be adequately calculated from a microwave emission model M with the general form

$$T_{B,k} = M\left(V_k, \theta_k^s, \theta_k^d(\theta_k^s, \ldots), T_{soil}, T_{veg}\right) \qquad (3)$$

where V_k denotes aspects of the status of the vegetation (as represented in the LDAS) that influences microwave emission and T_{soil} and T_{veg} represent the soil temperature profile and canopy temperature modeled in the LDAS. In this paper, M is the microwave emission model used in MICRO-SWEAT, θ_k^s corresponds to the average soil moisture in the eight modeled

soil layers above 5 cm depth and θ_k^d to that in the 12 modeled soil layers below 5 cm depth, which is a known function of θ_k^s [Note: bare soil and open water patches are special cases of M].

At any time L-band remotely sensed data are available, the value of V_k and any variables other than θ_k^s in M are specified by the LDAS for the patch k. Thus, M is in effect a well-specified function only of θ_k^s. The only measurement of brightness temperature (T_B) that would be available from a microwave radiometer for assimilation into the LDAS grid square is the area weighted average of the brightness temperatures in each patch ($T_{B,M}$)

$$T_{B,M} = \sum_{k=1}^{N} a_k M\left(V_k, \theta_k^s, \theta_k^d(\theta_k^s, \ldots), T_{soil}, T_{veg}\right) \Big/ \sum_{k=1}^{N} a_k \tag{4}$$

where a_k is the area of each patch, and N is the total number of patches in a grid-square.

The essential purpose of using a mosaic-patch LDAS is to allow representation of the effect of different patches of vegetation within a grid-square on surface exchanges and moisture and energy stores. Variations in forcing variables between LDAS grid-squares can be taken into account within the limits of availability and realism of the observational data used. However, it is not obvious how to preserve patch-specific soil moisture when assimilating the observed value of area-average surface brightness temperature for an LDAS grid-square with several different patches of land cover. Numerical studies of assimilation procedures aiming to preserve the distinct patch specific soil-moisture pattern calculated by the LDAS and, at the same time, modifying the area-average soil moisture field consistent with the observed area-average surface brightness were explored. Three alternative assimilation procedures are discussed.

1) Method 1—Fractional Change in Patch-Specific Soil Moisture: In this method, it is assumed that the LDAS has calculated the patch-to-patch differences in soil moisture adequately at the time the remotely sensed area-average brightness temperature is available, but the calculated values may all be systematically too high or too low by a factor that is independent of the patch. In this case, the required correction is to adjust the values of soil moisture for all N patches in the grid square by a common factor f so that the modeled value of surface brightness temperature becomes equal to the observed value. If $\theta_k^s(t_b)$ is the value of surface soil moisture for patch k modeled by the LDAS immediately prior to the availability of remotely sensed data, then $\theta_k^s(t_a)$, the modified value of soil moisture for this patch that is to be assimilated by the LDAS is given by

$$\theta_k^s(t_a) = f\theta_k^s(t_b). \tag{5}$$

Because the model M is not necessarily linear and differs between patches, it is necessary to solve for the value of $\theta_k^s(t_a)$ using the iterative equation

$$[\theta_k^s]_{j+1} = [f]_j\,[\theta_k^s]_j \tag{6}$$

where $[\theta_k^s]_{j+1}$ is the estimated value of $\theta_k^s(t_a)$ during the $(j+1)$th iteration, and $[f]_j$ is given by the ratio between $T_{B,O}$, the observed, area-average surface brightness temperature for the grid square and the value calculated using the microwave emission model, with the surface soil moisture modeled by the LDAS ($T_{B,M}$), thus

$$[f]_j = \frac{T_{B,O}}{T_{B,M}}. \tag{7}$$

In this equation, $T_{B,M}$ is given by (4). During the first iteration, $[\theta_k^s]_j$ is set equal to $\theta_k^s(t_b)$ in (6).

2) Method 2—Incremental Change in Patch-Specific Soil Moisture: In this method, it is assumed that the LDAS realistically calculates patch-specific soil moisture but that the calculated values may all be systematically too high or too low by a fixed amount which is independent of the patch. In this case, the required correction is to adjust the values of soil moisture for all the patches in the grid square by an amount $\Delta\theta$ so that $T_{B,M}$ becomes equal to $T_{B,O}$. The modified value of soil moisture for the patch that is to be assimilated by the LDAS, $\theta_k^s(t_a)$ is given by

$$\theta_k^s(t_a) = \theta_k^s(t_b) + \Delta\theta. \tag{8}$$

As in the previous case, it is necessary to solve for $\Delta\theta$ iteratively. An (arbitrary) first-guess value $[\Delta\theta]_0$ is assumed, and then successive estimates of $\Delta\theta$ are made from the iterative equation

$$[\Delta\theta]_{j+1} = [\Delta\theta]_j \frac{\left(T_{B,O} - [T_{B,M}]_j\right)}{\left([T_{B,M}]_j - T_{B,M}\right)}. \tag{9}$$

Where $[T_B]_j$ is the area-average surface brightness temperature calculated from the estimated surface soil moisture during the jth iteration, given by (4).

3) Method 3—Fractional Change in Soil Moisture Since Last Assimilation: In this method, it is assumed that errors in the soil moisture of each patch are primarily due to weaknesses in the common forcing (e.g., precipitation, radiation, etc.) to which all of the patches have been exposed since the last soil moisture data assimilation took place. Further, it is assumed that the response of the soil-moisture store to these common forcing variables is approximately linear. In this case, the required correction is to modify the modeled change in the soil moisture of each patch that took place since the last assimilation by a factor that is assumed to be the same for all patches. Again, this factor needs to be defined in such a way that $T_{B,M}$ becomes equal to $T_{B,O}$.

Let the LDAS-modeled value of soil moisture for patch k immediately before the present update be $\theta_k^s(t_b)$, and let the change in LDAS-modeled soil moisture for patch k since the last assimilation be $\Delta\theta_k$. Thus, the modified value of soil moisture for this patch to be assimilated, $\theta_k^s(t_a)$, is given by

$$\theta_k^s(t_a) = \theta_k^s(t_b) + f\Delta\theta_k. \tag{10}$$

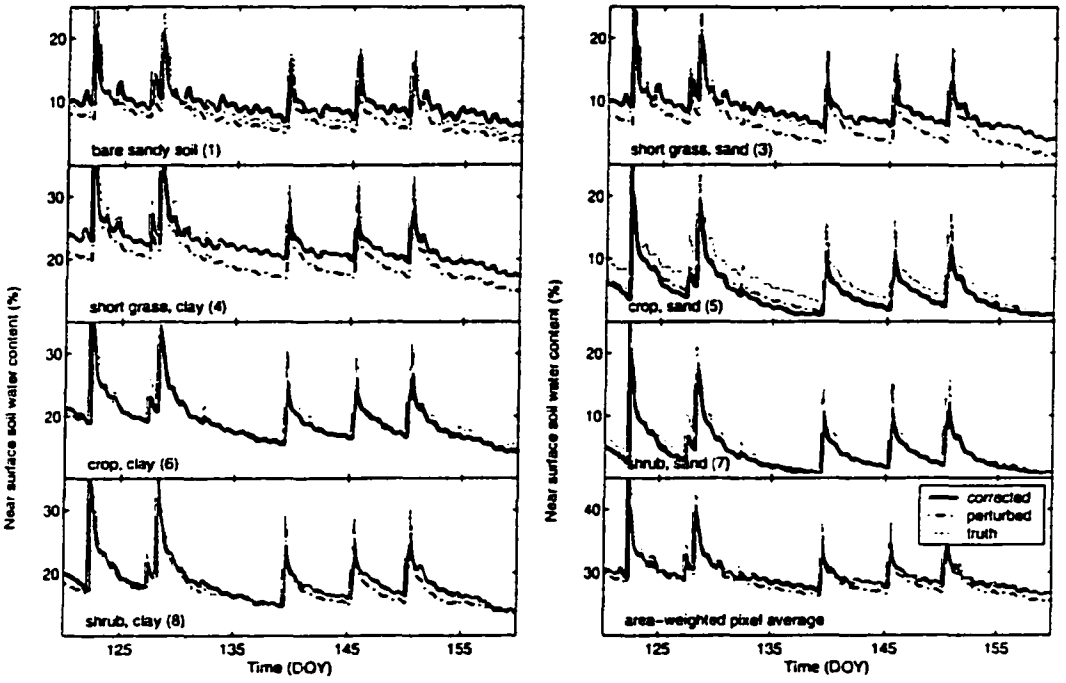

Fig. 3. Time series of the true, perturbed, and corrected top 5 cm soil moisture for the seven nonwater patches within the grid square, plus the area weighted average of the grid square.

Again, it is necessary to solve for f iteratively. An (arbitrary) first-guess value $[f]_0$ is assumed. Then successive estimates of $[f]_j$ are made from the iterative equation

$$[f]_{j+1} = [f]_j \frac{\left(T_{B,O} - [T_{B,M}]_j\right)}{\left([T_{B,M}]_j - T_{B,M}\right)} \tag{11}$$

where $[T_B]_j$ is given by (4).

IV. Results

The ability of the previously described three area-average assimilation methods to successfully modify the area-average and patch-specific soil moisture was tested using MICRO-SWEAT applied to the multipatch grid square mentioned above and documented in detail in Table I. MICRO-SWEAT was run for a one-year period using the Mesonet data for El Reno for 1997 taken from the SGP97 data base [22], and the area-weighted average microwave brightness temperature was forward calculated. This simulation is referred to as the "true" simulation and these modeled soil-moisture states and brightness temperatures are assumed to provide the truth against which other simulations are judged. The forcing data were then perturbed. In the present study, the precipitation was systematically reduced by 40%, and the resulting calculated values are referred to as the "perturbed" simulation. The true microwave brightness temperature was then assimilated into a similar multipatch MICRO-SWEAT simulation made by using the perturbed forcing data once every three days at 6:00 am. This is referred to as the "corrected" simulation.

Fig. 3 compares the time series of soil moisture in the top 5 cm for the true, perturbed, and corrected simulations during a representative three-month period with correction made using Method 2 (the results when using Methods 1 and 3 are not shown but appear very similar). Fig. 4 shows the same simulations but in this case, for the simulated deep soil moisture. The corrected simulation illustrated in Fig. 4 is that in which the values of deep soil moisture assimilated every three days for each patch k are calculated from (1) (again, the results when using (2) are not shown but appear very similar).

Table II gives the root mean square error (RSME) and bias relative to the true soil moisture calculated for the entire year for the perturbed soil moisture and for the corrected simulations using the three alternative assimilation methods. As might be expected, the area-weighted average plot shown in Fig. 3, the area-mean values of RSME and, particularly, the area-mean bias given in Table II indicate that the area-weighted mean surface soil moisture is significantly improved by assimilating the area-average microwave brightness temperature, regardless of which of the three assimilation methods (1, 2, or 3) is used. However, results on a patch-by-patch basis are varied. Some patches show improvement and some show degradation. For the short grass growing both on sandy and clay soils, the surface soil moisture is fairly well-corrected, for instance, while the crop and shrubs on the sandy soil have less well-corrected soil moisture. The relative improvement does not appear to be

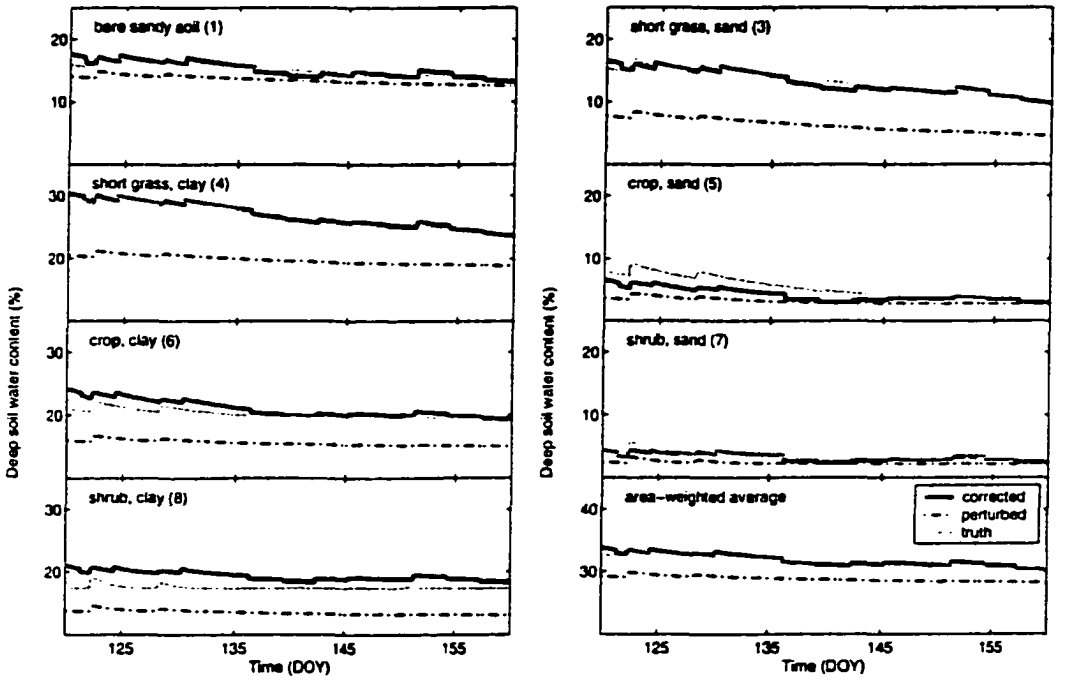

Fig. 4. Time series of the true, perturbed, and corrected deep soil moisture for the seven nonwater patches within the grid square, plus the area weighted average of the grid square.

TABLE II

COMPARISON OF THE SURFACE SOIL MOISTURE (IN %) RELATIVE TO THE TRUE SIMULATION FOR THE PERTURBED SIMULATION AND CORRECTED SIMULATIONS USING THREE DIFFERENT ASSIMILATION METHODS IN (a) AND (c) IN TERMS OF ROOT MEAN SQUARE ERROR (RSME) AND (b) AND (d) IN TERMS OF BIAS FOR EACH PATCH AND FOR THE AREA WEIGHTED AVERAGE FOR THE WHOLE GRID-SQUARE. THE VALUES GIVEN IN (a) AND (b) ARE FOR THE CASE WHEN ASSIMILATED ESTIMATES OF DEEP SOIL MOISTURE ARE CALCULATED FROM (1). THOSE IN (c) AND (d) ARE FOR THE CASE WHEN ASSIMILATED ESTIMATES OF DEEP SOIL MOISTURE ARE CALCULATED FROM (2)

	(a) Surface Soil Moisture (rmse, in %)				(b) Surface Soil Moisture (bias, in %)			
Patch	Perturbed	Method 1	Method 2	Method 3	Perturbed	Method 1	Method 2	Method 3
1	1.30	1.45	1.54	1.39	-1.10	0.82	0.93	0.53
2	0.00	0.00	0.00	0.00	0.00	0.00	0.00	0.00
3	2.35	1.43	1.11	1.38	-2.23	-0.96	-0.02	-0.48
4	3.51	2.41	1.79	1.82	-3.18	1.36	-0.56	-0.45
5	2.03	2.85	2.74	2.66	-1.84	-2.62	-2.51	-1.60
6	2.13	1.56	1.97	1.87	-1.83	-0.73	-1.52	-0.64
7	1.72	2.16	2.13	2.44	-1.36	-1.73	-1.69	-1.11
8	1.51	1.64	1.44	2.70	-0.87	0.23	-0.11	0.72
Mean	1.49	0.86	0.91	1.01	-1.35	-0.28	-0.46	-0.25

	(c) Surface Soil Moisture (rmse, in %)				(d) Surface Soil Moisture (bias, in %)			
Patch	Perturbed	Method 1	Method 2	Method 3	Perturbed	Method 1	Method 2	Method 3
1	1.30	1.65	1.89	2.28	-1.10	0.91	0.92	1.05
2	0.00	0.00	0.00	0.00	0.00	0.00	0.00	0.00
3	2.35	3.25	2.31	3.51	-2.23	-2.55	-1.05	-1.58
4	3.51	2.25	3.68	3.78	-3.18	-0.66	-2.85	-1.78
5	2.03	2.99	2.21	2.01	-1.84	-2.71	-1.09	-2.85
6	2.13	2.06	3.08	3.21	-1.83	-0.91	-2.04	-1.91
7	1.72	2.22	2.53	2.41	-1.36	-1.66	-0.29	-1.52
8	1.51	1.91	2.40	1.99	-0.87	0.11	-1.21	-1.11
Mean	1.49	1.25	1.65	1.85	-1.35	-0.66	-0.37	-0.85

TABLE III

COMPARISON OF THE DEEP SOIL MOISTURE (IN %) RELATIVE TO THE TRUE SIMULATION FOR THE PERTURBED SIMULATION AND CORRECTED SIMULATIONS USING THREE DIFFERENT ASSIMILATION METHODS IN (a) AND (c) IN TERMS OF RSME, AND (b) AND (d) IN TERMS OF BIAS FOR EACH PATCH AND FOR THE AREA-WEIGHTED AVERAGE FOR THE WHOLE GRID-SQUARE. THE VALUES GIVEN IN (a) AND (b) ARE FOR THE CASE WHEN ASSIMILATED ESTIMATES OF DEEP SOIL MOISTURE ARE CALCULATED FROM (1). THOSE IN (c) AND (d) ARE FOR THE CASE WHEN ASSIMILATED ESTIMATES OF DEEP SOIL MOISTURE ARE CALCULATED FROM (2)

Patch	(a) Deep Soil Moisture (rmse, in %)				(b) Deep Soil Moisture (Bias, in %)			
	Perturbed	Method 1	Method 2	Method 3	Perturbed	Method 1	Method 2	Method 3
1	1.84	0.87	1.16	1.38	-1.67	-0.11	0.10	-0.57
2	0.00	0.00	0.00	0.00	0.00	0.00	0.00	0.00
3	6.55	1.79	1.51	2.04	-6.55	-1.45	-0.03	-0.76
4	6.52	4.11	2.53	2.45	-6.35	3.11	0.74	0.87
5	2.72	1.42	1.52	3.62	-2.46	-1.09	-1.16	0.54
6	5.02	2.80	1.91	3.15	-4.95	1.90	0.74	2.03
7	1.76	0.76	1.07	3.04	-1.53	-0.28	-0.53	0.39
8	4.24	2.80	2.43	4.01	-4.19	2.05	1.60	2.63
Mean	2.98	0.96	0.91	1.30	-2.93	0.40	0.16	0.46

Patch	(c) Deep Soil Moisture (rmse, in %)				(d) Deep Soil Moisture (Bias, in %)			
	Perturbed	Method 1	Method 2	Method 3	Perturbed	Method 1	Method 2	Method 3
1	1.84	0.95	1.29	1.55	-1.67	-0.23	-0.85	-0.95
2	0.00	0.00	0.00	0.00	0.00	0.00	0.00	0.00
3	6.55	6.71	5.59	5.68	-6.55	-5.73	-5.18	-5.26
4	6.52	2.15	5.57	5.61	-6.35	-0.35	-5.36	-5.37
5	2.72	2.83	2.30	2.37	-2.46	-2.49	-1.44	-1.49
6	5.02	1.02	3.91	4.05	-4.95	-0.06	-3.83	-3.92
7	1.76	1.55	2.07	2.07	-1.53	-0.99	-0.42	-0.47
8	4.24	1.01	3.38	3.47	-4.19	0.43	-3.31	-3.38
Mean	2.98	1.18	2.31	2.37	-2.93	-0.87	-2.12	-2.18

strongly dependent on the method used to ascribe patch-specific estimates of soil moisture during assimilation, although Method 2 tends to give smaller values of RSME, while Methods 1 and 3 give less bias.

There is also a significant improvement in the deep soil moisture for all patches within the grid square and for the grid square as a whole, and a particularly noticeable decrease in the bias (Fig. 4 and Table III), regardless of which of the two equations [(1) and (2)] is used. This is encouraging because the deep soil moisture used in the correction procedure is only indirectly estimated from the microwave brightness temperature based on the LDAS-modeled relationship between surface and deep soil-moisture status.

Fig. 5 and Table IV give the difference in cumulative daily evaporation for each patch and the average value for the whole grid-square. When compared to the true simulation, the cumulative daily evaporation for the whole multipatch grid-square is greatly improved for the corrected simulation relative to the perturbed simulation. Again, results on a patch-by-patch basis are varied. The best prediction of evaporation is for short grass growing in sandy and clay soils, while the worst prediction of evaporation is for the clay soil with shrub vegetation cover.

In general, the results do not make a strong case for selecting one particular method for assimilating area-average surface soil moisture, although the simulation of deep soil moisture is best both as an area average and for individual patches when Method 2 is used, i.e., when the soil moisture is increased by a common amount for all the modeled patches. Neither do the results make a strong case for choosing between the use of (1) and (2) when calculating the deep soil-moisture estimate to be assimilated. However, in this particular study with this particular LDAS, assuming continuity before and after assimilation (1) produces slightly better results than using a historical analysis (2) and is obviously much more readily applied. In this example, the historical analysis was run for only one year. If it were run for ten years for example, (2) is likely to show improved results.

V. DISCUSSION AND CONCLUSIONS

In the preceding analyses, no explicit mention is made of the resolution at which they apply. However, it is assumed that the LDAS for which corrections are being made is running with a resolution that is broadly equal to the resolution at which remotely sensed surface soil moisture is available. This might well be a significant issue if the analysis is applied to regional LDAS which currently run with a grid resolution of 0.125°, i.e., at a resolution that is about a factor of four less than the likely resolution of any near-term L-band soil-moisture mission. Additional assumptions will be necessary to apply some of the methods described. For example, in the case of Methods 1 and 2, it will be necessary to assume that the fractional/incremental changes in soil moisture necessary to match the observed and modeled surface brightness temperature are equal across the whole satellite grid square when it corresponds to several LDAS grid squares. Similarly, in the case of Method 3, it will be necessary to assume that the fractional adjustment to

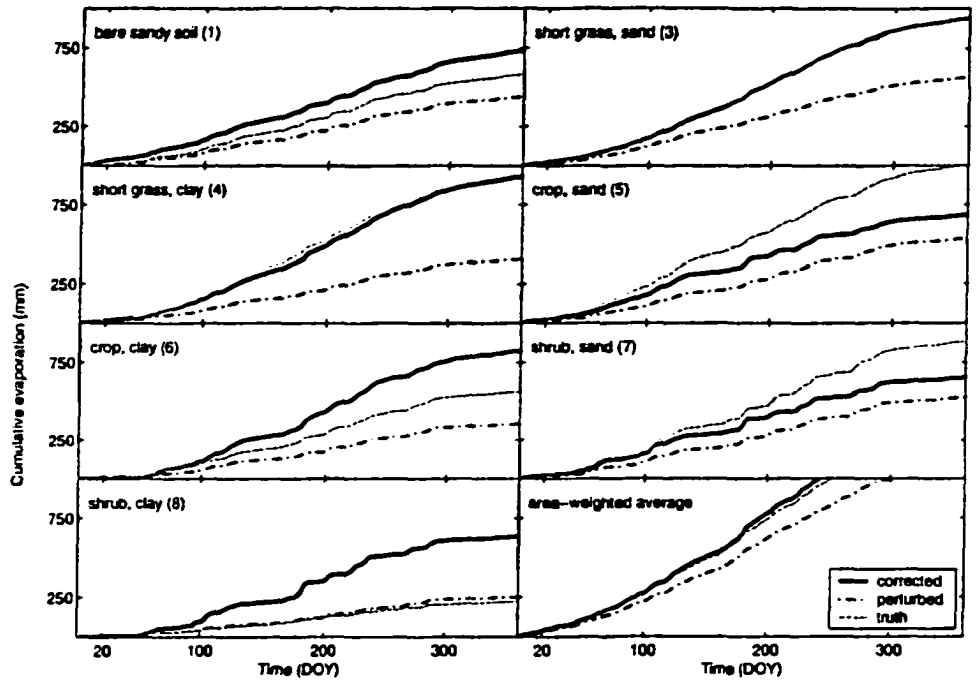

Fig. 5. Time series of the true, perturbed, and corrected cumulative evaporation for the seven nonwater patches within the grid square plus the area-weighted average of the grid square.

TABLE IV

COMPARISON OF THE CUMULATIVE EVAPORATION FOR THE EIGHT SEPARATE PATCHES AND THE AREA-WEIGHTED AVERAGE GRID SQUARE FOR THE ENTIRE YEAR. THE VALUES GIVEN IN (a) ARE FOR THE CASE WHEN ASSIMILATED ESTIMATES OF DEEP SOIL MOISTURE ARE CALCULATED FROM (1) WHILE THOSE IN (b) FOR THE CASE WHEN ASSIMILATED ESTIMATES OF DEEP SOIL MOISTURE ARE CALCULATED FROM (2)

Patch			(a) Equation 1			(b) Equation 2		
	Truth (mm)	Perturbed (mm)	Method 1 (mm)	Method 2 (mm)	Method 3 (mm)	Method 1 (mm)	Method 2 (mm)	Method 3 (mm)
1	588	445	716	740	667	722	732	713
2	3710	3710	3710	3710	3710	3710	3710	3710
3	930	567	839	938	892	580	771	765
4	951	409	1152	933	943	904	510	511
5	1006	537	707	687	1099	449	681	664
6	565	358	1008	828	1006	678	257	257
7	887	530	670	657	995	547	716	678
8	226	256	749	640	864	256	190	191
Mean	1302	1093	1394	1354	1452	1224	1399	1378

the change in soil moisture for each patch since the last assimilation cycle is the same for all the LDAS grid-squares present in each satellite pixel.

Notwithstanding the technical issues just mentioned, the primary conclusions of the present analysis are clear.

a) The recent and/or time average history of the LDAS description of soil water movement represents a plausible, LDAS-consistent way to use remotely sensed estimates of surface soil moisture to infer soil moisture at depth;
b) If such a relationship is defined, it is possible to use the LDAS description of soil and vegetation processes and microwave emission to allow approximate allocation of area-average soil moisture between the modeled patches using iterative techniques, which results in good area-average correction to soil moisture (and evaporation); good patch-specific deep soil moisture; but the patch-specific corrections to surface soil moisture are not as good;
c) The three iterative methods for allocating single area-average microwave brightness temperature between patches tested in the present study gave similar results, but Method 2 was arguably preferable, primarily because it was best in estimating deep soil moisture.

Notwithstanding the significant and general improvement in the area-average simulations when area-average microwave brightness temperature is assimilated for a multipatch LDAS grid square just described, the fact remains that the patch specificity of the soil moisture, especially that of the surface soil moisture, is less than perfectly captured. Presumably, this is because there is not enough remotely sensed information to accurately assign the microwave brightness temperature between patches, and the mosaic-patch representation of individual patches is not sufficiently powerful to fully compensate for this. It is possible that, given measurements of area-average microwave brightness temperatures at a range of look angles and with vertical and horizontal polarizations, it may be possible to disaggregate the area-average signal more effectively. The upcoming soil moisture ocean salinity (SMOS) [23]) L-band mission will, for example, provide this type of additional information, and detailed investigation of the potential value of SMOS observations for LDAS is the subject of our ongoing research.

ACKNOWLEDGMENT

The authors wish to thank C. Thies for editorial assistance.

REFERENCES

[1] A. C. M. Beljaars, P. Viterbo, M. J. Miller, and A. K. Betts, "Anomalous rainfall over the U.S. during July 1993: Sensitivity to land surface parameterization," *Mon. Weather Rev.*, vol. 124, pp. 364–383, 1993.

[2] A. K. Betts, J. H. Ball, A. C. M. Beljaars, M. J. Miller, and P. Viterbo, "The land-surface-atmosphere interaction: A review based on observational and global modeling perspectives," *J. Geophys. Rev.*, pp. 7209–7225, 1996.

[3] C. A. Clark and R. W. Arritt, "Numerical simulations of the effect of soil moisture and vegetation cover on the development of deep convection," *J. Appl. Meteorol.*, vol. 34, pp. 2029–2045, 1995.

[4] J. D. Fast and M. D. McCorkle, "The effects of heterogeneous soil moisture on a summer baroclinic circulation in the central United States," *Mon. Weath. Rev.*, vol. 119, pp. 2140–2167, 1991.

[5] M. J. Fennessey and J. Shukla, "Impact of initial soil wetness on seasonal atmospheric prediction," *J. Climate*, vol. 12, pp. 3167–3180, 1999.

[6] R. D. Koster and M. J. Suarez, "A simple framework for examining the interannual variability of land surface moisture fluxes," *J. Climate*, vol. 12, pp. 1911–1917, 1999.

[7] R. J. Oglesby, "Springtime soil moisture, natural climate variability and North American drought as simulated by the NCAR Community Model 1," *J. Climate*, vol. 4, pp. 890–897, 1991.

[8] R. D. Koster and M. J. Suarez, "Modeling the land surface boundary in climate models as a composite of independent vegetation stands," *J. Geophys. Res.*, vol. 97, pp. 2697–2715, 1992.

[9] *LDAS Homepage*, [Online]. Available: http://ldas.gsfc.nasa.gov.

[10] K. Mitchell, C. Marshall, D. Lohmann, M. Ek, Y. Lin, P. Grunmann, P. Houser, E. Wood, J. Schaake, D. Lettenmaier, D. Tarpley, W. Higgins, R. Pinker, A. Robock, B. Cosgrove, J. Entin, and Q. Duan, "The collaborative GCIP land data assimilation (LDAS) project and supportive NCEP uncoupled land-surface modeling initiatives," in *Proc. 15th Amer. Meteorol. Soc. Conf. Hydrol.*, 2000.

[11] Y. A. Liou, E. J. Kim, and A. W. England, "Radiobrightness of prairie soil and grassland during dry-down simulations," *Radio Sci.*, vol. 33, pp. 259–265, 1998.

[12] J. F. Galantowicz, D. Entekhabi, and E. G. Njoku, "Tests of sequential data assimilation for retrieving profile soil moisture and temperature from observed L-band radiobrightness," *IEEE Trans. Geosci. Remote Sensing*, vol. 37, pp. 1860–1870, July 1999.

[13] E. J. Burke, R. J. Gurney, L. P. Simmonds, and T. J. Jackson, "Calibrating a soil water and energy budget model with remotely sensed data to obtain quantitative information about the soil," *Water Resources Res.*, vol. 33, pp. 1689–1697, 1997.

[14] E. J. Burke, R. J. Gurney, L. P. Simmonds, and P. E. O'Neill, "Using a modeling approach to predict soil hydraulic properties from passive microwave measurements," *IEEE Trans. Geosci. Remote Sensing*, vol. 36, pp. 454–462, 1998.

[15] C. C. Daamen and L. P. Simmonds, "Measurement of evaporation from bare soil and its estimation using surface-resistance," *Water Resources Res.*, vol. 32, pp. 1393–1402, 1996.

[16] T. T. Wilheit, "Radiative transfer in a plane stratified dielectric," *IEEE Trans. Geosci. Remote Sensing*, vol. GE-16, pp. 138–143, 1978.

[17] J. R. Wang and T. J. Schmugge, "An empirical model for the complex dielectric permittivity of soils as a function of water content," *IEEE Trans. Geosci. Remote Sensing*, vol. GE-18, pp. 288–295, 1980.

[18] J. R. Wang and B. J. Choudhury, "Remote-sensing of soil-moisture content over bare field at 1.4 GHz frequency," *J. Geophys. Res.*, vol. 86, pp. 5277–5282, 1981.

[19] F. T. Ulaby, R. K. Moore, and A. K. Fung, *Microwave Remote Sensing—Active and Passive*. Reading, MA: Addison-Wesley, 1986.

[20] "Effect of vegetation characteristics on SMOS soil moisture retrievals.", to be published.

[21] P. R. Houser, W. J. Shuttleworth, J. S. Famiglietti, H. V. Gupta, K. H. Syed, and D. C. Goodrich, "Integration of soil moisture remote sensing and hydrological modeling using data assimilation," *Water Resources Res.*, vol. 34, pp. 3405–3420, 1998.

[22] *SGP97 Homepage*, [Online]. Available: http://daac.gsfc.nasa.gov/CAMPAIGN_DOCS/SGP97/sgp97.html.

[23] *SMOS Homepage*, [Online]. Available: http://www-sv.cict.fr/cesbio/smos.

Eleanor J. Burke, photograph and biography not available at the time of publication.

W. James Shuttleworth, photograph and biography not available at the time of publication.

Khil-ha Lee, photograph and biography not available at the time of publication.

Luis A. Bastidas, photograph and biography not available at the time of publication.

APPENDIX D: ESTIMATION OF AREA-AVERAGE SENSIBLE HEAT FLUX USING A LARGE APERTURE SCINTILLOMETER DURING THE SEMI-ARID LAND-SURFACE-ATMOSPHERE (SALSA) EXPERIMENT, by A. Chehbouni, Y.H. Kerr, C. Watts, O. Hartogensis, D. Goodrich, R. Scott, J. Schieldge, K. Lee, W.J. Shuttleworth, G. Dedieu, and H.A.R. De Bruin, in *Water Resources Research,* 35(8): 2505-2511, 1999.

Estimation of area-average sensible heat flux using a large-aperture scintillometer during the Semi-Arid Land-Surface-Atmosphere (SALSA) experiment

A. Chehbouni,[1,2] Y. H. Kerr,[3] C. Watts,[4] O. Hartogensis,[5] D. Goodrich,[6] R. Scott,[7] J. Schieldge,[8] K. Lee,[7] W. J. Shuttleworth,[7] G. Dedieu,[3] and H. A. R. De Bruin[5]

Abstract. The use of a large-aperture scintillometer to estimate sensible heat flux has been successfully tested by several investigators. Most of these investigations, however, have been confined to homogeneous or to sparse with single vegetation-type surfaces. The use of the scintillometer over surfaces made up of contrasting vegetation types is problematic because it requires estimates of effective roughness length and effective displacement height in order to derive area-average sensible heat from measurements of the refractive index. In this study an approach based on a combination of scintillometer measurements and an aggregation scheme has been used to derive area-average sensible heat flux over a transect spanning two adjacent and contrasting vegetation patches: grass and mesquite. The performance of this approach has been assessed using data collected during the 1997 Semi-Arid Land-Surface-Atmosphere field campaign. The results show that the combined approach performed remarkably well, and the correlation coefficient between measured and simulated area-average sensible heat flux was ~0.95. This is of interest because this approach offers a reliable means for validating remotely sensed estimates of surface fluxes at comparable spatial scales.

1. Introduction

The turbulent heat fluxes near the ground surface are strongly affected by the ability of the surface to redistribute the radiative energy absorbed from the Sun and the atmosphere into sensible and latent heat. These fluxes play a key role in regulating the energy balance of the atmosphere, which in turn drives atmospheric circulation. For this reason, recent efforts have concentrated on improving the parameterization of land-surface processes in atmospheric models by taking into account the effect of surface heterogeneities on the exchanges processes [*Avissar*, 1995]. The problem, however, is the difficulty in validating model simulations at regional and certainly at the global circulation model (GCM) scale. On the other hand, it is necessary to validate GCM output because unless these models can reliably simulate the observed water and energy cycles in the present climate, future predictions of climate change are rather tenuous [*Kinter and Shukla*, 1990]. To address this issue, the international community has coordinated several multidisciplinary field experiments for collecting hydrologic, atmospheric, and remote sensing data over a range of spatial and temporal scales. One of the unique features of these field experiments has been the deployment of a network of several single-point measurements of surface fluxes, i.e., eddy correlation or Bowen ratio stations for validating atmospheric and hydrologic models. There are technical limitations on using such systems related to the required horizontal homogeneity of the surface layer, the expensive, and the training [*De Bruin et al.*, 1995].

Several investigations recently demonstrated the potential of using scintillometers to obtain areally averaged sensible heat fluxes over path lengths of several kilometers, which are similar to satellite measurement scales [*Wesely and Derzko*, 1975; *Wesely*, 1976a, b; *Kohsiek*, 1985, 1987; *De Bruin et al.*, 1995; *McAneney et al.*, 1995; *Green et al.*, 1994; *Lagouarde et al.*, 1996; *Hartogensis*, 1997]. The scintillation method works by transmitting a beam of electromagnetic radiation and measuring the intensity variations of the received signal. This leads to a direct measure of the strength of the refractive index of the air and then to the structure parameter for the refractive index (C_n^2), which can then be related to the structure function parameter of temperature (C_T^2) used to derive sensible heat flux.

The objective of this study is to use a large-aperture scintillometer (LAS) to estimate areally averaged sensible heat flux over a transect made up of two adjacent patches (a grass-covered patch and a primarily mesquite-covered patch) with contrasting water status and roughness length. Scintillometer-based sensible heat flux is compared to a weighted average of those measured over each individual patch using two independent three-dimensional eddy correlation systems. The experiment took place in the San Pedro Basin within the context of

[1]Institut de Recherche pour le Développement/Instituto del Medio Ambiente y Desarrollo Sustentable, Reyes and Aguascalientes Esq., Hermosillo, Mexico.
[2]Permanently at Institut de Recherche pour le Développement, Paris, France.
[3]Le Centre d'Etudes Spatiales de la Biosphère, Toulouse, France.
[4]Instituto del Medio Ambiente y Desarrollo Sustentable, Hermosillo, Mexico.
[5]Department of Meteorology, Wageningen Agricultural University, Wageningen, Netherlands.
[6]Agricultural Research Service, United States Department of Agriculture, Tucson, Arizona.
[7]Department of Hydrology and Water Resources, University of Arizona, Tucson.
[8]Jet Propulsion Laboratory, California Institute of Technology, Pasadena.

Paper number 1999WR900111.
0043-1397/99/1999WR900111$09.00

the Semi-Arid Land-Surface-Atmosphere (SALSA) research program [*Goodrich et al.*, 1998].

2. Physical Background

2.1. Theoretical Principles

In a turbulent medium such as the Earth's atmosphere the turbulent refractive index fluctuations η are affected by fluctuation of temperature, humidity, and pressure. However, the contribution of atmospheric pressure fluctuation to the refractive index is known to be small, and its effect can be neglected [*Hill*, 1989]. According to *Andreas* [1989] the refractive index fluctuation η is related to temperature T' and humidity q' fluctuations, thus

$$\eta = A_T(\lambda, P, T, q)\frac{T'}{T} + A_q(\lambda, P, T, q)\frac{q'}{q} \qquad (1)$$

where A_T and A_q are known functions that depend on the optical wavelength λ, the total atmospheric pressure P, the air temperature T, and the specific humidity, q. In the visible and near-infrared region of the electromagnetic spectrum the dependence of A_T and A_q on λ is very small. For $\lambda = 0.94$ μm, which is the wavelength of the scintillometer used in this study, these functions can be parameterized following *Andreas* [1989] as

$$A_T = -0.78 \times 10^{-6}\frac{P}{T} \qquad (2)$$

$$A_q = -57.22 \times 10^{-6} q \qquad (3)$$

The refractive index fluctuations η in a turbulent medium are a random function of time t and position x. In turbulence theory it is common to describe the spatial variability or "structure" of a variable by the so-called structure function $D_A(r)$ [*Panofsky and Dutton*, 1984]. The structure function of refractive index fluctuations η for separation distances r in the inertial subrange of scales about a point x is

$$D_n(r) = \overline{[\eta(x) - \eta(x + r)]^2} = C_n^2 r^{2/3} \qquad l_0 < r < L_0 \qquad (4)$$

where C_n^2 is the refractive index structure parameter representing the amplitude of the variations in the refractive index and the overbar denotes a time or ensemble average [*Lagouarde et al.*, 1996]. The inertial subrange for which (4) is valid is the range in the turbulent spectrum in which turbulent energy is transferred from larger to smaller wavelengths. The inner scale l_0 marks the transition between the inertial and viscous energy dissipating range of eddy sizes and is of the order of 0.5–1.0 cm near the surface. The integral or outer scale L_0 describes the scale of the dominant inhomogenities, which is of the order of half the height of measurement above the surface.

On the basis of *Tatarskii*'s [1961] theory, *Clifford et al.* [1974] showed that for a LAS the variance of the natural logarithm of the irradiance I incident at the receiver is

$$\sigma_{\ln(I)}^2 = \overline{[\ln(I) - \overline{\ln(I)}]^2} = \int_0^1 C_n^2(u) W(u) du \qquad (5)$$

where $W(u)$ is a spatial weighing function given by

$$W(u) = 16\pi^2 k^2 L \int_0^\infty dK K \Phi_n(K) \sin^2[K^2 L u(1 - u)/2k] \cdot [2J_1(x_1)2J_1(x_2)/(x_1 x_2)]^2 \qquad (6)$$

$u = x/L$ is the normalized pathlength; L is the path length; $k = 2\pi/\lambda$ is the optical wave number; $x_1 = KD_R u/2$ and $x_2 = KD_T u/2$, where D_R and D_T are the receiver and transmitter apertures, respectively; K is the three-dimensional spatial wave number; J_1 is a Bessel function of the first kind of order one; and Φ_n, the three-dimensional Kolmogorov spectrum of the refractive index, describes the turbulent medium in terms of its Fourier components K:

$$\Phi_n(K) = 0.033 C_n^2 K^{-11/3} \qquad (7)$$

After integrating (6) and using (5) and (7), *Wang et al.* [1978] obtained

$$C_n^2 = C\sigma_{\ln(I)}^2 (D_R/D_T)^{7/3} L^{-3} \qquad (8)$$

where C is a calibration constant, which is a function of the ratio D_R/D_T. For equal receiver and transmitter apertures, as is the case here, C_n^2 can be described as a linear function of $\sigma_{\ln(I)}^2$ measured by the scintillometer as

$$C_n^2 = C\sigma_{\ln(I)}^2 D^{7/3} L^{-3} \qquad (9)$$

where $C = 1.12$ for C_n^2 ranges from 10^{-17} to 10^{-12} m$^{-2/3}$ and D is the diameter of the receiver/transmitter.

2.2. Sensible Heat Flux

A scintillometer is an instrument that measures the intensity of a light beam fluctuation after propagating through a turbulent medium. It is assumed that these intensity fluctuations are caused by inhomogeneities in the refractive index, which are due to turbulent eddy motions along the scintillometer path. The eddy motions are generated by temperature and humidity fluctuations and can be regarded as a collection of converging and diverging lenses focusing and defocusing the scintillometer beam [*McAneney et al.*, 1995]. In the visible and infrared region, assuming that temperature and humidity fluctuations are perfectly correlated, the spatially averaged refractive index structure parameter measured directly by a LAS is related to the temperature structure parameter as

$$C_T^2 = C_n^2\left(\frac{T^2}{-0.78 \times 10^{-6} P}\right)^2\left(1 + \frac{0.03}{\beta}\right)^{-2} \qquad (10)$$

where β is the Bowen ratio that is incorporated as a humidity correction such that C_T^2 decreases with increasing evaporation rate. The study by *De Wekker* [1996] showed that this term can be neglected whenever the Bowen ratio is >0.6, which is generally the case over natural surfaces in arid and semiarid areas. The sensible heat and momentum fluxes together determine atmospheric stability, and this in turn influences turbulent transport, thus an iterative procedure is needed to calculate sensible heat flux from the scintillometer measurement [*Lagouarde et al.*, 1996].

We first define the dimensionless temperature scale θ^* as

$$\theta^* = H/\rho c_p u^* \qquad (11)$$

where ρ is the density of the air, c_p is the heat capacity at constant pressure, and u^* is the friction velocity given from

$$u^* = \frac{ku}{\ln\left(\frac{z-d}{z_0}\right) - \psi_m\left(\frac{z_0-d}{L_{mos}}\right)} \tag{12}$$

where z is the measurement height, z_0 is the roughness length, d is the displacement height, ψ_m is the integrated stability function, and L_{mos} is the Monin-Obukhov length defined as

$$L_{mos} = \frac{Tu_*^2}{kg\theta_*} \tag{13}$$

Under unstable conditions, *De Bruin et al.* [1993, 1995] found that the temperature structure parameter C_T^2 and θ^* are related by

$$\frac{C_T^2(z-d)^{2/3}}{\theta_*^2} = 4.9\left(1 - 9\frac{z-d}{L_{mos}}\right)^{-2/3} \tag{14}$$

Sensible heat flux can then be derived using (10)–(14) via iteration.

2.3. Derivation of Area-Average Sensible Heat Flux Over Patchy Surfaces

Inferring area-average sensible heat flux using scintillometer from (10)–(14) requires an aggregation rule that allows for the derivation of effective value of the roughness length z_0 and the displacement height d. This is a classical "aggregation problem," where a link needs to be established between the relevant parameters at the patch scale and at the grid scale. Fortunately, there has been substantial progress in specifying area-average parameters using either empirical [*Mason*, 1988; *Blyth et al.*, 1993; *Blyth and Harding*, 1995; *Noilhan and Lacarrere*, 1995; *Shuttleworth*, 1988, 1991; *Arain et al.*, 1996] or theoretical approaches [*Lhomme*, 1992; *Lhomme et al.*, 1994; *Chehbouni et al.*, 1995; *Raupach*, 1991, 1995; *Raupach and Finnigan*, 1995]. Following *Shuttleworth et al.* [1997], effective roughness length can be formulated as

$$\ln^{-2}\left(\frac{z_b-d}{z_0}\right) = \sum_i w_i \ln^{-2}\left(\frac{z_b-d_i}{z_{oi}}\right) \tag{15}$$

while the effective displacement height can be formulated as

$$d = \sum_i w_i d_i \tag{16}$$

where z_{0i} and d_i are the patch scale roughness length and displacement height, respectively, which were derived as functions of the vegetation height; w_i is the fraction of the surface covered by the patch i; and z_b is the blending height, which is expressed as a function of the friction velocity, wind speed, and horizontal length scale [*Wieringa*, 1986].

3. Experiment

3.1. Site Description

This study took place in the Upper San Pedro Basin (USPB), which represents the focus study region for the SALSA program. The basin originates in northern Sonora, Mexico, and flows north into southeast Arizona. (see Figure 1 for site location). The basin embodies a number of characteristics that make it an exceptional outdoor laboratory for addressing a large number of scientific challenges in arid and semiarid hydrology, meteorology, ecology, and social and policy science [*Goodrich et al.*, 1998]. The basin is a transition area between the Sonoran and Chihuahuan Deserts. It is an international basin spanning the Mexico-United States border with significantly different cross-border legal and land-use practices, significant topographic and vegetation variation, and a highly variable climate. The annual rainfall ranges from ~300 to 750 mm, with the majority of annual precipitation (~65%) occurring during the July through September monsoon season from high-intensity convective thunderstorms and ~30% coming from less intense winter frontal systems. Major vegetation types include desert shrub-steppe, grasslands, oak savannah, pinyon-juniper, and ponderosa pine. For this study an experimental site made up of two adjacent patches (i.e., a sacaton grass site adjacent to a mixed mesquite/grassland site) on the San Pedro River flood plain was chosen. The aerodynamic characteristics of the two patches were very different: the grass was ~1 m in height, and the mesquite was ~3.5 m in height.

3.2. Instrumentation

During the monsoon period, measurements include basic meteorological data, i.e., wind speed and direction at different heights, incoming radiation, air temperature, and humidity. Additionally, soil moisture, vegetation sampling, and surface reflectance and temperature were also taken. Fluxes of sensible heat and water vapor were measured above both grass and the mesquite patches using an eddy covariance-based method. Over the grass patch the eddy covariance station consisted of a three-dimensional sonic anemometer and krypton hygrometer manufactured by Campbell Scientific, Inc. Over the mesquite patch the eddy covariance system comprises a three-axis sonic anemometer manufactured by Gill instrument (Solent A1012R) and an IR gas analyzer (LI-COR 6262 model), which was used in close path mode. The system is controlled by specially written software that calculates the surface fluxes of momentum, sensible and latent heat, and carbon dioxide from the output of the sonic and IR gas analyzer and displays them in real time. During the first portion of the campaign an intercomparison of flux instruments was conducted over a homogeneous region of the sacaton grass.

The LAS used in this study was designed and built at the Department of Meteorology of the Wageningen Agricultural University, and the electronics are those described by *Ochs and Wilson* [1993]. The LAS has an aperture size of 0.15 m, and the light source is a light-emitting diode (LED: TIES-16A, Texas Instruments), operating at a peak wavelength of 0.94 μm, placed at the focal point of a concave mirror (see Figure 2 for a picture of the LAS). The reflected beam emitted by the transmitter diverges slightly (by ~0.002°). The irradiance distribution over the beam is completely uniform. The receiver employs an identical mirror to focus light on a photo diode detector. To distinguish the light emitted by the LAS from ambient radiation, it is excited by a 7 kHz square wave. Scintillations appear as amplitude modulations on the carrier wave. For beam alignment, telescope rifle sights are mounted on both the receiver and emitter housings.

In this study the receiver and the emitter were ~900 m apart, spanning a transect made up of 25% grass and 75% mixed mesquite and grass. The average measurement height was 10.5 m above the soil surface. The receiver electronics are designed in such a way that after setting the path length it gives an output voltage such that C_n^2 can be derived from $C_n^2 = 10^{(V_{out}-12)}$, where V_{out} is the output voltage of the scintillometer. Ten minute average values of the scintillometer output

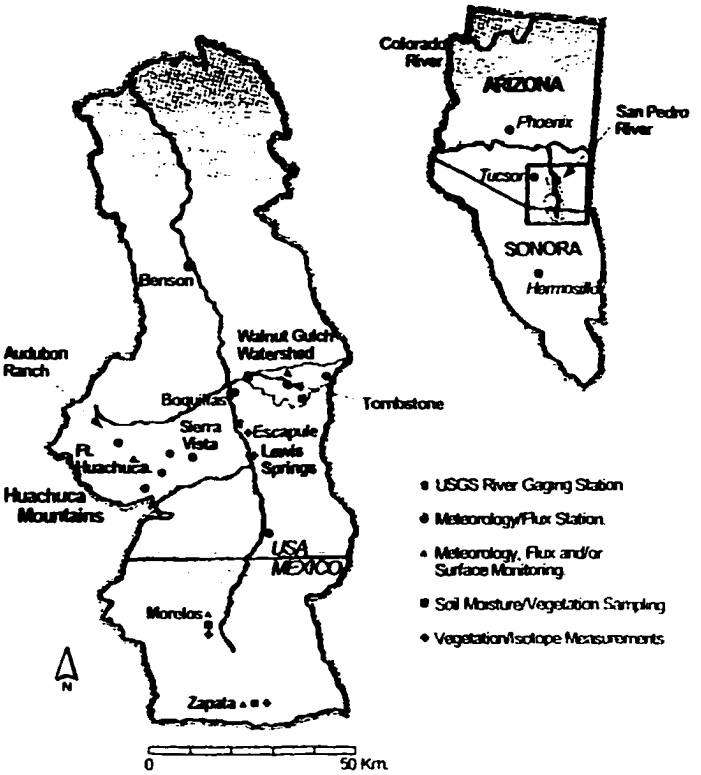

Figure 1. Location map of the Upper San Pedro Basin.

V_{out} were stored on a data logger (Campbell Scientific, Inc., 21X). These data were linearly averaged to provide 30 min average values.

4. Results

4.1. Intercomparison of Measurement Systems

During the first part of the intensive campaign, two eddy correlation instruments were deployed next to each other over a homogeneous sacaton grass. At the same time the scintillometer was installed over the same patch, sampling a transect of ~300 m corresponding to the footprint of the eddy correlation instruments. In Figure 3a, sensible heat flux estimated by the scintillometer is compared to the values obtained using the

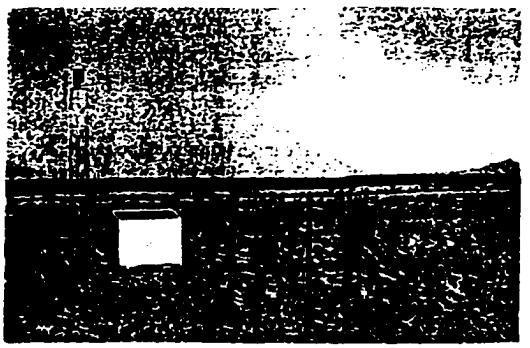

Figure 2. Picture of the emitter of the large-aperture scintillometer (the receiver looks similar).

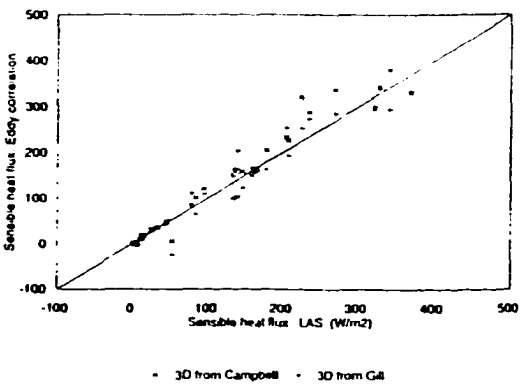

Figure 3a. Comparison between sensible heat flux obtained with the scintillation method and the corresponding values measured with eddy correlation systems during the intercomparison period: Gill, pluses, and Campbell, crosses.

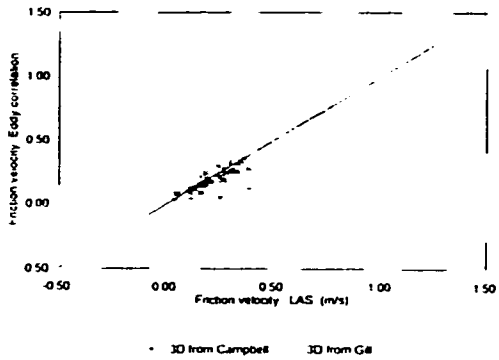

Figure 3b. Comparison between friction velocity with the scintillation method and the corresponding values measured with eddy correlation systems during the intercomparison period: Gill, pluses, and Campbell, crosses.

eddy correlation instruments. Figure 3b presents the same comparison for friction velocity. It is seen that except for a few outliners the correspondence is good. The differences between the scintillometer and eddy correlation estimates for both sensible heat flux and friction velocity are of the same magnitude as the difference between the two eddy correlation systems. The statistical results comparing the different systems are given in Table 1a for sensible heat flux and in Table 1b for the friction velocity. This confirms the result obtained elsewhere [*De Bruin et al.*, 1996; *Lagouarde et al.*, 1996], where comparisons of sensible heat flux measured by the scintillometer and eddy correlation over short distances are within experimental error. Therefore no adjustment of the two eddy correlation measurements has to be made.

After the intercalibration period one of the eddy correlation systems (Gill) was deployed over the mesquite patch, while the other (Campbell) was deployed over the grass patch. At the same time the transmitter and the receiver of the scintillometer were set ~900 m apart to sample a transect made up of 75% mesquite and 25% grass. Figures 4a and 4b present the difference in measured sensible heat flux and friction velocity between the grass and mesquite patches. Figures 4a and 4b demonstrate that there are significant differences between the two patches, which can be up to 150 W m^{-2} for sensible heat flux and 0.5 m s^{-1} for u^*. This contrasted behavior can be explained by the difference in terms of the canopy height and the root system depth between the grass and the mesquite. These parameters greatly influence the aerodynamic flow above the canopy and the partitioning of available energy into sensible latent heat flux.

Table 1a. Statistical Results of the Intercomparison Between the Sonic From Campbell, the Sonic from Gill, and the Large Aperture Scintillometer (LAS) in Estimating Sensible Heat Flux

	N	MAD	RMSD	X_{coeff}	R^2	Const
Gill/Campbell	29	23.04	34.89	1.04	0.92	1.59
Gill/LAS	29	20.88	28.40	0.95	0.94	5.34
Campbell/LAS	29	22.64	31.63	0.88	0.94	8.86

N is the number of observations, MAD is the mean absolute difference, RMSD is the Root Mean Square Difference; X_{coeff} is the slope of the linear regression; R^2 is the correlation coefficient, and Const is the constant of linear regression.

Table 1b. Statistical Results of the Intercomparison Between the Sonic From Campbell, the Sonic from Gill, and the LAS in Estimating Friction Velocity

	N	MAD	RMSD	X_{coeff}	R^2	Const
Campbell/LAS	29	0.04	0.06	0.89	0.70	0.88
Gill/Campbell	29	0.05	0.07	0.62	0.39	1.04
Gill/LAS	29	0.05	0.07	0.71	0.45	0.95

4.2. Validation and Discussion

Equations (10)–(14) were used in conjunction with effective roughness length and effective displacement height obtained from (15) and (16) to derive area-average sensible heat flux and friction velocity using scintillometer measurements taken under unstable conditions from days of the year (DOYs) 225–231. To verify the performance of the scintillometer, it is necessary to derive an area-average friction velocity and area-average sensible heat flux from eddy correlation measurements independently from each patch.

Simple weighted averages of the fluxes measured by the three-dimensional sonics over the grass and the mesquite patches were used for the area-average sensible heat flux. However, estimating area-average friction velocity is not trivial. The approach adopted here was to obtain area-average momentum flux (ρu^{*2}) as a weighted average of the fluxes measured independently over each patch and then match it with that formulated in terms of effective friction velocity. This leads to the following relationship between effective friction velocities u^* and components friction velocities u_i^*:

$$u^* = \left(\sum w_i u_i^{*2}\right)^{0.5} \tag{17}$$

Figure 5 presents a comparison between the scintillometer-based friction velocity and that obtained using (17) in conjunction with measured component friction velocities. The scatter

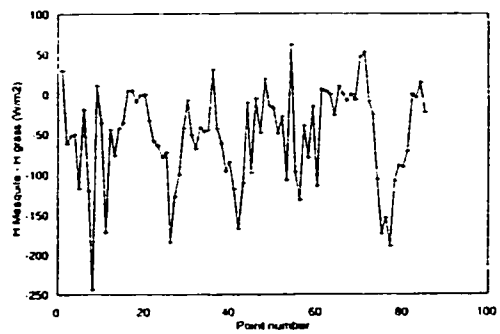

Figure 4a. Differences of sensible heat flux measured over mesquite and over grass.

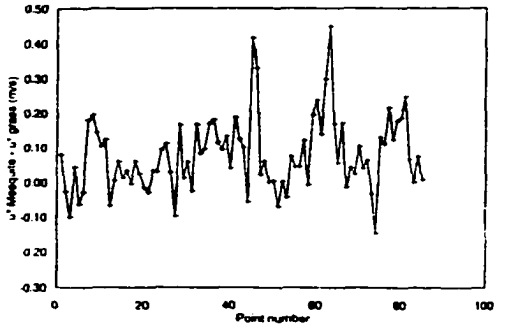

Figure 4b. Differences of friction velocity measured over mesquite and over grass.

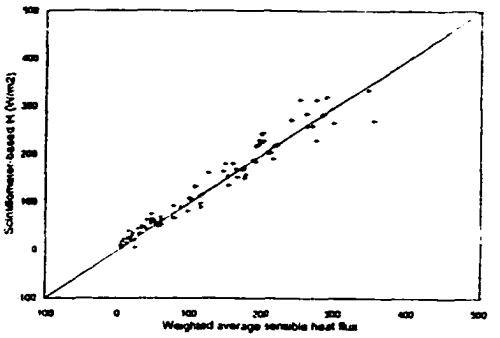

Figure 6. Comparison between measured area-average sensible heat flux and the corresponding values derived from the scintillometer measurements.

in Figure 5 is larger than those reported in the literature. However, it is important to remember that this study is for a very complex surface where heterogeneity is present at both patch and grid scales. Figure 6 presents a comparison between measured values of area-average sensible heat flux and the corresponding values estimated by the scintillometer. The correspondence between the two are very good. Statistical analysis of the performance of the LAS in estimating area-average H and u^* are presented in Table 2. The performance of the scintillometer in estimating area-average sensible heat flux over contrasting patches in this study is very similar to that reported over a single patch [*McAneney et al.*, 1995]. This suggests the robustness of the scintillometer approach over nonuniform surfaces.

This result is very encouraging because it suggests that reliable area-average estimates of sensible heat flux can be obtained to validate large-scale atmospheric models without the need to deploy a network of hydrometeorological devices such as eddies. However, a number of issues need to be addressed before it is possible to generalize the results obtained in this study. As can be seen from (10), estimating C_T^2 from C_n^2 requires a humidity correction factor that has been legitimately neglected here. This is not necessarily always the case. The problem arises when the scintillometer measurements are made over transects that comprised several patches with significantly different evaporating rates (and different low Bowen ratios). In this case it is necessary to derive an effective Bowen ratio, and this may not be trivial. Additionally, there is a need to investigate the case where the sign of the heat flux changes along the transect because the scintillometer cannot distinguish between stable and unstable conditions. Finally, the issue associated with changes in wind direction from downpath to cross-path needs to be investigated.

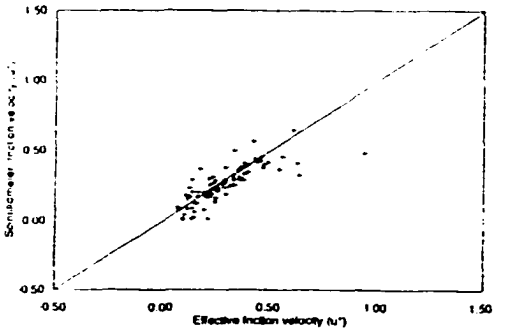

Figure 5. Comparison between effective friction velocity derived from eddy correlation measurements and the corresponding values evaluated with the scintillometer. Units are m s^{-1}.

5. Conclusions

Several successful studies have investigated the use of the scintillometer in estimating area-average sensible heat flux over homogeneous surfaces. The objective of this study was to test the performance of the scintillometer over a surface made up of two contrasting patches. The approach used was to combine scintillometer measurements with an aggregation scheme to derive effective roughness length and effective displacement. The result showed that the agreement between the measured and simulated area-average sensible heat flux values is very good. The LAS has several major advantages for measuring sensible heat flux: (1) it is not sensitive to flow distortions near the instrument; (2) it is easy to operate and to maintain, (3) it gives statistically more reliable data, which allowed for averaging over a short time period. More importantly, it can provide a reliable tool for estimating sensible heat flux at spatial scales compatible with meteorological models and remote-sensing satellites.

Table 2. Statistical Results of the Comparison Between Measured and Scintillometer-Based Area-Average Sensible and Friction Velocity

	N	MAD	RMSD	X_{slope}	R^2	Const
Sensible heat flux	84	16.9	22.5	0.97	0.95	11.10
Friction velocity	84	0.06	0.10	0.62	0.63	0.06

Acknowledgments. We acknowledge financial support from CONACYT, the French remote sensing program PNTS, and the European Commission and ESA through VEGETATION and ERS2/ATSR2 projects. This research is situated within the framework of NASA Mission to Planet Earth (MTPE): NASA/EOS grant NAGW2425. Additional support was also provided by the USDA-ARS Global Change Research Program and NASA grant W-18-1997. Many thanks to ARS-Tombstone staff for helping during the course of the experiment and to B. Heusinkveld from WAU for his help during the processing of the scintillometer data. We are thankful to C. Thies and F. Santiago for their editorial assistance.

References

Andreas, E. L., Two-wavelength method of measuring path-averaged turbulent surface heat fluxes, *J. Atmos. Oceanic Technol.*, *6*, 280–292, 1989.

Arain, A. M., J. D. Michaud, W. J. Shuttleworth, and A. J. Dolman, Testing of vegetation parameter aggregation rules applicable to the Biosphere-Atmosphere Transfer Scheme (BATS) at the FIFE site, *J. Hydrol.*, *50*, 3751–3774, 1996.

Avissar, R., Scaling of land-atmosphere interactions, an atmospheric modelling perspective, *Hydrol. Processes*, *9*, 679–695, 1995.

Blyth, E. M., and R. J. Harding, Application of aggregation models to surface heat flux from Sahelian tiger bush, *Agric. For. Meteorol.*, *72*, 213–235, 1995.

Blyth, E. M., A. J. Dolman, and N. Wood, Effective resistance to sensible and latent heat flux in heterogeneous terrain, *Q. J. R. Meteorol. Soc.*, *119*, 423–442, 1993.

Chehbouni, A., E. G. Njoku, J.-P. Lhomme, and Y. H. Kerr, An approach for averaging surface temperature and surface fluxes over heterogeneous surfaces, *J. Clim.*, *5*, 1386–1393, 1995.

Clifford, S. F., G. R. Ochs, and R. S. Lawrence, Saturation of optical scintillation of strong turbulence, *J. Opt. Soc. Am.*, *64*, 148–154, 1974.

De Bruin, H. A. R., W. Kohsiek, and B. J. J. M. van den Hurk, A verification of some methods to determine the fluxes of momentum, sensible heat, and water vapour using standard deviation and structure parameter of scalar meteorological quantities, *Boundary Layer Meteorol.*, *63*, 231–257, 1993.

De Bruin, H. A. R., B. J. J. M. van den Hurk, and W. Kohsiek, The scintillation method tested over a dry vineyard area, *Boundary Layer Meteorol.*, *76*, 25–40, 1995.

De Bruin, H. A. R., J. P. Nieveen, S. F. J. de Wekker, and B. G. Heusinkveld, Large aperture scintillometry over a 4.8 km path for measuring areally-average sensible heatflux, paper presented at 22nd AMS Symposium on Agricultural and Forest Meteorology, Am. Meteorol. Soc., Atlanta, Ga., 1996.

De Wekker, S. F. J., The estimation of areally-averaged sensible heat fluxes over complex terrain with a large-aperture scintillometer, M.S. thesis, Dep. of Meteorol., Wageningen Agric. Univ., Wageningen, Neth., 1996.

Goodrich, D. C., et al., An overview of the 1998 activities of the Semi-Arid Land-Surface Program, paper presented at 1998 American Meteorological Society Meeting, Phoenix, Ariz., 1998.

Green, A. E., K. J. McAneney, and M. S. Astill, Surface-layer scintillation measurements of daytime sensible and momentum fluxes, *Boundary Layer Meteorol.*, *68*, 357–373, 1994.

Hartogensis, O., Measuring areally-averaged sensible heat fluxes with a large aperture scintillometer, M.S. Thesis, Dep. of Meteorol., Wageningen Agricultural University, Wageningen, Neth., 1997.

Hill, R. J., Implications of Monin-Obukhov similarity theory for scalar quantities, *J. Atmos. Sci.*, *6*, 2236–2244, 1989.

Kinter, J. L., and J. Shukla, The global hydrologic and energy cycles: Suggestions for studies in pre-global energy and water cycle experiment (GEWEX) period, *Bull. Am. Meteorol. Soc.*, *71*, 181–189, 1990.

Kohsiek, W., A comparison between line-averaged observations of C_n^2 from scintillation of a CO_2 laser beam and time averaged in situ observations, *J. Clim. Appl. Meteorol.*, *24*, 1099–1102, 1985.

Kohsiek, W., A 15 cm aperture LED scintillometer for C_n^2 and cross-wind measurements, *KNMI Sci. Rep. WR 87-3*, Royal Neth. Meteorol. Inst., DeBilt, 1987.

Lagouarde, J.-P., K. J. McAneney, and E. F. Green, Scintillometer measurements of sensible heat flux over heterogeneous surfaces, in *Scaling Up in Hydrology Using Remote Sensing*, edited by J. B. Stewart et al., pp. 147–160, John Wiley, New York, 1996.

Lhomme, J. P., Energy balance of heterogeneous terrain: Averaging the controlling parameters, *Agric. For. Meteorol.*, *61*, 11–21, 1992.

Lhomme, J. P., A. Chehbouni, and B. Monteny, Effective parameters of surface energy balance in heterogeneous landscape, *Boundary Layer Meteorol.*, *71*, 297–309, 1994.

Mason, P. J., The transformation of areally-averaged roughness lengths, *Q. J. R. Meteorol. Soc.*, *114*, 399–420, 1988.

McAneney, K. J., A. E. Green, and M.S. Astill, Large aperture scintillometry: The homogeneous case, *Agric. For. Meteorol.*, *76*, 149–162, 1995.

Noilhan, J., and L. Lacarrere, GCM gridscale evaporation from mesoscale modelling: A method based on parameter aggregation tested for clear days of Hapex-Mobilhy, *J. Clim.*, *8*, 206–223, 1995.

Ochs, G. R., and J. J. Wilson, A second-generation large-aperture scintillometer, *NOAA Tech. Memo ERL WPL-232*, NOAA Environ. Res. Lab., Boulder, Colo., 1993.

Panofsky, H. A., and J. A. Dutton, Atmospheric turbulence, in *Models and Methods for Engineering Applications*, 397 pp., John Wiley, New York, 1984.

Raupach, M. R., Vegetation-atmosphere interaction in homogeneous and heterogeneous terrain: Some implications of mixed-layer dynamics, *Vegetatio*, *91*, 105–120, 1991.

Raupach, M. R., Vegetation-atmosphere interaction and surface conductance at leaf, canopy and regional scales, *Agric. For. Meteorol.*, *73*, 151–179, 1995.

Raupach, M. R., and J. J. Finnigan, Scale issues in boundary-layer meteorology: Surface energy balances in heterogeneous terrain, *Hydrol. Processes*, *9*, 589–612, 1995.

Shuttleworth, W. J., Macrohydrology: The new challenge for process hydrology, *J. Hydrol.*, *100*, 31–56, 1988.

Shuttleworth, W. J., The modellion concept, *Rev. Geophys.*, *29*, 585–606, 1991.

Shuttleworth, W. J., Z.-L. Yang, and M. A. Arain, Aggregation rules for surface parameters in global models, *Hydrol. Earth Syst. Sci.*, *1*, 217–226, 1997.

Tatarskii, V. I., Wave propagation in a turbulent medium, 285 pp., *McGraw-Hill*, New York, 1961.

Wang, T. I., G. R. Ochs, and S. F. Clifford, A saturation-resistant optical scintillometer to measure, *J. Opt. Soc. Am.*, *69*, 334–338, 1978.

Wesely, M. L., The combined effect of temperature and humidity on the refractive index, *J. Appl. Meteorol.*, *15*, 43–49, 1976a.

Wesely, M. L., A comparison of two optical methods for measuring line-averages of thermal exchanges above warm water surfaces, *J. Appl. Meteorol.*, *15*, 1177–1188, 1976b.

Wesely, M. L., and Z. I. Derzko, Atmospheric turbulence parameters from visual resolution, *Appl. Opt.*, *14*, 847–853, 1975.

Wieringa, J., Roughness dependent geographical interpolation of surface wind speed averages, *Q. J. R. Meteorol. Soc.*, *112*, 867–889, 1986.

A. Chehbouni, IRD/IMADES, Reves and Aguascalientes Esq., Col San Benito, Hermosillo CP 83190, Sonora, Mexico (ghani@cideson.mx)

H. De Bruin and O. Hartogensis, Department of Meteorology, Wageningen Agricultural University, Duivendaal 2, 6701 AP Wageningen, Bodenummer 1, Netherlands.

G. Dedieu and Y. H. Kerr, CESBIO, 31055 Toulouse, France.

D. Goodrich, Agricultural Research Service, United States Department of Agriculture, Tucson, AZ 85719.

K. Lee, R. Scott, and W. J. Shuttleworth, Department of Hydrology and Water Resources, University of Arizona, Tucson, AZ 85721.

J. Schieldge, Jet Propulsion Laboratory, California Institute of Technology, Pasadena, CA 91109-8099.

C. Watts, IMADES, Hermosillo CP 83190, Sonora, Mexico.

(Received August 3, 1998; revised March 29, 1999; accepted March 31, 1999.)